AQUAPORIN-1 AND PRESSURE-DRIVEN WATER TRANSPORT ACROSS AORTIC ENDOTHELIA.

AQUAPORIN-1 EXPRESSION, DISTRIBUTION AND REGULATION

BY

JIMMY DEON TOUSSAINT

A dissertation submitted to the Graduate faculty in Chemical Engineering in fulfillment of the requirements for the degree of Doctor of Philosophy, The City University of New York

2009

This manuscript has been read and accepted for the Graduate Faculty in Engineering in satisfaction of the dissertation requirement for the degree of Doctor of Philosophy

Professor David S. Rumschitzki

August 10, 2009

Date

Chair of Examining Committtee

Professor Mumtaz Kassir

August 10, 2009

Date

Executive Officer

Professor Alexander Couzis

Professor Lane Gilchrist

Professor John Tarbell

Professor Mark Pezzano

Dr. Kung-Ming Jan M.D.

Supervisory Committee

THE CITY UNIVERSITY OF NEW YORK

ABSTRACT

AQUAPORIN-1 AND PRESSURE-DRIVEN WATER TRANSPORT ACROSS AORTIC ENDOTHELIA.AQUAPORIN-1 EXPRESSION, DISTRIBUTION AND REGULATION

BY JIMMY DEON TOUSSAINT

ADVISOR: PROFESSOR DAVID RUMSCHITZKI

CO-ADVISOR: DR. KUNG-MING JAN

Atherosclerosis is responsible for over 50% of deaths in the US and in all Western countries. The earliest events of atherosclerosis occur when pressure-driven convection transports low-density lipoproteins (LDLs) from the blood into the subendothelial intimae (SI) of high-pressure, large and intermediate sized arteries, resulting in a cascade of events whose consequences can include stroke and/or heart attack. Over short time scales (minutes), studies have shown that macromolecular tracers focally cross the endothelium of these vessels via transient leaks that are associated with the junctions around rare (~1 cell every few thousand) endothelial cells that are temporarily not tight (mean lifetime~1 hr). Some of these leaks are associated with cells that are either dying or dividing. Yet transmural pressure drives far more liquid from the blood across the normal (non-leaky) arterial endothelium through the vessel wall, and this flow can further advect tracer that has entered the wall through a focal leak. Thus the transmural pressure-driven water flow both advects (large) tracers into the SI, where they can bind to extracellular matrix and dilutes unbound lipid in the SI, thereby decreasing the kinetics of such binding, and

sweeps unbound lipid from the SI deeper into the wall. Thus the nature of this overall convective trans-wall water flux is of critical interest.

It has generally been accepted that water crosses the endothelium paracellularly, that is, through both the tight and leaky junctions between endothelial cells. Since 1990, however, a family of ubiquitous transmembrane proteins called aquaporins (AQP), which very efficiently facilitate transmembrane water transport with great specificity and little or no ATP cost, has been identified. It is therefore natural to ask whether AQPs are present in arterial endothelial cells and, if so, if their presence suggests a functional transcellular contribution to transmural water transport. In that case, vessels might have the capacity to control this transmural water process actively by control of their AQP expression levels. As noted, this would affect the further transport of LDL that had already crossed the SI paracellularly through leaky junctions and in its kinetics of binding to SI ECM.

In this thesis we utilize quantitative immunohistochemistry techniques to identify and show the existence and distribution of Aquaporin-1 (AQP1) on both the luminal and abluminal membranes of whole vessel rat aortic endothelial cells. We also note evidence from the theses of my labmates (T. Nguyen, S. Russell, Y. Xue) that either blocking aquaporins chemically or knocking down their expression reduces endothelial hydraulic conductivity (the ratio of the transmural water flux to the driving pressure difference), both in cultured cell monolayers and in excised whole vessels ex vivo.

Hypertension is a known risk factor for atherosclerosis and we postulate that one external condition that may influence a vessel's AQP expression is its transmural pressure. We

confirm this hypothesis in two male rat models: 1. Normotensive Wistar Kyoto rats and their genetically modified hypertensive cousins, the Spontaneously Hypertensive rats (SHR). 2. Non-genetically modified normotensive Sprague-Dawley rats, Sprague-Dawley rats made hypertensive by having undergone the Goldblatts procedure that induces the renin-angiotensin pathway to hypertension and Sprague-Dawleys that have undergone a sham operation. Using quantitative immunohistochemistry we show that endothelial cells from the both groups of chronically hypertensive rats appear to express far more AQP than their normotensive analogues. This evidence, in aggregate, supports the hypothesis that aortic endothelial cells may be able to actively regulate their aquaporin expression in response to chronic hypertensive conditions, which results in partial control of their transmural transport processes.

Water flows as discrete entities through an AQP, however we used the continuum Navier Stokes approach for modeling this flow and calculating its hydraulic conductivity; the results obtained were in close proximity to experimental data and molecular simulations results. We also present simple kinetic models based on the Law of Mass Action to describe molecular transcription and translation processes that describe our observed transmural pressure-induced differential AQP1 expression. This mechanism assumes that changes in transmural pressure impact the transcription factors (TFs) that serve as a regulatory point for the control of gene expression. We first examine the model's steady states for different transmural pressures and compare with data from our lab. From these data we extract certain model kinetic parameters and find ranges for them. We then extend our findings by numerically solving (using Matlab®7.3.0) the dynamical version of our model. In particular, we predict the time dependence of the concentration of TFs,

mRNA and AQP1 in response to step changes in transmural pressure. We also postulate that siRNA against AQP1 mRNA destroys or degrades these mRNAs with second order kinetics, and in the process themselves are consumed. This loss of siRNA subsequently affects gene expression until the siRNA concentration is severely depleted and the mRNA and its protein can recover. We solve for the corresponding dynamics of several cases of AQP1 reduction upon siRNA introduction and its subsequent recovery with siRNA depletion.

Improved understanding of AQP1 regulation by, e.g., transmural pressures, may lead to novel therapies, not just in the case of atherosclerosis, but also for a wide variety of human diseases.

ACKNOWLEDGEMENTS

First of all I would like to acknowledge my heavenly father for the breath of life and a spirit of persistence for seeing me through this endeavor; with him all things are possible. I would like to also thank all my former lab members, Dr. Sun Yu, Dr.Tieuvi Nguyen, Dr. Stewart Russell, Chirag Raval, Yan Xue and Shripad Joshi for all those wonderful, trying and inspiring moments that we had as a team. I would like to extend the deepest gratitude to my following friends for their moral support and encouragement. They include Dave Trim, David Babb, Kurt Pierre, Yvette Austin, Kelvin "Chun" Alleyne, Reemell Hercules, Marion Kent and Curtis Thorpe and Dave Bartholomew. I would also like to thank my advisors, David Rumschitzki and Dr. Kung-ming Jan for their dedicated guidance and words of encouragement in seeing my project to the end. Very special thanks to Gloria "Nana" Asare for all your support and encouragement. Finally I would like to acknowledge my family who, without their support, this would not have been possible. They include Jimechia (daughter) along with her mother, Karen Mark, Viola Orr (grandmother), Shirma Fung (mother), Lamont Toussaint (father), Sandra Orr (aunt), brothers; Lamont, Al, Otis, Shermann, Andre and sister, Carla.

TABLE OF CONTENTS PAGE

LIST OF TABLES

Page

CHAPTER 5

LIST OF FIGURES

CHAPTER 1 **Page**

CHAPTER 2

CHAPTER 3

CHAPTER 4

CHAPTER 5

CHAPTER1

INTRODUCTION

Atherosclerosis is responsible for over 50% of all deaths in the US and the Western world. Two-thirds of these deaths are caused by heart attacks when the coronary arteries are affected; clots that can affect other organs such as the brain, which results in strokes, and the kidneys, liver, gastrointestinal tract and limbs are responsible for the remaining one-third (Guyton and Hall 2000). Atherosclerosis is a progressive systemic pathological condition of large and intermediate sized arteries. It involves the passage, deposit and accumulation of cholesterol from the blood, across the endothelium and into the subendothelial intima (SI) of these vessels. This build up of cholesterol deposits eventually grow and coalesce leading to the complicated process of atheromatous plaque development. In addition, smooth and fibrous muscle tissues proliferate there to form larger plaques. These plaques can become large enough to bulge into the arterial lumen, leading to stenosis and reduction of blood flow in these

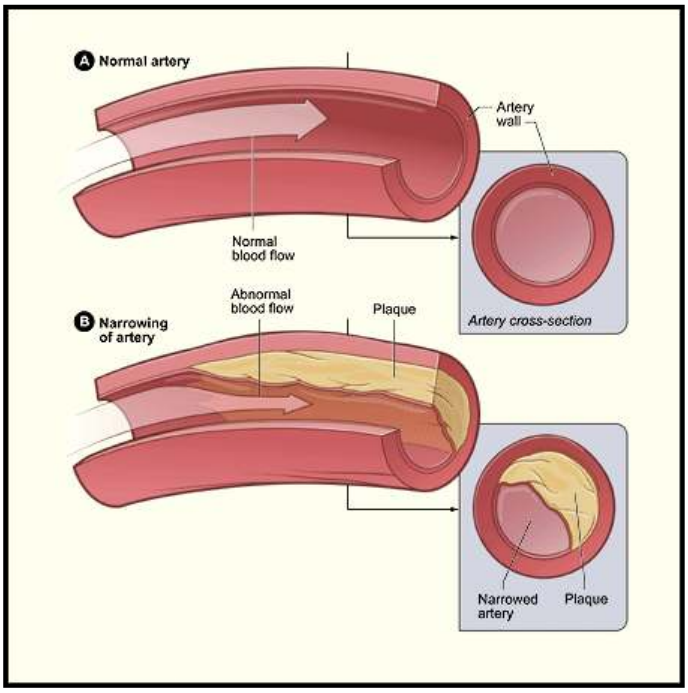

Figure 1: (www.nhlbi.nih.gov) A shows normal artery with normal blood flow**. B** shows artery with plaque build up

vessels as shown in figure 1 (Guyton and Hall 1996).They can also rupture, releasing debris into the blood stream that can clog downstream vessels.

One significant function of the endothelium is to provide a major barrier to the entry of macromolecules such as low-density lipoprotein (LDL) cholesterol (see below), from the blood into the walls of blood vessels. The mechanism whereby LDL cholesterol is transported across the endothelium is not fully understood and this has given birth to several controversial issues spanning several decades (Rippe, Rosengren et al. 2002). In order to fully characterize these transport mechanisms, several fundamental details such as the biological structures and functions of cholesterol molecules and arteries and their biochemical interactions need to be understood.

Cholesterol belongs to a class of substances known as lipids. Lipids maintain the integrity of the cell membranes, among other functions. All lipids have a low solubility in blood, and as a result, nature has devised a mechanism whereby cholesterol is transported to and from the cell by special transporters called "lipoproteins." A class of lipoprotein called low-density lipoprotein (LDL) or "bad" cholesterol, shown in figure 2, is the major cholesterol carrier in the body and principally delivers cholesterol to the body's cells. Human serum LDLs are between 17-26nm in

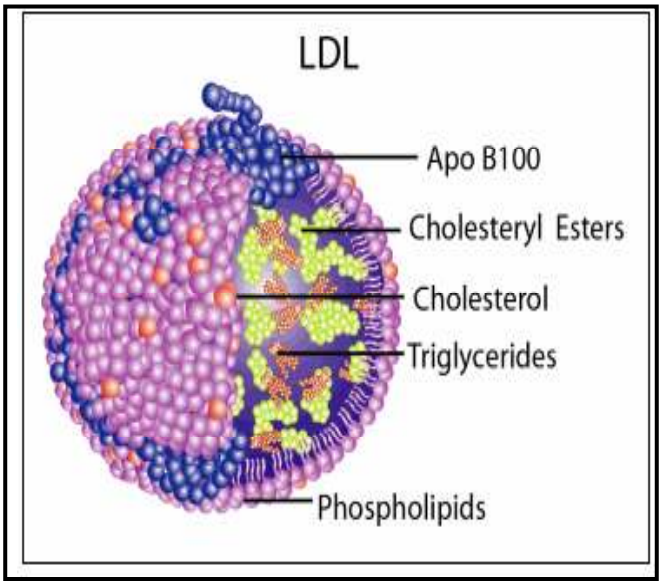

Figure 2: (www.sigmaaldrich.com) structure of LDL

diameter and have a molecular weight of between 2.2 to 2.3 million Daltons. LDLs are comprised of approximately 21% protein, 11% triglycerides, 22% phospholipids, 37% cholesteryl esters and 8% cholesterol by weight (Scanu 1973).

The structure of LDL is well suited for the solubilization of lipids in plasma. The non-polar lipids, such as cholesterol ester and triglycerides, are present in the core of the LDL molecule, surrounded by a monolayer of proteins, polar lipids, unesterified cholesterol and phospholipids. This outer monolayer is negatively charged and hydrophilic, thereby allowing the lipoproteins to remain soluble in blood plasma (Patton 1989; Guyton and Hall 1996). There is also a single apoprotein molecule (apo-B100) at one pole of the LDL molecule.

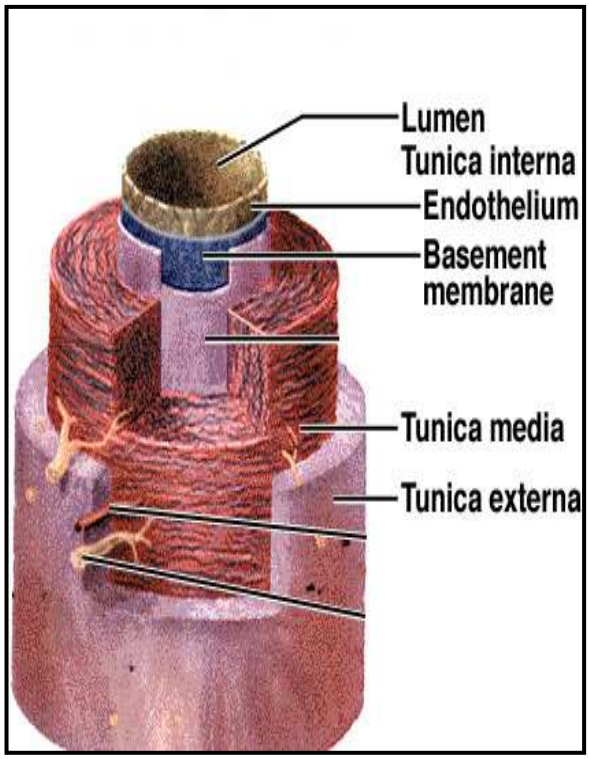

Figure 3: (www.bmb.psu.edu 2005) Generalized structure of the artery

This protein allows the recognition of the LDL molecule by the LDL receptors on the membranes of virtually all cells, such as endothelial cells, in the body (Guyton and Hall 1996). The walls of all arteries consist of three different layers, the intima, media and adventitia, as shown in figure 3. These layers surround a central blood-containing space called the lumen of these vessels (Marieb 1999; Libby 2001)**.** Lining the surface of the intima is the endothelium, which is a continuous monolayer of closely-fitting flat endothelial cells (EC) that also serves as a slick surface to minimize friction with blood

components as blood flows through the lumen. In fact, it is one of the only surfaces that can maintain blood in its liquid state over long contact times (Marieb 1999; Libby 2001).

Intercellular clefts of varying sizes and shapes exist between adjacent endothelial cells. The widths of these clefts have been found to be between 4 to 20 nm and consist of both tight and gap junctions (Bundgaard 1984; Huang, Jan et al. 1992). Some of these clefts appear linear and winding, while others are interdigitated, irregular and dumbbell-shaped (Huang, Jan et al. 1992).

The sub-endothelial region of the intima is mostly acellular, consisting of an extracellular matrix of collagen fibers, elastins and proteoglycans (Frank and Fogelman 1989; McGuire, Brocks et al. 1989). In the normal rat aorta, the thickness of the SI varies between 0.15μm and 0.6μm when subjected to physiological pressure conditions (Huang, Jan et al. 1998). This represents less than one percent of the thickness of the entire arterial wall (Huang, Rumschitzki et al. 1994). The outermost portion of the SI is separated from the media by an internal elastic lamina (IEL). The IEL contains numerous fenestrations or openings that contain proteoglycans and collagen fibers (Lindsay 1979).

The entry of large solutes into the vessel wall

The transendothelial transport pathway controversy to determine the major route or routes of macromolecular transport across the arterial endothelium has stimulated numerous experimental (Bratzler, Chisolm et al. 1977; Fry 1983; Lin, Jan et al. 1988; Lin, Jan et al. 1990) and theoretical studies (Fry 1985; Weinbaum, Tzeghai et al. 1985; Huang, Rumschitzki et al. 1994) over the decades. This noteworthy debate has aptly been captured by Rippe et al in their review article entitled “The Vesicle Controversy” (Rippe,

Rosengren et al. 2002). Ever since the discovery of "plasmalemma" vesicles by electron microscopy (Palade 1953), one belief that has taken prevalence is that the major route for macromolecular transendothelial transport is through these vesicles. It is termed "transcytosis" and it involves a type of "shuttling mechanism" of macromolecules from the luminal to abluminal regions of the endothelium. Proponents of this belief, such as Wagner et al, injected eel capillaries with electron dense macromolecular tracers at various times. They then performed three-dimensional continuous serial sectioning of the samples and reported that the tracers were found bound and confined to regions of the capillary wall at considerable distances away from intercellular junctions associations. As a result of this, they concluded that transcellular transport was the major route for macromolecular tracers used in their study (Wagner and Chen 1991). However, in their review, Rippe et al report that patches of tracer bounded to pericytes were also found and they were higher in concentration than those found in the plasmalemma vesicles. Rippe et al state that this indicates a transcellular tracer route such as could be found in a channel formed from fused plasmalemma vesicles (Rippe, Rosengren et al. 2002). On the other side of the coin, and the one whose extensive evidence has convinced us, is the importance of a paracellular route as a major transendothelial pathway. Investigators have for decades observed regional variations in the permeability of the arterial wall to macromolecules that were too large to pass through normal junctions (Majno, Palade et al. 1961; Packham, Rowsell et al. 1967; Bell, Adamson et al. 1974; Bell, Adamson et al. 1974; Sprague, Frankel et al. 1980). Based on these observations, Weinbaum et al formulated a mathematical "cell turnover hypothesis" model in an attempt to explain this phenomenon. They proposed that, during cell turnover, i.e., during cell mitosis and

apoptosis, cell junctions become temporarily widened and "leaky," providing a pathway for macromolecules to focally cross the endothelium; they proposed this as the major transendothelial route instead of via vesicles ferrying macromolecules across ECs. Although these junctions account for less than 10^{-5} of the *en face* endothelial surface area, the model predicts that these focal leaks enhance endothelial permeability by 50-100% in the larger, artheriosclerosis-prone arteries (Weinbaum, Tzeghai et al. 1985). The cell-turnover approach took a new look at an old problem and has since been the impetus for several subsequent experimental studies. Lin et al investigated macromolecular leakage in rat thoracic aortas by injecting rats with both the 6nm diameter Evan Blue Albumin (EBA) and the 22nm Lucifer Yellow Low Density Lipoprotein (LY-LDL) tracers. They allowed these tracers to circulate for three to five minutes before sacrificing the rats, excised and scanned their thoracic aortas and identified their dividing endothelial cells with hematoxylin stain. They found that although mitotic cells are very rare (1.4 in 10^4), 99% of these cells are associated with EBA leakage and 80% with (LY-LDL) conjugate leakage. These leaks however only account for 30% of all leakage found of EBA and 45% of LY-LDL (Lin, Jan et al. 1988; Lin, Jan et al. 1989). Chen et al also conducted similar permeability studies and found that when the smaller sized (4-5nm diameter) horseradish peroxidase (HRP) molecule was used, 90- 100% of all mitotic cells showed junctional leakage; however, these cells accounted for only between 3.9-8.6% of all leakages (Chen, Jan et al. 1997). Truskey et al. investigated the association of mitotic cells with macromolecular leakage in rabbit aorta. They found that 25% of all mitotic cells exhibited higher ^{125}I-LDL leakage and permeability than non-mitotic cells (Truskey, Roberts et al. 1992). Lin et al conducted similar experiments to account for

other non-mitotic-associated leakage. They found that although dead or dying cells are also infrequent (0.48% in 12 rats), 63% of them associate with EBA leakage (Lin, Jan et al. 1990). These independent studies not only support the cell turnover postulation but they also suggest that mitotic cell/macromolecular leakage association is species-independent.

Chuang et al conducted time-dependant studies of the growth of HRP and EBA leakage as a function of the circulation time after intravenous injection of these tracers. Both studies showed the same trend that, as time progressed, the observed tracer spot sizes increased rapidly. In the case of the HRP, these spots became steady ~250μm diameter at about 4 minutes (Chuang, Cheng et al. 1990). Both the speed of growth and the nearly steady spot size suggested the influence of a convective flux.

Transport models

These studies galvanized the search for mathematical models to explain macromolecular transport into the artery wall. Yuan et al. put forward for the first time a two-dimensional, convective-diffusive intimal transport model that proposed a non-uniform subendothelial pressure field resulting from the differences between the hydraulic conductance of the leaky and normal endothelial junctions. This model considered the SI as a separate region and, by doing so, looked at the unique role of the IEL in regulating the transport of macromolecules parallel to the endothelium after they had passed through the rare leaky junctions, some of which, as noted, are associated with dying or dead cells and those cells undergoing mitosis (Yuan, Chien et al. 1991). Previous one-dimensional models (Fry 1985; Fry 1987) only considered diffusion or diffusion coupled to convection only in a direction normal to the endothelial surface.

Because of its very small relative thickness (~0.1-0.6μm; less than 1% of the media thickness) to the media, it was impossible to experimentally measure the transport parameters such as the Darcy permeability (Kp) and hydraulic conductivity (Lp) of the SI. As such, Yuan et al took the SI and media to have equal parameters. This assumption resulted in the model grossly underestimating the early time rise seen in experiments. Huang et al.1994 subsequently overcame this obstacle by using the experimental observations of Frank and Fogelman and Nievelstein et al. These investigators used a rapid freeze etching technique without any chemical fixation followed by rotary shadow imaging to view with extraordinary details the three dimensional ultrastructure of the extracellular subendothelial proteoglycan and collagen matrix of both Wantanabe Heritable Hyperlipidemic (WHHL) and normal, cholesterol fed (10 days~ 3months) White New Zealand rabbits (Frank and Fogelman 1989; Nievelstein, Fogelman et al. 1991). Examination of these studies resulted in the astute observation that the ultrastructure of the intima and the media were vastly different (Huang, Rumschitzki et al. 1994). These observations were supported by the immunolocalization studies conducted by (Lark, Yeo et al. 1988) that showed that the media and intima have very different proteoglycan compositions. Using values obtained from Frank and Fogelman's work, Huang et al's constructed an *ab initio* theory for these unknown transport parameters and the results predicted that the Kp of the SI to was ~$10^{-12}$$cm^2$, two orders of magnitude larger than the measured Kp for the media (Vargas, Vargas et al. 1979). Their predicted values for the hydraulic conductivity were 40-75 times larger in the SI than in the media. Huang et al therefore concluded that the SI behaves as a sparse flexible matrix in which the glycoaminoglycan (GAG) chains offer little transport resistance to

tracer advection parallel to the endothelium away from the leaks. Their model, axisymetric in nature, along with these newly found – not fitted - SI parameters, was able to successfully predict the early time rise growth followed by the near plateau of the macromolecular tracer spot sizes observed by Chuang et al experimentally *in vivo* without the introduction of any adjustable (i.e., neither measured nor calculated *ab initio*) parameters. The model allows blood plasma to pass through both the normal and the leaky junctions of the endothelium of vessels. It advects macromolecules through the leaky junctions of the endothelium into arterial SI where they can bind to extracellular matrix to form extracellular lipid liposomes that can progress to form pre-atherosclerotic lesions. This fluid subsequently spreads parallel to the endothelium away from the leak in the SI before seeping through the fenestrae of the IEL and into the media. Water also passes through the normal junctions of the endothelium and, interestingly, this flow, in aggregate far larger than the flow through the rare leaky junctions, dilutes the local LDL concentration of the subendothelial intima and flushes unbound SI LDL into the media. Clearly plasma (or water) transport is critical in modulating the macromolecular transport of LDL cholesterol from the blood into the arterial wall and the investigation of convective fluid transport is central to the greater understanding of the pre-arteriosclerotic processes. Such pressure-driven transport should increase with transmural pressure, but pressure induced ultrastructural changes in the wall /intimal structure can diminish their effects since they can dramatically increase wall resistance to such flow.

Hydraulic conductivity

Investigations conducted by Ernest Henry Starling in 1896 on transmembrane convective flow in biological system are considered the earliest work of significance in the area of water flow through biological tissue. He looked at the effect of hydrostatic or osmotic pressure difference on fluid flow across membranes in micro-vessels (Michel 1997). He found that the rate of fluid flow across the micro-vessel wall was proportional to the hydrostatic pressure difference ΔP minus the osmotic pressure difference ΔΠ, or

$$\mathbf{J_V = LpS\ (\Delta P - \Delta \Pi\ )} \quad \text{(Trusky 2004)} \qquad \mathbf{(1)}$$

where Jv is the fluid volume flow rate, **S** is the surface area of the endothelium and **Lp** (the ratio of the transmural flux to pressure difference) is the hydraulic conductivity of the vessel wall. Equation 1 is called the *Starling's law of fluid filtration*; it serves as the definition of Lp and the basis of its measurement.

Physiologically, hydrostatic pressure pushes fluid out of the capillary. It is highest at the arteriolar end and lowest at the venular end of the capillary. The hydrostatic pressure difference is counterbalanced by an "*oncotic pressure"* difference caused by variations in protein concentration in the blood of these micro-vessels and in the *interstitial* space surrounding them. A higher protein concentration tends to draw water across the membrane to dilute it. Physiologically, a net pressure difference exists to produce a flow of fluid from the arterial capillaries into the tissue. Basically, this fluid movement enhances the convective transport of macromolecules that enter the interstitial space when those molecules are small enough to get through the micro-vessel's wall (Trusky 2004). Starling's law can accurately predict the flux of fluid based on the pressure and osmotic

differences across the membrane and the hydraulic conductivity for membranes with macroscopically uniform structures. The capillary wall can be treated as a membrane because its thickness is one order of magnitude smaller than the circumference of the vessel. However it is still non-uniform having at least three barriers to fluid transport: the glycocalyx, the endothelium, and basement membrane (Marieb 1999; Tarbell 2003).

Starling's law also has its limitations when it is used to analyze fluid flow across biological membranes. The structure of the endothelium is non-uniform, containing endothelial cells, endothelial clefts and junctional proteins. As a result, if this non-uniformity is not taken into consideration, it can lead to inconsistencies between experimental data and the predictions offered by this law. For example (Michel and Phillips 1987) did transient perfusion studies on single frog mesenteric micro-vessels and observed brief reabsorption for 15-30 seconds from the tissue to the blood vessel when the capillary pressure was dropped below the osmotic pressure across the capillary wall. Beyond 2-5 minutes however, only a small filtration from the blood vessel to the tissue was seen. The model therefore safely predicted the transient 15-30 seconds aspect of the experiment but failed in the steady state 2-5 minute period. Another limitation of Starling's law is its inability to accurately predict the hydraulic conductivity when the walls of micro-vessels are permeable or semi-permeable to those solutes such as albumin and fibrinogen that contribute significantly to the maintenance of the osmotic pressure difference across the micro-vessel wall. Kedem and Katchalsky conducted studies based on irreversible thermodynamics and demonstrated that when this happens, one must modify this law must to include an *osmotic reflection coefficient* σ_S. The modified Starling's law of filtration now becomes

$$\mathbf{Jv = LpS\ (\Delta P - \sigma_S \Delta \Pi)} \qquad \mathbf{(2)}$$

The value of σ_S varies between zero and unity, with typical values between 0.7 and 0.9 for plasma proteins. When σ_S is equal to unity, the vessel wall is impermeable to the solute. If the solute permeability of the micro-vessel is extremely high, σ_S approaches zero (Marieb 1999; Tarbell 2003).

Several different experimental techniques to measure Lp of large vessels have been developed by different authors. Tedgui and Lever looked at the effects of luminal pressure and endothelial removal on the fluid filtration across the thoracic aortas of male New Zealand white rabbits (2.0-2.5kg) *ex vivo* at conditions where **ΔΠ**was zero. They excised these blood vessels in such a way as to prevent vessel shortening and depressurization, filled them with 4% albumin-Tyrode solution and measured the Lp at two different controlled pressures. They found Lp values (mean ± SD) for the rabbit thoracic aorta were $4\pm1.31 * 10^{-8}$ and $2.44\pm0.80 * 10^{-8}$ cm/sec.mmHg at 70 and 180 mmHg respectively, for the total wall with intact endothelium and $5.36\pm1.62*10^{-8}$ and $5.27\pm0.84 * 10^{-8}$ cm.sec.mmHg at 70 and 180 mmHg respectively for the total wall with denuded endothelium, as shown in table 1. They concluded that the hydraulic conductivity of the intact total wall exhibited a pressure-dependence at these two pressures, whereas for the damaged wall this dependence did not appear to exist (Tedgui and Lever 1984).

Pressure (mmHg)	Hydraulic conductivity * 10^8 (cm/sec. mmHg)	
	Intact Vessel	Endothelium denuded
70	4.00±1.31	5.36±1.62
180	2.44±0.80	5.27±0.84

Table1. **(Tedgui and Lever 1984)** Hydraulic conductivities measured with and without endothelium in rabbit aortas

Tedgui and Lever's data, as shown in table 1, imply that Lp might be a function of the distension of the vessel caused by the perfusion pressure in the vessel's lumen, beyond its area inclusion in the calculation of the flux. However, because they did not use the same rabbit aorta for Lp measurements at the two control pressures, Balwin et al suggested that one could not draw a definite inference. Baldwin, Wilson et al (1992) then adapted Tedgui and Lever's technique and conducted similar ex-vivo experiments to measure the Lp, but this time doing measurements at all pressures of interest, both with intact and then with denuded endothelium, on the each aorta. They studied two groups of the same strain of male New Zealand white rabbits (2.0-2.5kg) as Tedgui et al, at five different transmural pressures to determine whether Lp is influenced by vascular strain and hence by mechanical strain.

Balwin et al found that that the Lp values (mean± SD) at 50,100 and 150 mmHg from group 1 rabbits were 3.8± 2.8*10^{-8}, 3.5± 1.3*10^{-8} and 4.1± 1.1*10^{-8} cm/sec.mmHg, while group 2 rabbits gave values of 4.2± 1.6*10^{-8}, 3.8± 1.1*10^{-8}, 3.8± 1.1*10^{-8}, 4.2± 1.1*10^{-8} cm/sec. mmHg at pressures of 75,100,125 and 150mmHg respectively as shown in table 2.

Pressure (mmHg)	Hydraulic conductivity * 10^8 (cm/sec. mmHg)	
	Group1	Group 2
50	3.8± 2.8	
75		4.2± 1.6
100	3.5± 1.3	3.8± 1.1
125		3.8± 1.1
150	4.1 ±1.1	4.2± 1.1

Table 2.**(Baldwin, Wilson et al. 1992)** Hydraulic conductivities measured with and without endothelium in rabbit aortas

Annie Yixin Shou in our group adapted and modified Baldwin et al's method to measure the hydraulic conductivities of aortas from far smaller male Sprague- Dawley rats. These results are shown in figure 4, and are compared with the results obtained by Tedgui and Lever on rabbit aortas.

Interestingly, her results agree quantitatively with Tedgui and Lever (1984) and qualitatively with Baldwin and Wilson (1992). All three of these Lp studies show similar trends, that is, Lp decreases rapidly by about ~40% as the pressure increases from 50 to 80 mmHg. They then remain constant as the pressure is increased to 180 mmHg. When the endothelium is removed, the Lp values increase overall by about a factor of two and the Lp appears to be independent of the transmural pressure drop (Shou, Jan et al. 2006). Huang, Rumschitzki et al (1997) proposed a new hypothesis and mathematical model to explain these similar trends found in Tedgui and Lever's (1984) and Baldwin and Wilson's (1992) *ex vivo* rabbit aorta studies.

They suggested that, because the SI is much less dense than the media, it compresses far more easily under transmural-pressure load than the media, leading to large depressions in the vicinity of the fenestral pores of the IEL that can occlude or partially occlude them. This proposal was based on the ultrastructural observations of Frank and Fogelman (1988) and the *ab initio* calculations of intimal permeability done by Huang et al (1994). The purported differences in the matrix structure were also supported by immunulocalization studies. These studies showed that the proteoglycan structure in the SI is conspicuously different from that in the media. In fact, the matrix in the fenestral

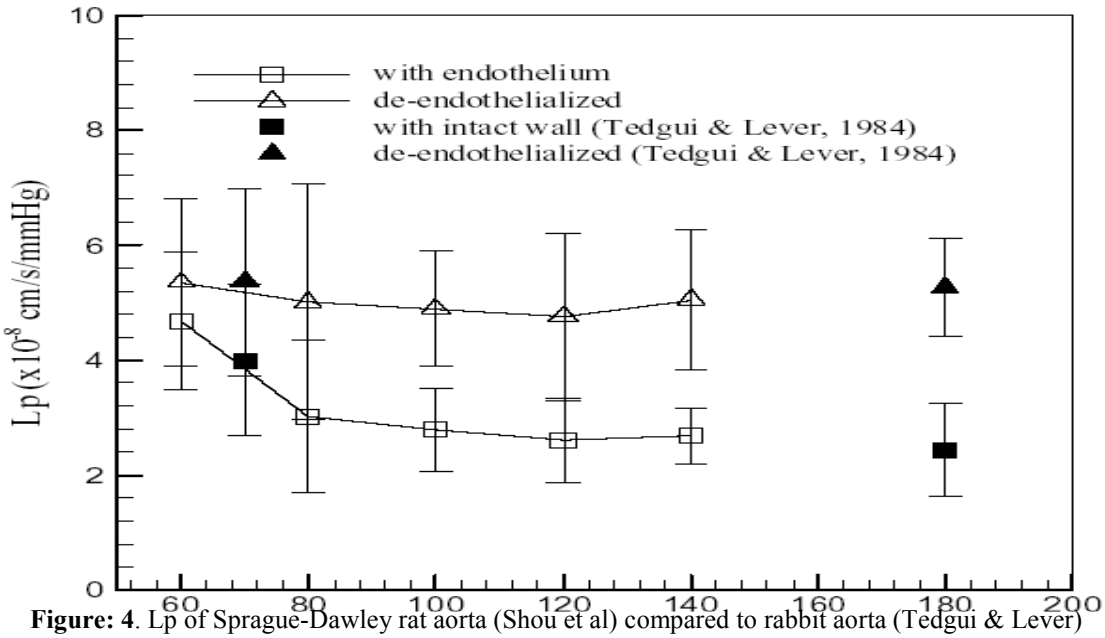

Figure: 4. Lp of Sprague-Dawley rat aorta (Shou et al) compared to rabbit aorta (Tedgui & Lever)

pores of the IEL appears to be just a continuation of the SI matrix (Wight and Hascall 1983; Lark, Yeo et al. 1988). They predicted that at lower pressures of ~50mmHg, just below the physiological range, the intima is relaxed and hardly compressed; because of its sparse nature, it presents very little hydraulic resistance to fluid flow. At higher pressures however, they claim, the endothelium compresses the SI up to its maximal values, which is determined by the stiffness of the SI extracellular matrix's (ECM)

collagen fibers. This compression increases the fiber density and decreases the Kp of the SI. More importantly, it can possibly lead to the blocking of the fenestral pores, which can cause significant changes in the flow through them and, therefore, across the wall of the vessel. They also hypothesized that, beyond this maximal compaction, there is little change in SI thickness with increase in pressure. When the endothelium, a major layer of flow resistance due in part to its ability to block IEL fenestrae, is removed however, and only the dense media remains, the Lp of the total wall almost doubles. Moreover, there no longer being an agent that can block IEL fenestrae, Lp becomes independent of pressure. We can therefore see that the endothelium, by virtue of its Lp and its ability to occlude IEL fenestrae accounts for a major portion of the hydraulic conductivity of the whole wall.

We have seen that transendothelial water transport is central to LDL transport from the blood into the wall of artherosclerosis-prone arteries. It has also been accepted that this fluid flows through normal and leaky junctions. However studies conducted over the twenty years have left some intriguing possibilities of other pathways across the endothelium for water passage.

Aquaporins

During the last two decades, Agre and coworkers, while attempting to isolate a 32kDa Rhesus (Rh) polypeptide from erythrocytes, also identified, purified and partially characterized an abundant 28kDa novel integral membrane protein. They subsequently isolated this 28kDa protein from the renal tubules of kidneys. This 28kDa protein was

mistakenly believed to be a breakdown product of a larger 32kDa molecular weight protein. (Agre, Saboori et al. 1987; Denker, Smith et al. 1988; Saboori, Smith et al. 1988). It was later named CHIP28 (channel –like integral membrane protein of 28Kda) (Preston and Agre 1991) but subsequently called aquaporin-1 (AQP1). Subsequent structural characterization studies done found that CHIP28 was related to the major intrinsic protein from bovine lenses (MIP26), presently known as Aquaporin-0 (AQP0), a channel that allows lens fibers to absorb interstitial fluid. Subsequently CHIP28 were expressed in oocytes from *Xenopus laevis* and their osmotic permeabilities measured to test whether they were indeed water channels (Preston, Carroll et al. 1992).

Since the initial discovery of AQP1, an entire family of aquaporins (AQP0-12) has since been identified and characterized in numerous diverse tissues in animals such as the testes, brains, kidneys, eyes, salivary and tear glands and plants. (Connolly, Shanahan et al. 1998; Ishibashi, Kuwahara et al. 1998; Koyama, Ishibashi et al. 1998; Yasui, Kwon et al. 1999; Hatakeyama, Yoshida et al. 2001; Itoh, Rai et al. 2005; Morishita, Matsuzaki et al. 2005).

Channel proteins can be characterized by their rates of permeation and selectivity. Aquaporins increases the water permeation of plasma membranes by lowering their activation energy from 10-20 kcal/mol to less than 5 kcal/mol. This allows the channels to maintain a high water flux (~10^9 water molecules s^{-1}channel^{-1}) when they are subjected to transmembrane osmotic pressure differences (Heymann and Engel 1999) Aquaporins are highly specific for water transport and prevent nearly all other small molecules, solutes and ions such as hydroxide (OH^-) ions, ammonia (NH_3) and urea,

from crossing the membrane. Protons (H^+) however present a particularly difficult challenge for a water channel because of their positive charge. As such, they can move along a column of water by hydrogen bond exchange; however, aquaporins succeed in preventing even the passage of individual protons (Zeidel, Nielsen et al. 1994; Agre, Lee et al. 1997). It has been suggested that aquaporin-1 is selective even to protons because of its strongly charged entrances that act as an electrostatic filter. Or, this selectivity may arise because of steric hindrances caused when H^+ associates with a molecule of water to form H_3O^+, which is too large to fit through the channel neck (diameter ~2.8 Å), just large enough for the passage of a single water molecule (Heymann and Engel 1999).

Submillimolar concentrations of Hg^{2+} are known to pharmacologically inhibit water channels. Agre and coworkers found that 1mM mercuric chloride ($HgCl_2$) inhibited the osmotic permeability of proteoliposomes reconstituted with purified aquaporin-1

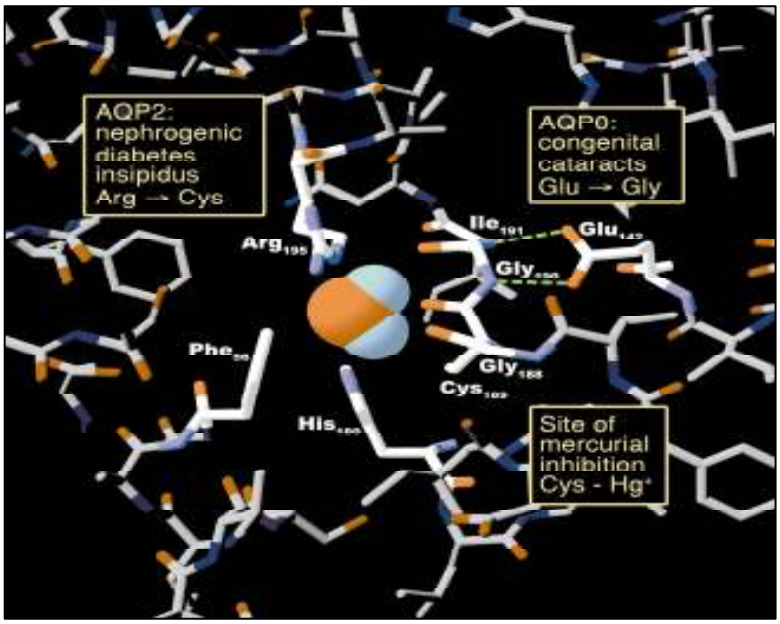

Figure 5: (Kozono, Yasui et al. 2002) Human disease mutation and pharmacologically active sites projected onto an atomic model of and AQP1 pore at the narrowest constriction point (transverse section). The model is based on Protein Data Bank coordinates 1H61 of human red cell AQP1. The side chains of three residues (Arg-195, His –180 and Phe-56) plus the backbone carbonyl groups of two residues (Gly-188 and Cys-189) line the pore. The side chain of Cys-189 lies proximal to the pore. Binding of a mercuric ion to the sulfhydryl group of this residue inhibits the water permeability of AQP1.

by 87%. Other mercurial agents such as fluorescein mercuric acetate (FMA), p(chloromercuri) benzenesulfonate also showed similar inhibition but to varying degrees as shown in table 3. *2*-mercaptoethanol however rapidly reverses this inhibition (Zeidel, Nielsen et al. 1994). Site- directed mutagenesis subsequently confirmed that four cystenes (87,102,152 and 189) are sensitive to Hg^{2}+ as shown in figure 5 (Preston, Jung et al. 1993). 2- mercaptoethanol however reduces the cistene-Hg^{++} bond.

The structure of bovine AQP1 (bAQP1), which has a high degree of sequence homology to human AQP1 (hAQP1), was solved by X-ray crystallography to 2.2Å resolution. The basic unit of AQP1 is a tetramer with each monomer providing an independent water pore and having a dumbbell-like shape when viewed along its axis, as shown in figure 6. The pore's structure consists of an extracellular vestibule, a selectivity filter and a cytoplasmic vestibule.

Inhibitor	% decrease in RBC Pf	%decrease in CHIP Pf
1mM $HgCl_2$	87± 6	90
1mM pCMBS	90	83± 8
0.5 mM FMA	45-50	70± 6
$HgCl_2$ + NEM	90	79± 5
$HgCl_2$+*B*-ME	0	30± 9

Table3: Effect of different blockers on water inhibition of red blood cells and CHIP-28

The extracellular vestibule is conical in shape, has a 15 Å mouth diameter and is 20 Å in length. It tapers down to 2.8 Å to form the constriction region. This very narrow region

begins the 20 Å long selectivity filter that ends in the 20 Å long cytoplasmic vestibule that also has a 15 Å mouth, as shown in figure7 (Sui, Han et al. 2001).

Hydropathy analysis allows one to measure the hydrophobic nature of amino acids. It is useful for studying the secondary structure from the primary sequence of a protein (Kyte and Doolittle 1982; Cherry and Ragan 1986). Hydropathy analysis done on the polypeptide chain of AQP1 predicts highly hydrophobic regions spanning the plasma membrane bilayer six times. Further studies show that both the N and C termini of the protein are cytoplasmic. This therefore suggests that a potential model would have three of the five connecting loops (loops A, C and E) to be intracellular and the other two to be extracellular (loops B and D), as shown in figure 8 (Preston and Agre 1991).

The selectivity filter is highly hydrophobic. However there are hydrophilic nodes that allows a pathway for mediating rapid water transport (Sui, Han et al. 2001). Experimental transport studies have been done by Agre and coworkers using purified human red blood cell AQP1 embedded in proteoliposomes of a defined lipid composition. Osmotic water permeabilities (P_F) were then measured by exposing the proteoliposomes to an osmotic gradient at zero transmural pressure difference in a stopped flow fluorometer. The calculated AQP1 conductance (P_F) was found to be $4.7*10^{-13}$ cm^3/sec per AQP1 tetramer. (Zeidel, Ambudkar et al. 1992).

Pressure-induced water transport studies by molecular dynamics were also conducted on AQP1. Such calculations are quite tricky and subject to interpretation. It was found that the osmotic water permeability for one set of experiments was

$1.16\pm0.4*10^{-12}$ cm^3/ per AQP1 tetramer and $5.6\pm 0.1*10^{-13}$ cm^3/sec per AQP1 tetramer for the second set of experiments

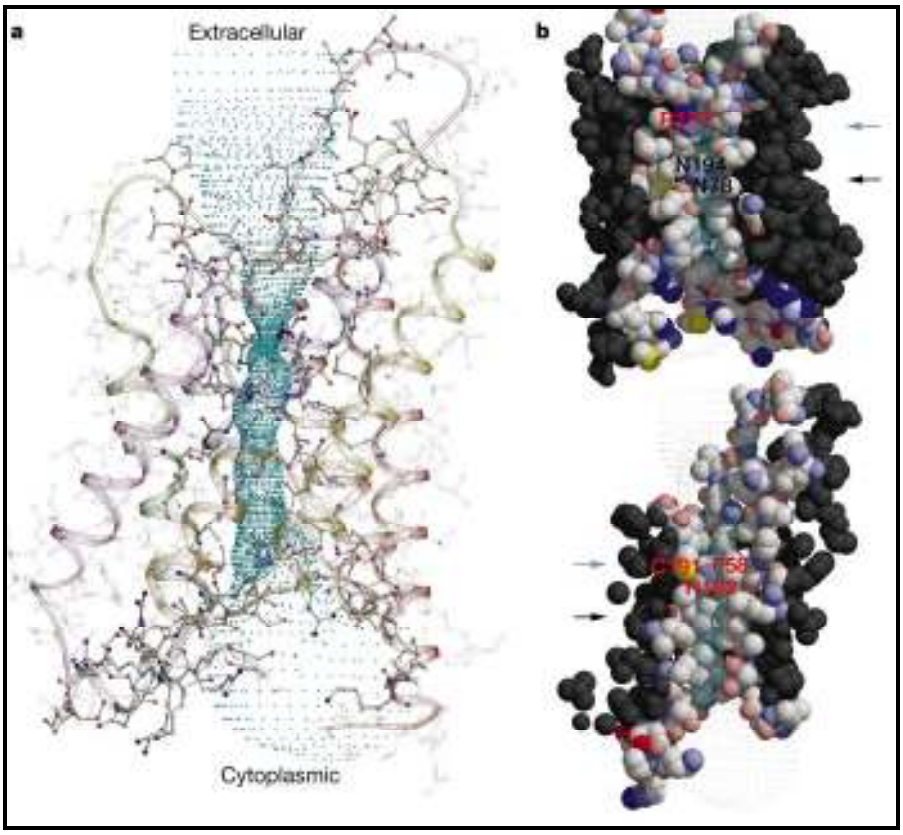

Figure6: (Sui, Han et al. 2001) Side view of AQP1. a, backbone in ribbon format, residues depicted in ball and stick representation; residues lining the pore are shown in opaque colors. The pore profile is highlighted by an array of blue dots generated by the program HOLE. The constriction region is visible as the pinched-in area in the extracellular half of the profile. **b,** Side-view cutaway of a space filling model. Residues not in direct contact with the pore are dark grey. The pore lining in the top figure consists primarily of polar groups distributed along the length of the selectivity filter; the complementary half is predominantly hydrophobic in nature. The constriction region and pseudo two fold axis (centered about the NPA motifs) are indicated by blue and black arrows respectively. The pore profile (blue dots) is superimposed on each channel half. The figure was produced using MOLSCRIPT and Raster.

Using the conversion factor derived from the Van't Hoff's equation

$$\mathbf{P_f = (RT/V_W)L_p} \quad \textbf{(Zhu, Tajkhorshid et al. 2002)} \qquad \textbf{(3)}$$

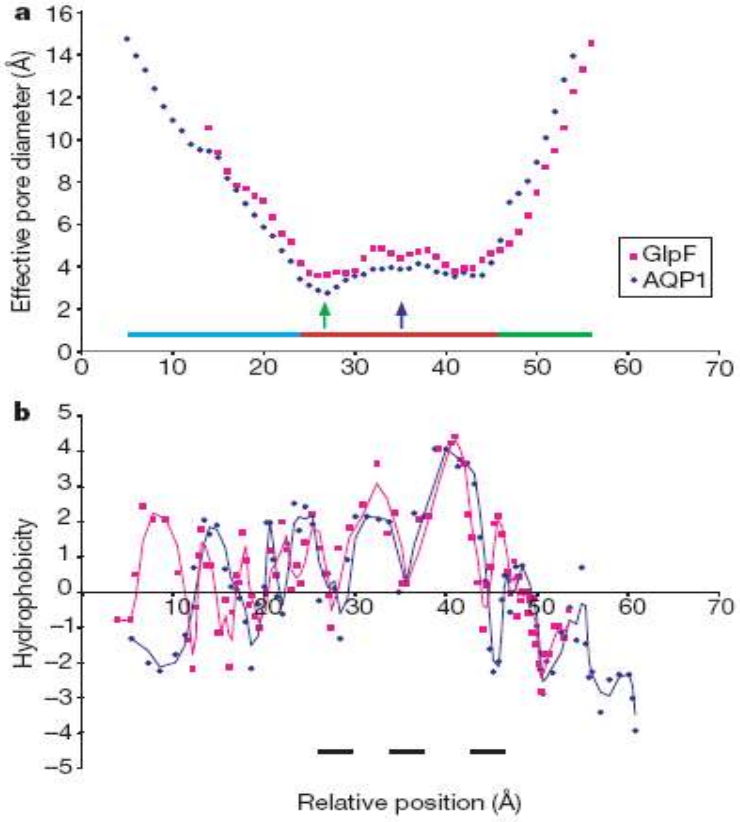

Figure 7: (Sui, Han et al. 2001) The effective pore diameter (a) and hydrophobicity (b) of the AQP1 and GlpF channels. Green and dark blue arrows indicate the locations of the constriction region and pseudo-two –fold axis respectively. Below these arrows a light blue bar indicates the location of the vestibule, a red bar the selectivity filter and a green bar, the cytoplasmic vestibule. The three black bars in the hydropathy profile identify hydrophilic nodes within the selectivity filter. Pore diameters were determined with AMBER-based van der Waals radii and analysed using the program HOLE. Hydrophobicity was characterized using the Kyte and Doolittle amino-acid hydropathy scale and a four point averaging window across the pore-lining residues.

where R is the gas constant and T is the absolute temperature, the hydraulic conductivity Lp was found to be, respectively, 8.0± 0.3*10^{-17} cm^5/ N.sec per AQP1tetramer and 3.8± 0.7*10^{-17} cm^5/ N.sec per unit AQP1 tetramer (Zhu, Tajkhorshid et al. 2002)

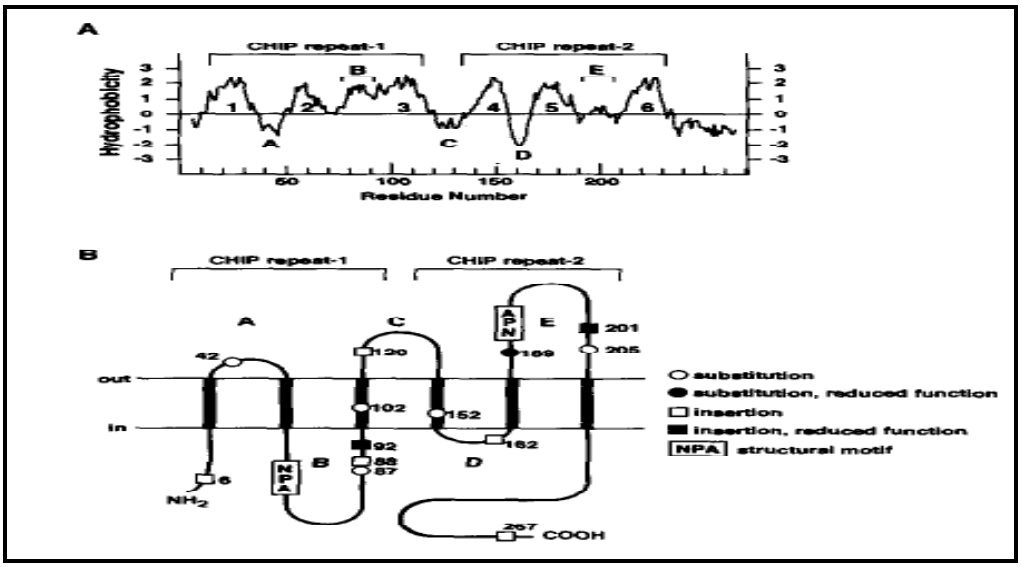

Figure8: ((Jung, Preston et al. 1994) Tandem repeat within NH_2- and COOH- terminal halves of Aquaporin CHIP. a, hydropathy of deduced CHIP amino acid sequence as analyzed by the algorithm of Kyte and Doolitle with a 7-residue window. b, deduced membrane topology of CHIP revealing locations and functional and functional P_f of site-directed mutants; single residue substitutions;1-or 2 residue insertions. Extracellular (out) and cytoplasmic(in) surfaces of the lipid bilayer are noted

Until now, arterial endothelial permeability to water has been ascribed to junctional and possibly vesicular transport (Kao, Chen et al. 1994). In chapter two, we identify and show the existence of AQP1 in/on the endothelial cells of rat aorta using immunohistochemistry and confocal microscopy. Our general goal, however, is to investigate whether aquaporins play any role in transendothelial transport. This work was done simultaneously with and complements the work done by my (former) fellow PhD students, Drs. Annie Yixin Shou, Tieuvi Nguyen and Stewart Russell in our lab, who demonstrated the suppression of the hydraulic conductivity of both bovine aortic endothelial cell monolayers and of whole, intact rat aorta *ex vivo* by treatment with very low doses (chosen to avoid artifacts due to mercury toxicity, etc.) of $HgCl_2$, or, in the monolayer case, by siRNA knockdown of AQP1 expression. We detail this work below.

Hypertension is a known risk factor for atherosclerosis. It is therefore conceivable to believe that the higher the transmural pressure, the greater the convective macromolecular transendothelial transport. Whereas it is well-known that chronic hypertension leads, over a period of many months, to medial thickening and therefore likely to a lowering of the overall conductivity of the arterial media, we suspect that, if aquaporin-1 indeed plays a significant role in determining vessel wall hydraulic conductivity, then vessels may be able to actively regulate their aquaporin-1 expression far more rapidly in response to chronic hypertensive conditions. Such a regulation may allow them to actively influence their homeostatic transmural transport processes, both in the short and longer terms. In chapter three we use quantitative immunohistochemistry to detect the presence, distribution and to quantify and compare the endothelial AQP1 in both genetically modified normotensive Wistar Kyoto rats (WKY) and their hypertensive Spontaneous Hypertensive (SHR) cousins. In chapter four, in order to eliminate the possibility that chapter three's observed aquaporin expression differences were due to genetic differences between the two strains of rats, we repeat these quantitative immunohistochemistry studies using instead normotensive Sprague Dawley (SD) rats and SDs rendered hypertensive by the well-known Goldblatt procedure. In chapter five, we attempt to model our results obtained in chapter four using a simple deterministic kinetic model. The results of this study will hopefully lead to improved understanding which may direct us to novel therapies for not only atheriosclerosis but for a wide range of diseases.

CHAPTER 2: IMMUNOCYTOCHEMICAL LOCALIZATION AND DISTRIBUTION OF AQP1 AND AQP1 FUNCTIONALITY: STUDIES ON BOVINE AORTIC ENDOTHELIAL CELL MONOLAYERS AND ON RAT AORTIC ENDOTHELIAL CELLS IN WHOLE VESSELS EX VIVO

I. INTRODUCTION

As detailed in the introduction, several noteworthy experimental investigations have shown that pressure-driven convective water flux plays a central role in the transmural transport of macromolecules (Duncan, Cornfield et al. 1962; Tedgui and Lever 1985; Tedgui and Lever 1987). This transmural pressure difference, typically on the order of ~100 mmHg across large artery walls, drives a flow of plasma, consisting of mostly water and small solutes, that advects solutes across these vessels from the blood in the lumen into and through the tissue. This transport method, in conjunction with transport from the *vasa vasorum* in large, thick-walled arteries, allows for the provision of nutrients to medial cells. However, this process also sweeps harmful solutes such as low-density lipoproteins (LDL), across the endothelium in regions where there are focal gaps between endothelial cells that are large enough to allow passage of such large molecules. The LDL then enters the subendothelial intima (SI) where it can accumulate and bind to the subendothelial extracellular matrix (ECM), leading to pre-atherosclerotic lesions (Guyton and Hall 1996) There is not yet general agreement on the mechanisms whereby LDL cholesterol is transported across the endothelium and this has given birth to competing theories – vesicle transport through ECs, transport across denuded regions or transport through rare inter EC junctions that are temporarily widened – theories that have been discussed over several decades (Rippe, Rosengren et al. 2002). This

controversy has stimulated several experimental (Bratzler, Chisolm et al. 1977; Fry 1983; Lin, Jan et al. 1988; Lin, Jan et al. 1990) and theoretical studies (Fry 1985; Weinbaum, Tzeghai et al. 1985; Huang, Rumschitzki et al. 1994). One sticking point for the denuded regions theory has been the overwhelming evidence that showed that the endothelial monolayer is continuous except for areas where lesions are already present (Schwartz 1980; Schwartz, Gajdusek et al. 1980; Schwartz, Gajdusek et al. 1981). The fact remains that the EC membrane normally has tight interendothelial cell junctions (~4-7nm width) (Leach, Lammiman et al. 2000; Karakotchian and Fraser 2007). However, blood-borne LDL particles, which are ~22nm in diameter, are apparently still able to traverse this boundary and for decades investigators have observed regional variations in the permeability of the arterial wall to such macromolecules that are too large to pass through normal junctions. Extensive corroborative evidence reveals that the paracellular transport routes between endothelial cells (EC) junctions act as a major transendothelial pathway for such molecules (Majno, Palade et al. 1961; Packham, Rowsell et al. 1967; Bell, Adamson et al. 1974; Bell, Adamson et al. 1974; Sprague, Frankel et al. 1980). Based on these observations, Weinbaum et al formulated a mathematical model based on a "leaky junction/ cell turnover hypothesis" in an attempt to explain this phenomenon. They proposed that, during cell turnover, i.e., cell mitosis and apoptosis, rare cell junctions become temporarily widened and "leaky" providing a pathway for macromolecules to focally cross the endothelium . Although these junctions account for less than 10^{-5} of the *en face* area of the endothelium, the model predicts they could increase endothelial permeability by 50-100% in the larger artheriosclerotic prone arteries (Weinbaum, Tzeghai et al. 1985)

The cell-turnover approach took a new look at an old problem and has since been the impetus for several subsequent experimental studies. Lin et al investigated macromolecular leakage in rat thoracic aortas by injecting rats with both 6μm Evan Blue Albumin (EBA) and 22μm Lucifer Yellow Low Density Lipoprotein (LY-LDL) preparations, allowing these tracers to circulate for three to five minutes before sacrificing the rats. Their thoracic aortas were then excised and scanned and the dividing cells identified by hematoxylin staining. They found that, although mitotic endothelial cells are very rare (~1.4 in 10^4 cells), 99% of these cells were associated with EBA leakage and 80% with (LY-LDL) conjugate leakage. These leaks, however, only account for 30% of all leakage found for EBA and 45% for LY-LDL (Lin,

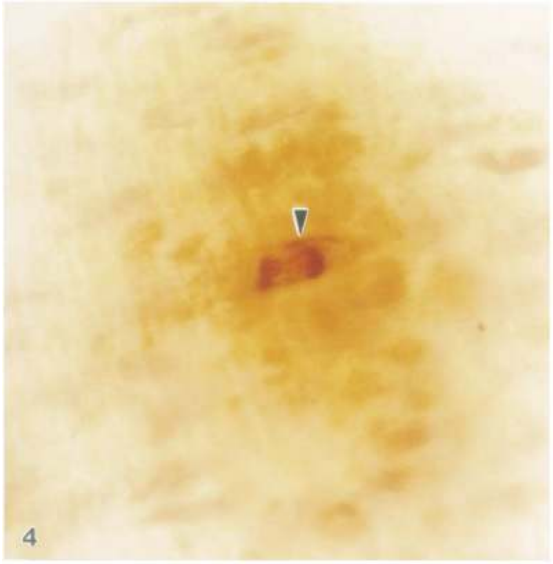

Figure 1: Light micrograph of an en face preparation of aortic endothelium with hematoxylin staining at 3 min after HRP injection showing association of HRP with mitotic endothelial cell (arrowhead) in anaphase. x2200 (Chen, Jan et al. 1997)

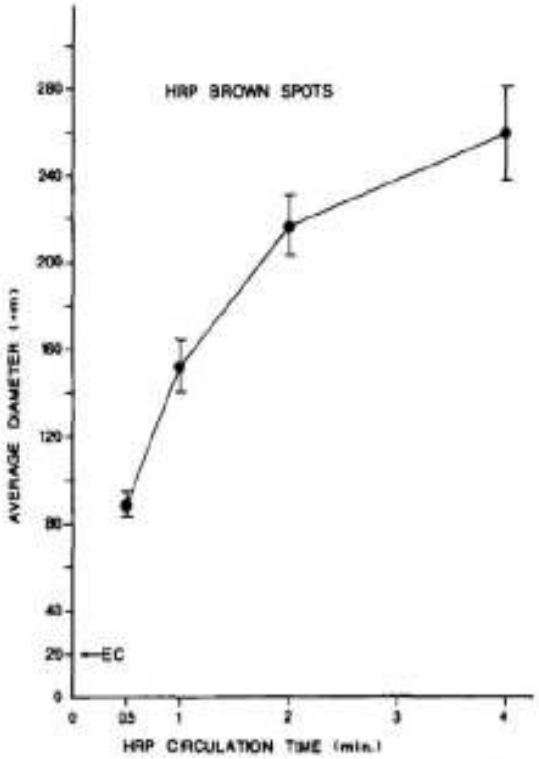

Figure 2: The average diameter of the HRP brown spots measured on an enface preparation of rat thoracic aorta at various HRP circulation time (Chuang, Cheng et al. 1990)

Jan et al. 1988; Lin, Jan et al. 1989). Chen et al also conducted similar permeability studies and found that, when the smaller sized (4-5μm) horseradish peroxidase (HRP) molecule was used, 90-100% of all mitotic cells showed junctional leakage, as shown in figure1; however, these cells only accounted for between 3.9-8.6% of all leaks (Chen, Jan et al. 1997). Truskey et al. also investigated the association of mitotic cells with macromolecular leakage in rabbit aorta. They found that 25% of all mitotic cells exhibited higher ^{125}I-LDL leakage and permeability than non-mitotic cells (Truskey, Roberts et al. 1992). Since these studies demonstrated that dividing cells do not account for all leaks, Lin et al conducted similar experiments to account for non-mitotic leakage. They found that, although dead or dying endothelial cells are also infrequent (0.48% in 12 rats), 63% of them are associated with EBA leakage (Lin, Jan et al. 1990). These independent studies not only support the cell turnover postulation but also suggest that mitotic cell/macromolecular leakage association may be species independent.

Chuang et al conducted time dependent studies of the growth of both HRP and EBA leakages as a function of the circulation time of these tracers in rats after intravenous injection. For both tracers, they found that the tracer spot sizes grew rapidly with circulation time. For HRP, the spot diameters became nearly steady at ~250μm at about 4 minutes. This rapid growth and the achievement of a nearly steady spot radius suggest that convective tracer movement plays a strong role in tracer spot growth; see figure2 (Chuang, Cheng et al. 1990).

Until now, it has been natural to ascribe arterial endothelial water permeability to junctional transport (Kao, Chen et al. 1994). However fascinating this may be, one cannot

help but wonder if other important pathways exist. During the last two decades, Agre and coworkers while attempting to isolate a 32kDa Rhesus (RH) polypeptide from erythrocytes also identified, purified and partially characterized an abundant 28kDa novel integral membrane protein. They subsequently also isolated this 28kDa protein from the renal tubules of kidneys. This 28kDa protein was mistakenly believed to be a breakdown product of a 32kDa protein. (Agre, Saboori et al. 1987; Denker, Smith et al. 1988; Saboori, Smith et al. 1988). This 28kDa protein was later named CHIP28 (channel –like integral membrane protein of 28KDa) (Preston and Agre 1991) but subsequently called aquaporin-1 (AQP1). Structural characterization studies found that CHIP28 was related to the major intrinsic protein from bovine lens (MIP26), presently known as Aquaporin-0 (AQP0), a channel that allows lens fibers to absorb interstitial fluid. Studies were subsequently conducted on CHIP28 by expressing them in oocytes from *Xenopus laevis* and measuring their osmotic permeabilities. These proteins were found to function as water channels, which were reversibly inhibited by mercury chloride ($HgCl_2$), a known inhibitor of water channels (Preston, Carroll et al. 1992).

Since their discovery, an entire family of aquaporins (AQP0-12) has also been identified and characterized in several diverse tissues such as the testes, brains, kidneys, eyes, salivary and tear glands in animals and in plants. (Brown, Katsura et al. 1995; Ishibashi, Kuwahara et al. 1997; Connolly, Shanahan et al. 1998; Ishibashi, Kuwahara et al. 1998; Koyama, Ishibashi et al. 1998; Yasui, Kwon et al. 1999; Hatakeyama, Yoshida et al. 2001; Itoh, Rai et al. 2005; Morishita, Matsuzaki et al. 2005).

Let us recap. AQP1 are found to be expressed in various systemic organs and also play an obvious role in their permeability to water. Convective fluid flow across the

endothelium of large arteries is critical for both the influx and efflux of transendothelial lipid transport. This transport, in turn has been implicated in the earliest events of artherogenesis. It is therefore natural to ask what role, if any, aquaporins may play in this type of fluid transport across large arteries.

Our general goal in this thesis is to investigate whether aquaporins play any role in this type of transendothelial fluid transport and how their expression is affected by chronic hypertension, a known risk factor of atherosclerosis. In particular, we are firstly interested in knowing whether the rat aorta's endothelium expresses AQP1. Immunohistochemistry and confocal microscopy will be used to address this concern.

II. MATERIALS and METHODS

Cell Culture *(performed by Stewart Russell, Ph.D., a fellow researcher in our lab).* Bovine aortic endothelial cells (BAECs) from passage 4 through 7, obtained from VEC Technologies (Rensselaer, NY, USA) were plated at an initial concentration of 32,000 cells per cm^2 on 12-well filters (Corning 3460) that had previously been treated for 1 hour with fibronectin. Subsequently the cells were cultured in Minimum Essential Medium containing 10% fetal bovine serum, 100U/ml penicillin-streptomycin and 2.5μg/ml L-glutamine. Filters were maintained in an incubator at 37^oC and 5% CO_2 and 95% air for 3 days until confluent. The polyester membranes of the 12-well filters were then removed and placed on Superfrost Plus slides (Fisher Scientific, Pittsburgh, PA).

Aortic Tissue Preparation

Male Sprague –Dawley rats weighing between 250-300g were anesthetized with sodium pentobarbital (Abbot Laboratories, North Chicago, IL; 30mg/100g i.v.). The left femoral vein was located and cannulated with PE50 polyethylene tubing attached to two syringes, one containing excess sodium pentobarbital and the other containing 0.3 ml of heparin (5000USP unit/ml; China Chemical &Pharmaceutical, Tapei, R.O.C). The carotid artery was also cannulated with PE50 polyethylene tubing connected to two pressurized syringes; one containing 60ml PBS with 0.3ml heparin, the other containing Accustain Bouin's fixative (Sigma Chemical, St. Louis, MO). The trachea was then intubated and mechanically ventilated. The rat was perfused through the femoral vein with the heparin, immediately followed by an overdose of sodium pentobarbital through the same vein to stop the heart. The carotid artery was perfused with the PBS/Heparin solution at a pressure of 70 mmHg until the efflux from the femoral arteries appeared clear.

The perfusate was then switched to Bouin's solution at the same pressure with the femoral arteries serving as exit points. The abdomen was opened by a midline incision and the aorta removed and placed in the Bouin's fixative for one hour. After the aorta was removed from the fixative, the connective tissue, including the adventitia, was carefully removed under a dissecting microscope with fine forceps. The aorta was sectioned into several segments. These segments were washed in 70% alcohol plus several drops of ammonium hydroxide until all the yellow color disappeared. The segments were placed in 30% sucrose and left overnight at 4^{O}C. Subsequently, the excess solution was absorbed away and the pieces embedded in O.C.T (Optimal Cutting Temperature compound Tissue-Tek, Sakura Finetek, Torrance, CA). The pieces were

then sectioned in a cryostat (Microtome Cryostat Cryostar HM 560 MV) to form 10μm-thick specimens. The specimens were collected on Superfrost Plus slides (Fisher Scientific, Pittsburgh, PA).

Autofluorescence Mitigation

From our preliminary fluorescent immuno-histochemical studies, we noticed that the elastin layers of the rat aorta had a significant, broad auto-fluorescent spectrum. We decided to restrict this autofluorescence to one part of the spectrum (see the appendix to this chapter for consideration of other options) and to use a suitable fluorescent tag for imaging the epitopes in another, disjoint part of the spectrum. This was done using the following method. The slides containing the samples were incubated in 0.5 % Pontamine Sky Blue 6BX (Alfa Aesar, Haverhill, MA) for five minutes followed by a five minute washing in PBS. This restricts tissue autofluorescence to the red (Cowen, Haven et al. 1985; www.uhnresearch.ca/facilities/wcif/PDF/Autofluorescence.pdf 2000).

Immunohistochemistry

For the immunohistochemical study, the slides and the polyester membrane of the 12-well filters were incubated in blocking solution (3% goat serum, 0.3%Triton-X, 20mM sodium phosphate, 0.9mM sodium chloride, 0.05% saponin) for 30 minutes followed by three five minutes washings in PBS. They were subsequently exposed to rabbit anti-rat AQP1 antiserum (category AQP11-A, Alpha Diagnostic International, San Antonio, TX [ADI]) diluted in PBS plus 3% goat serum, 0.2% bovine serum albumin (Sigma) in PBS

for 18 –24 hours at 6^{O}C. After trying different concentrations, we settled on the primary antibody at a dilution of 1:500 (i.e. 2μg/ml) because this concentration created the least amount of non- specific staining with the secondary antibody when analyzed. Afterwards, the slides and 12-well filter membranes were washed in PBS three times and incubated with Alexa 488 conjugated goat anti-rabbit IgG (Molecular Probes, Carlsbad, CA) at a dilution of 1:50 in PBS for 90 minutes at room temperature.

Control Studies

There were two control experiments done in the immunohistochemical study. For the first control, PBS replaced the primary antibody and the experiment was conducted as mentioned before. For the second control, rat AQP1 control/blocking peptide (category AQP11-P Alpha Diagnostic International, San Antonio, TX [ADI]) was used. Excess blocking peptide was incubated in primary antibody (50:1) and left for 90 minutes at 6^{O}C. This mixture then replaced the primary antibody as previously mentioned in the other control and the immunohistochemical study done as before.

Nuclear Counterstaining and Mounting

To view the nuclei of the individual cells in the specimens, the slides and filter membranes were stained with Hematoxylin solution, Gill #2 (Sigma) according the following procedure (Presnell and Schreibman 1979). The sections were rehydrated with two changes of five minutes each of 100% alcohol followed by 70% alcohol, followed by five minutes of running water. The slides were then dipped ten times in 2% Hematoxylin solution for two minutes each. This was followed by dips in water until the water looked

clear. The slides were dipped in 0.3% ammonium hydroxide and rinsed twice again for one minute each in water. The blue intensity was then checked under a microscope and the procedure repeated if the stain is too dark or too light to permit proper identification of the nuclei. Some of the samples were also incubated with Slow Fade® Gold antifade containing DAPI, which also stains the nuclei of cells (Invitrogen, Carlsbad,CA). Samples were washed in PBS three times and mounted with Vectashield mounting media for fluorescence (Vector laboratories, Burlingame, CA). Cover slips were securely applied to the samples using clear nail polish. The samples were then kept in the dark to prevent damage to the Alexa 488 tag and subsequently viewed and captured using a Leica TCS SP2 AOBS confocal microscope using a 488nm Argon laser. Image analysis was done with the Leica confocal software TCS SP/NT version 2.5 1347d. For control experiments, both the antigen peptide and PBS replaced the primary antibody.

Custom Software

The z slices of the present chapter as well as of the internal standards and those that were used for quantification in later studies (see Chapter 3) were analyzed using a specially-coded custom software that uses active contours or snakes to find the boundaries of objects in an image (Kass, Witkin et al. 1998). This

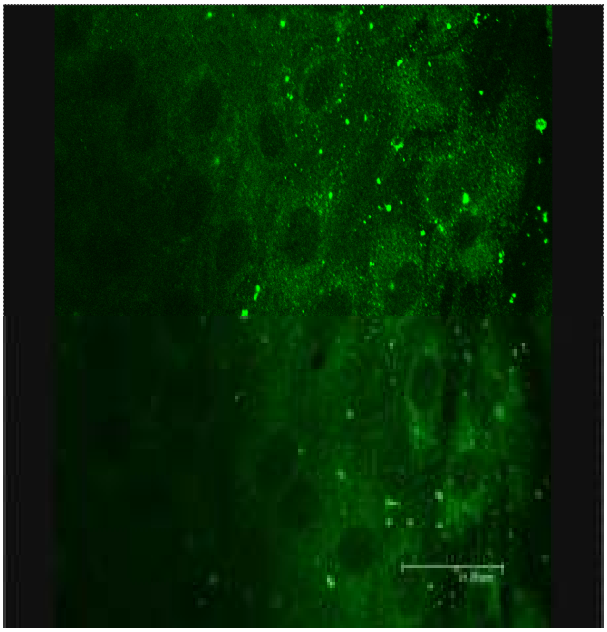

Figure 3: Confocal images of BAECs with Alexa 488-tagged AQP1 (green). Nuclei are stained with hematoxylin

software tightly outlines and encloses the region, corresponding to the endothelium, of intense green staining beyond the IEL in each of the confocal sections/images of the confocal z-stack taken of the aorta. It then integrates the intensity of the Alexa 488 fluorescence enclosed in this region and calculates the perimeter and area of the enclosed region. Simpson's rule is used to calculate integrated intensity, the total surface area and the total volume of the z stack region of the aortic endothelium. We thank Mr. Hadi Fadaifard and Professor George Wolberg both of Department of Computer Science at City College of the City University of New York for working with us on this program.

III. RESULTS

Figures 3 shows a confocal extended focus image of a BAEC monolayer that clearly expresses AQP1 (green fluorescence). These were taken from ±3μm in the z coordinate

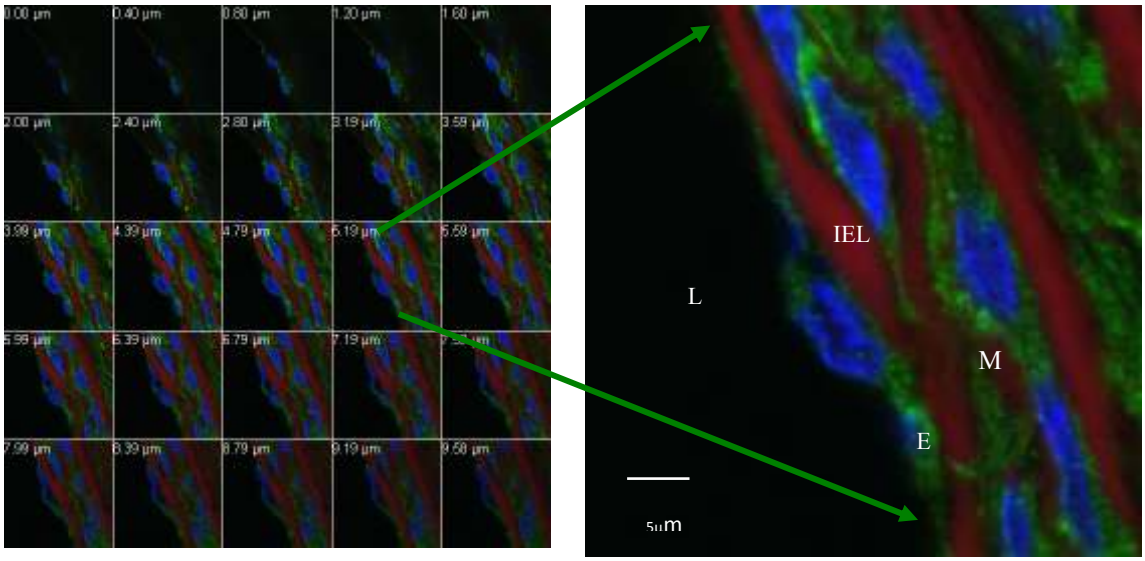

Figure 4:0.4 μm z confocal sections of Sprague Dawley rat endothelial cells with green Alexa 488 showing the presence of AQP1 proteins. Nuclei are stained in blue with DAPI. L=Lumen; E=Endothelium; IEL=Internal Elastic Lamella; M=Media

center of the monolayer. The AQP1 concentration appears higher in the cytoplasmic structures around the nucleus than at the cell borders. Figure 4 shows a confocal z stack gallery image of RAECs expressing AQP1 in a whole vessel *ex vivo*. There are 25 optical serial sections in this gallery representing a total thickness of ~ 10μm. These slices were obtained using a Leica confocal microscope and analyzed using its software, as described above. Arrows in the magnified image of one of the slices indicate the presence of AQP1 antibody (green Alexa 488 fluorescence) predominantly restricted to the plasma membrane of both the luminal and abluminal sides of the endothelial cells and to the medial cells. This figure also shows the well-known fact that the smooth muscle cells of the media also express AQP1(Shanahan, Connolly et al. 1999). Figure 5 smashes 50 higher magnification optical serial slices (from a Spontaneously Hypertensive rat (SHR)) together to form a two-dimensional image. Superimposed on it is the blurry black and white transmission image.

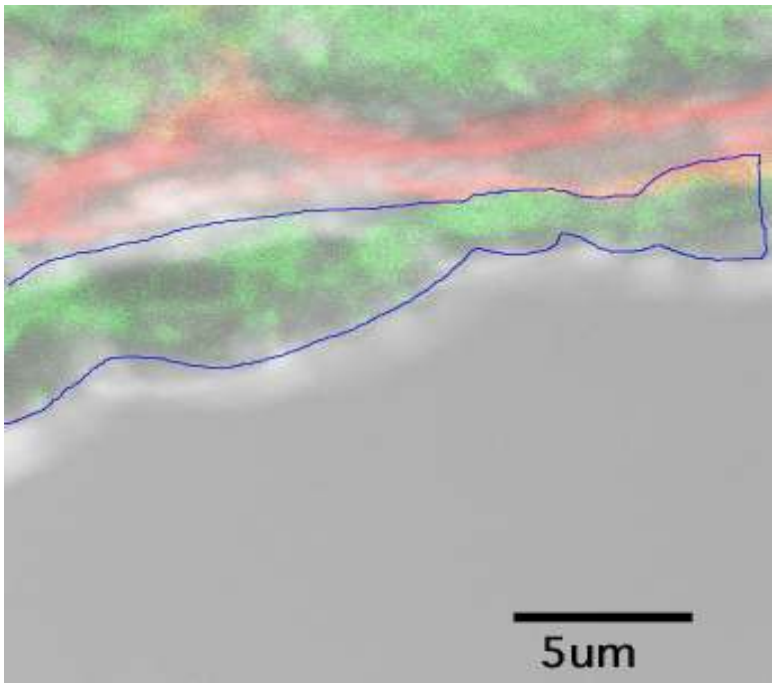

Figure 5: Extended focus image of 50 high magnification optical confocal slices from thoracic aorta of an SHR with transmission image (blurry at high magnification) superimposed. Near coincidence of blue outline and transmission EC image indicates AQP1 expression throughout cell

The tight blue outline was done by our custom software, which uses active contours or snakes

to find the boundaries of objects in an image, in this case, the significant green fluorescence between the IEL and the lumen, indicative of the presence of AQP1. The near coincidence of the blue line and the transmission image boundary shows that AQP1 is expressed throughout the intracellular compartments of the cell. The AQP1s therefore form a potential pathway for transendothelial water transport. There were two control experiments used in this study; where both PBS and a mixture of the primary antibody and its blocking peptide replaced the primary antibody. These control experiments both produced similar qualitative results. Since no primary antibody is used in the first control, there are no binding sites (except non-specific binding on the tissue) available for the secondary antibody; therefore we expect little or no Alexa 488 fluorescent signal. For the second control, the blocking peptide binds to the primary antibody 90 minutes prior to secondary antibody incubation, thereby occupying available binding sites that would have normally been available for this antibody. Again we expect little or no Alexa 488 fluorescent signal. Figure 6 confirms our expectations; it shows a confocal z stack gallery image of control RAECs in whole vessels *ex vivo* using the blocking peptide/antibody mixture. These optical serial sections of this RAEC control do not show any detectable fluorescent signal.

IV. DISCUSSION

AQP1 are found to be expressed in many endothelial cell types involved in fluid transport such as the choroids plexus of the brain, the cornea of the eyes and the hepatic bile ducts suggesting a transport role for them in these environments (Nielsen, Smith et al. 1993). We have localized AQP1 in BAEC monolayers and on RAECs in whole vessels *ex vivo,* as shown in figure 3 and 4

The predominance of AQP1 throughout the plasma membrane and the intracellular regions of the endothelial cells shown in figure 5 demonstrate a feasible potential pathway for pressure driven transcellular water transport. Thus water may enter the ECs from the lumen, and pass through the cell, possibly or partly through the inner organelles, before exiting the cell and entering the deeper regions of the wall.

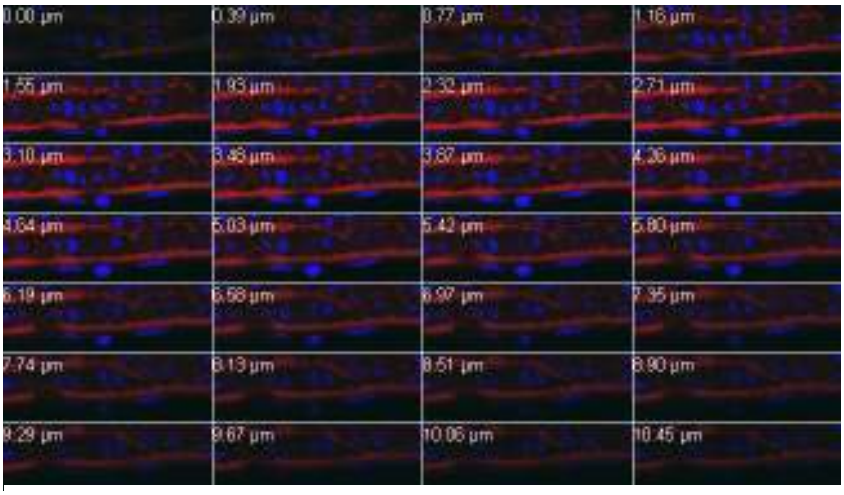

Figure 6: Control image; primary antibody replaced by both PBS and control serum

Osmotic filtration studies done by Ziedel and coworkers using purified human red blood cell AQP1 embedded in proteoliposomes of defined lipid composition have shown that they play a functional role in the permeability of cells to water (Zeidel, Ambudkar et al. 1992). In order to address whether the AQP1 found here in aortic ECs plays a similar functional role in pressure-driven transendothelial water transport, Drs. Tieuvi Ngugen, Annie Shou and Stewart Russel in our lab also did functional hydraulic conductivity (Lp) studies on both BAEC monolayers and whole rat thoracic aorta *ex vivo*. In BAECs, our group measured Lp of matched pairs of monolayers, one control and one exposed to $HgCl_2$ (T. Nguyen), a known AQP1-blocker, and one control and one whose AQP1 level was knocked down using siRNA (S. Russell), which are silencing RNA that interferes with a specific gene expression, in this case AQP1 (Elbashir, Harborth et al. 2001). In the

ex vivo whole vessel studies, Y. Shou and T. Nguyen measured Lp at various transmural pressures, introduced $HgCl_2$, remeasured Lp at the same transmural pressures, then denuded and repeated the Lp measurements a third time, all on the same vessel. In both the monolayer and the whole vessel studies, extensive $HgCl_2$ titrations were done so as to eliminate any artifacts due to $HgCl_2$ toxicity. (Y. Xue in our lab is currently working on the complementary experiment: measuring Lp at various transmural pressures on whole vessels *ex vivo*, where the ECs in the excised vessel have undergone AQP1 knockdown with siRNA. These results are not yet available.) Figure 7 shows a confocal image of a BAEC monolayer knockdown with siRNA then subjected to the previously mentioned immunohistochemical preparation. Quantitative analysis of this image compared to figure 3 shows a 50% reduction in the strength of the Alexa 488 fluorescent signal.

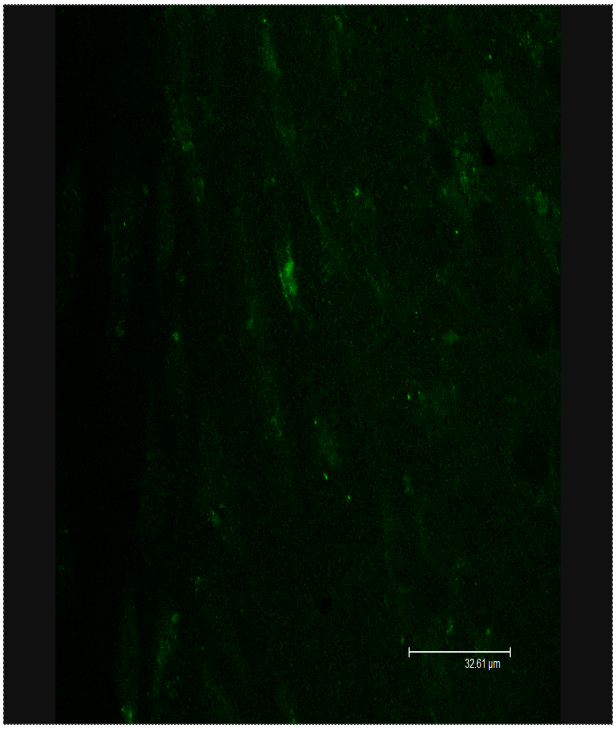

Figure 7: Confocal images of BAECs knockdown with siRNA and Alexa 488-tagged AQP1 (green). Nuclei are stained with hematoxylin

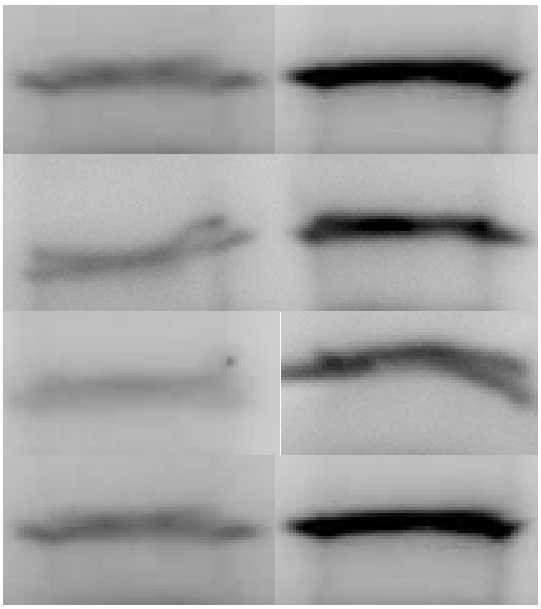

Figure 8: Western blot showing BAEC monolayer AQP1 (target B) knockdown between 42-70% with siRNA

Yan Xue from our lab also did Western Blot knockdown experiments using siRNA on BAEC monolayers as shown in figure 8 showing that these proteins can be decreased between 42-70%. Her results corroborate our immunohistochemical findings of AQP1 knockdown via siRNA. Figure 9 shows the Lp studies done by S. Russell using BAEC monolayers incubated with and without siRNA. It shows that the water flux across the monolayer subjected to siRNA was reduced by up to 62% compared to the controls. T. Nguyen's *in vitro* water flux measurements across BAEC monolayer were either subjected to $HgCl_2$ blocker or to a blank solution. Her results showed that the monolayers subjected to the blocker showed an average of 22.1% ($p<0.05$) lower water fluxes than the untreated ones. Her

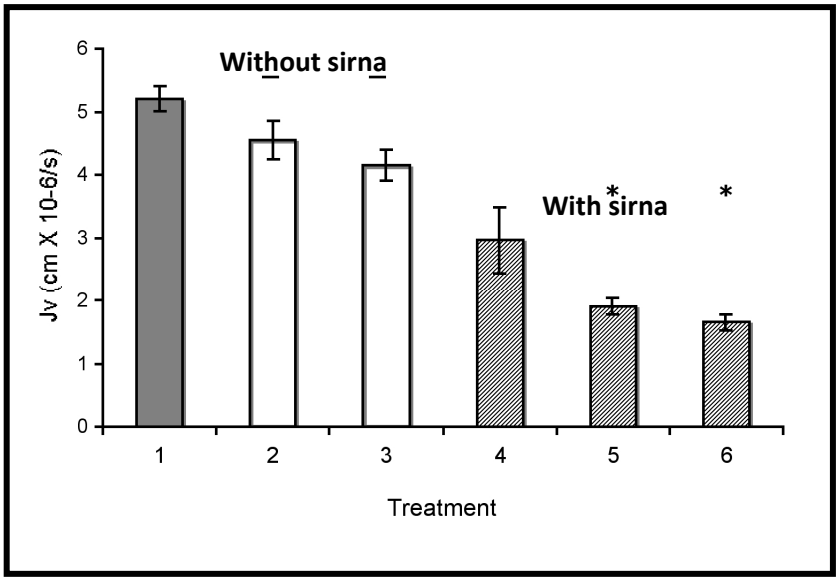

Figure 9: Steady-state water flux through BAEC monolayers treated with siRNAtargeting AQP-1 (S. Russell)

In-Vitro BAECs at $10cmH_20$ ($p<.01$, n(1)=10, n(2-6)=6,means +/- SEM)

results are shown in table1. T. Nguyen results on whole rat thoracic aortas *ex vivo* are shown in figure 10. Measurements of Lp (ΔP) were done at 60, 80 and 100mmHg. T. Nguyen found that every vessel subjected to $HgCl_2$ showed lower Lp values than those with intact endothelium at every pressure.This drop was largest at 60mmHg pressure, where the decrease was ~32%. These studies conducted by my labmates using the different techniques all separately show that knocking down or chemically blocking AQP1 in either BAEC monolayers or RAECs in whole vessels *ex vivo* significantly reduces transmural pressure-driven trans-endothelial water transport. These results argue that AQP1 facilitates a paracellular water pathway across aortic endothelial cells. Apart from certain small gaseous molecules(Herrera, Hong et al. 2006), AQP1 appears to only transport water; therefore, using this paracellular pathway water has the potential to dilute an existing subendothelial concentration of LDL, which can dramatically slow its kinetics of binding to ECM, a crucial prerequisite to pre-atherosclerotic lesion formation. A known risk factor for atherosclerosis is hypertension and we shall hypothesize that one condition that may influence a vessel's AQP expression is its transmural pressure. If transmural water transport were purely due to junctional transport, it would be a passive process that went up and down with a changing transmural pressure. If, on the other hand, as these data indicate, a portion of this transport is a protein-gated process, then a vessel might be able to actively regulate this transport by differential protein (AQP1) expression. This motivates the study in the next chapter, which begins by quantifying EC AQP1 expression and its response to changes in chronical transmural pressure. We will attempt to answer this question using Wistar Kyoto rats (WKY) and their chronically hypertensive cousins SHR as our animal model in Chapter 3 and normal Sprague-Dawley

rats and those made hypertensive by renovascular surgery, as the animal model in chapter four.

Pair	Control *Jv x 10^{-6} cm/s*	25m**M** $HgCl_2$ *Jv x 10^{-6} cm/s*
1	5.11	4.29
2	7.26	5.92
3	4.53	3.44
4	5.88	4.26
Average± SEM	5.70±1.18	4.44 ±1.05

Table 1: Jv of BAEC monolayer incubated in HgCl2 against control filter left in normal cell culture media. Pairs of control and experimental filters were run in parallel.

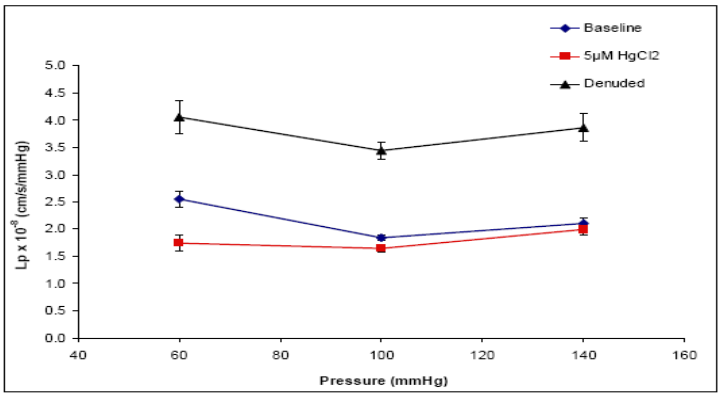

Figure 10: Lp vs ΔP: Baseline, 5μM $HgCl_2$, Denuded (T. Nguyen) means +/- SEM (n=6)

V. SUMMARY

Pressure-driven convective water flux plays a central role in the transmural transport of LDL; it advects these molecules from

the blood across rare, focal leaks in the arterial endothelium into the inner regions of atheriosclerotic prone vessels. It is naturally assumed that transendothelial water transport occurs paracellularly via cell junctions. However, since the discovery of the integral membrane water protein-AQP1 and its ubiquity in many tissues, it is reasonable to ask if it may play a role in transcellular water transport. We have used immunohistochemistry and confocal microscopy to show the existence and distribution of aquaporin-1 proteins on cultured BAECs and in whole rat aorta endothelium *ex vivo*. Image analysis done using our custom software showed these aquaporins to be well distributed throughout the aortic endothelial cells, including in the luminal and abluminal regions, thereby suggesting the possibility of these molecules serving as potential transendothelial water pathways across the endothelium. Functional Lp studies conducted by my colleagues (T. Nguyen, S. Russell and Y. Xue) using different techniques corroboratively show that knocking down or chemically blocking AQP1 in either BAEC monolayers or RAECs in whole vessels *ex vivo* significantly reduces transmural pressure-driven trans-endothelial water transport. These results strongly suggest that AQP1 supports a paracellular water pathway across aortic endothelial cells and changes in the concentration of active aquaporins affects transmural water transport. It would then follow that such changes likely affect on the dynamics of transendothelial transport of LDL, particularly over longer time scales.

VI. APPENDIX

Note on autofluorescence

The autofluorescence of the aorta of the rat is, in general, a major obstacle. The tissue appeared to emit a broad fluorescence spectrum from the green to the red region. In attempting to solve this problem, I first switched the fixative from Paraformalehyde Lysine Periodate (PLP) to Bouin's fixative in order to see whether this was the cause of the autofluorescence. This technique did reduce the autofluorescence but not to an acceptable level.

I also tested the unfixed tissue for autofluorescence. The test showed that the level of autofluorescence did decrease when compared to the fixed tissue but the level was still too high to provide good immuno-histochemical data. I searched the literature and found that the autofluorescence of blood vessels mainly results from either the fixation protocol or the elastin fibers or a combination of both (Cowen, Haven et al. 1985; www.uhnresearch.ca/facilities/wcif/PDF/Autofluorescence.pdf 2000). I then investigated and implemented a current chemical technique used for mitigating the autofluorescence of blood vessels. This technique as explained in the methods section basically pushes all the autofluorescence into the red region of the spectrum. One incubates the fixed tissue with 0.5% Pontamine Sky Blue dye. The tissue can then be tagged with the secondary antibody Alexa 488 affinity pure conjugated goat anti -rabbit IgG, which fluoresces in the green region of the spectrum.

CHAPTER 3: AQUAPORIN-1: ITS QUANTIFICATION IN THE ARTERIAL ENDOTHELIUM OF THE SPONTANEOUS HYPERTENSIVE (SHR) AND NORMOTENSIVE (WKY) WISTAR KYOTO RAT MODEL: HOW AQP1 EXPRESSION CHANGES WITH CHRONIC HYPERTENSION

I. INTRODUCTION

Atherosclerosis is responsible for over 50% of all deaths in the US and the Western world. About two-thirds of these deaths are caused by heart attacks as a result of blood clots in one or more coronary arteries. The other one third are caused by clots in vessels of the brain, which result in strokes, and the kidneys, liver, gastrointestinal tract, limbs etc (Guyton and Hall 2000).

Large arteries and/or aortic valves normally show a proclivity to develop atherosclerosis. However, the pulmonary arteries (PA) and veins do not generally exhibit this deleterious condition. In humans, the PA becomes susceptible only in the presence of pulmonary hypertension. Veins, on the hand, do not normally develop this condition (Lever, Jay et al. 1996), except in coronary bypass surgeries where the saphenous vein is frequently used as an arterial bypass vessel, which places it in high-pressure arterial conditions. These veins subsequently remodel and rapidly develop atherosclerosis (Wong, Nili et al. 2008). Atherosclerosis involves the passage, deposit and accumulation of cholesterol from the blood, across the endothelium and into the subendothelial intima (SI) of these large vessels. The build-up of cholesterol deposits eventually grow and coalesce, leading to the complicated process of atheromatous plaque development. Smooth and fibrous muscle tissues proliferate to form larger plaques. These plaques can

become large enough to bulge into the arterial lumen, leading to stenosis and the reduction of blood flow in these vessels (Guyton and Hall 1996). Alternately, such plaques can rupture, sending debris that can catastrophically obstruct downstream vessels into the bloodstream. The quest to ferret out the transendothelial pathways for the transport of lipoprotein cholesterol from the blood into the arterial walls has generated several competing theories and, as a result, has stimulated numerous experimental studies (Bratzler, Chisolm et al. 1977; Fry 1983; Lin, Jan et al. 1988; Lin, Jan et al. 1990). For decades investigators have found regional variations in the permeability of the arterial wall to macromolecules that were too large to pass through normal junctions ((Majno, Palade et al. 1961; Packham, Rowsell et al. 1967; Bell, Adamson et al. 1974; Bell, Adamson et al. 1974; Sprague, Frankel et al. 1980). Based on these observations, Weinbaum et al formulated a mathematical model based on a "leaky junction/ cell turnover hypothesis" in an attempt to explain this phenomenon. They proposed that, during cell turnover, i.e., cell mitosis and apoptosis, cell junctions become temporarily widened and "leaky," providing a pathway for macromolecules to focally cross the endothelium. Although these junctions account for less than 10^{-5} of the *en face* endothelial surface area, their model predicted that they could account for a 50-100% increase in the endothelial permeability of large, artheriosclerosis-prone arteries to such large molecules (Weinbaum, Tzeghai et al. 1985). This cell turnover approach became the impetus for several subsequent permeability studies involving the transendothelial transport of macromolecules such as horseradish peroxidase (HRP), Evans Blue Albumin (EBA) and Lucifer Yellow Low Density Lipoprotein (LY-LDL) that experimentally

confirmed some of the model's predictions (Lin, Jan et al. 1988; Lin, Jan et al. 1989; Lin, Jan et al. 1990; Truskey, Roberts et al. 1992; Chen, Jan et al. 1997).

The findings from these studies further galvanized the search for mathematical models to explain the observed transmural macromolecular transport. Yuan et al invoked advection, as well as diffusion, to account for the observed rapid subendothelial tracer spread, but was unable to explain these data (Yuan, Chien et al. 1991). Huang et al.'s axisymmetric transport model extended Yuan's model. They used medial and endothelial parameters from experimental measurements (Huang, Rumschitzki et al. 1994), but due to its extreme thinness, there were no experimental values for the SI's transport parameters. Instead, they appealed to Frank, Fogelman and Nievelstein's (Frank and Fogelman 1989; Nievelstein, Fogelman et al. 1991) ultra-rapid freezing/rotary shadow etchings, which showed the (rabbit aorta's) SI's extracellular matrix (ECM) structure in exquisite detail. From the resulting characteristic matrix fiber sizes and spacings, they constructed an *ab initio* theory for these missing parameters, which turned out to be far different – up to two orders of magnitude - from the medial parameters. With these values, their two-dimensional, convective-diffusive transport theory was able to successfully predict the early time growth followed by the near plateau of the macromolecular tracer spot sizes that had been observed experimentally (Chuang, Cheng et al. 1990). This model assumes that the transmural pressure drives plasma (mostly water) through both regular and leaky junctions of the endothelium of susceptible vessels. The flow through the leaky junctions advects macromolecules from the blood through these leaks into the artery's SI where they can bind to ECM to begin to form pre-atherososclerotic lesions. This fluid advection spreads in the SI parallel to the

endothelium before seeping through the fenestrae of the internal elastic lamella (IEL) and into the media. As noted, water also passes through the normal non-"leaky" endothelium and can dilute the local low-density lipoprotein (LDL) concentration of the SI and flush it from the SI into the media. Clearly water transport is critical in modulating the macromolecular transport of cholesterol from the blood into the arterial wall and an investigation of convective fluid transport is central to the greater understanding of the pre-arteriosclerotic processes.

Aquaporins

Over the last two decades, Agre and coworkers have identified, purified and partially characterized an abundant 28kDa novel integral membrane water channel protein named aquaporin-1 (AQP1) from red blood cells and renal tubules of the kidneys (Agre, Saboori et al. 1987; Denker, Smith et al. 1988; Saboori, Smith et al. 1988). Since their discovery, an entire family of aquaporins has been identified and characterized in diverse tissues (AQP0-12) such as the testes, brains, kidneys, eyes, salivary and tear glands in animals and also in plants. (Brown, Katsura et al. 1995; Ishibashi, Kuwahara et al. 1997; Connolly, Shanahan et al. 1998; Ishibashi, Kuwahara et al. 1998; Koyama, Ishibashi et al. 1998; Yasui, Kwon et al. 1999; Hatakeyama, Yoshida et al. 2001; Itoh, Rai et al. 2005; Morishita, Matsuzaki et al. 2005). AQP1 has been found in mouse aortic and in human coronary endothelial cells (Shanahan, Connolly et al. 1999; Saadoun, Papadopoulos et al. 2005). In Chapter 2 above we have demonstrated that AQP-1 is also expressed in the endothelial cells of the rat thoracic aorta and have suggested that it plays a role in transendothelial water transport. In his review, Heyman et al states that all living cells are

subjected to osmotic and hydrostatic changes and as a result must be able to handle these changes. They go on to say that osmotic permeation studies have shown that aquaporins increase the water permeation of plasma membranes by lowering their activation energy from 10-20 kcal/mol to less than 5 kcal/mol. This allows aquaporin water channels to maintain a high water flux ($\sim 10^{9}$ water molecules $s^{-1}channel^{-1}$) when these membranes are subjected to a transmembrane osmotic pressure differences (Heymann and Engel 1999).

AQP1 are highly specific for water transport and prevent most other molecules, solutes and ions, such as ammonia (NH_3) and protons (H^{+}) from crossing the membrane (Holm, Jahn et al. 2005; Beitz, Wu et al. 2006). Protons, however present a particularly difficult challenge for this water channel because of their positive charge. They can move along a column of water by hydrogen bond exchange. AQP1 succeeds even in preventing the passage of these individual protons (Zeidel, Nielsen et al. 1994; Agre, Lee et al. 1997).

Aquaporins' distinct water specificity, their presence in rat thoracic aortic endothelial cells and their ability to enhance the transport of water across the plasma membranes of cells invite the intriguing possibility of a functional role for them in the atherosclerotic process. If so, then their expression, concentration and distribution numbers and factors that regulate them become important to pre-atherosclerotic processes. Identifying and investigating these factors therefore becomes crucial.

Regulation of gene expression

Several decades ago, Francis Crick enunciated the idea of *the central dogma.* This idea has remained one of, if not the most important, fundamental principle in modern day molecular biology. It states that genetic information or gene expression as we know it, flows when deoxyribonucleic acid (DNA) is transcribed to ribonucleic acid (RNA), which is then translated into proteins, but never the other way around (Crick 1958; Crick 1970). (The discovery of reverse transcriptase (Temin 1976; Baltimore 1995) showed that this dogma is not absolute, since it produces DNA from an RNA template.) Several of these gene expression steps can be modulated and, as such, these regulatory processes have been intensively studied. Monod and Jacob, using the *lac operon* system, published one of the first notable works done in the study of the regulation of protein expression (Jacob and Monod 1961). Since then, several works have also elucidated the fundamental mechanisms of the regulation of protein expression in several other systems (Krueger, Danke et al. 2006; Turner, Flagel et al. 2008; Fan, Ma et al. 2009) and, in particular, how the environment or external stimuli such as pH, temperature and osmolarity can affect this expression (Iliev, Xu et al. 2002; Wuertz, Urban et al. 2007; Georgianna, Hawkridge et al. 2008; Hall, Vullo et al. 2008).

Hypertension

Data obtained from clinical, pathological and experimental studies have shown that hypertension is a major risk factor for the development and progression of atherosclerosis (Davis and Klainer 1940; McGill, Carey et al. 1985; Kannel, Neaton et al.

1986; Chobanian, Lichtenstein et al. 1989). The mechanisms by which this occur are poorly understood, and some literature findings may not always seem consistent. Wu et al showed that Spontaneously Hypertensive Rats (SHR), a widely used animal model of essential hypertension, exhibit increase endothelial cell turnover, which leads to an enhancement of endothelial permeability to Evan Blue-albumin. In contrast, Bretherton et al found that hypertensive rabbits did not show significantly greater entry of ^{125}I LDL into the vessel wall over cholesterol-fed normortensive rabbits (Bretherton, Day et al. 1977; Wu, Chi et al. 1990). One however must be cautious in drawing conclusions in these experiments since these two macromolecules are different in several aspects, e.g., size. Several ultrastructural features have also been found to be common to both hypertension and atheriosclerosis. These include increased smooth muscle cell numbers and cell mass, endothelial changes, increased connnective tissue, and intimal thickening (Schwartz and Benditt 1977; Haudenschild, Grunwald et al. 1985; Alexander 1995). Although the mechanisms of these two deleterious conditions have not been well elucidated, it has been suggested that, as a result of the common features observed, they may share similarities in mechanism (Alexander 1995).

In Chapter 2, we used immunohistochemistry, confocal microscopy and image analysis to show that AQP1 is expressed throughout the rat aortic endothelial cells. Since it is well established that cellular environments such as pH, osmolality and temperature can influence gene expression, it is reasonable to hypothesize that chronic hypertensive situations, that is, chronic elevated transmural pressure, can also affect AQP1 gene expression. If AQP1 protein expression can be modulated by chronic hypertension and a transmural water functionality can be attributed to them in the atherosclerotic process

then it is imperative that we do a quantitative investigation of these numbers, since changes in these numbers would affect transendothelial water transport and, by implication, macromolecular transport processes as well. We have decided to begin with the genetically modified SHR and its normotensive cousin, the Wistar Kyoto rat (WKY)(Kurtz and Morris 1987). We will use quantitative immunohistochemistry and confocal microscopy along with our custom image analysis software to quantify AQP1 numbers in these two rat variants. We will also relate our findings to functional hydraulic conductivity (Lp) studies conducted by my colleague Dr. Tieuvi Nguyen from our lab, using these two animal models. We shall also construct two simple "unit operation" type models based on continuum fluid mechanics, one for the flow through a single aquaporin channel and the other for the water flux across the endothelium that includes both junctional and aquaporin-based transcellular flow. Finally, we will compare our very simple model's hydraulic conductivity lp value for a single AQP1 water channel with both experimental and molecular dynamics values found in the literature.

II. METHODS

Quantitative Immunohistochemistry

An immunohistochemical study was performed on the aortas of young healthy male WKYs and SHRs weighing between 250-300g. The rats were anesthetized with sodium pentobarbital (Abbot Laboratories, North Chicago, IL; 30mg/100g i.v.). The left femoral vein was located and cannulated with PE50 polyethylene tubing attached to two syringes, one containing excess sodium pentobarbital and the other containing 0.3 ml of heparin (5000USP unit/ml; China Chemical &Pharmaceutical, Tapei, R.O.C). The carotid

artery was also cannulated with PE50 polyethylene tubing connected to two pressurized syringes; one containing 60ml PBS with 0.3ml heparin, the other containing Accustain Bouin's fixative (Sigma Chemical, St. Louis, MO).

The trachea was intubated and mechanically ventilated. The rat was perfused through the femoral vein with the heparin, immediately followed by an overdose of sodium pentobarbital through the same vein to stop the heart. The carotid artery was perfused with the PBS/Heparin solution at a pressure of 70 mmHg until the efflux from the severed right femoral artery appeared clear.

The perfusate was switched to the Bouin's solution at the same pressure with the femoral arteries serving as exit points. The abdomen was opened by a midline incision and the aorta removed and placed in the Bouin's fixative for one hour. After the aorta was removed from the fixative, the connective tissue, including the adventitia, was carefully removed under a dissecting microscope with fine forceps. The aorta was sectioned into several smaller segments. These segments were washed in 70% alcohol plus several drops of ammonium hydroxide until all the yellow color disappeared. The segments were placed in 30% sucrose and left overnight at 4^{O}C. Subsequently, the excess solution was absorbed away and the pieces embedded in O.C.T (Optimal Cutting Temperature compound Tissue- Tek, Sakura Finetek, Torrance, CA). The pieces were then sectioned to a thickness of 10μm in a cryostat (Microtome Cryostat Cryostar HM 560 MV); and the specimens collected on Superfrost Plus slides (Fisher Scientific, Pittsburgh, PA).

To view the nuclei of the individual cells in the specimen, the slides were stained with Hematoxylin solution, Gill #2 (Sigma) according the following procedure (Presnell

and Schreibman 1979). The sections were rehydrated with two changes of five minutes each of 100% alcohol followed by 70% alcohol, followed by five minutes of running water. The slides were then dipped ten times in 2% Hematoxylin solution for two minutes each. This was followed by dips in water until the water looked clear. The slides were dipped in 0.3% ammonium hydroxide and rinsed twice for one minute each in water. The blue intensity was then checked under a microscope and the procedure repeated if the stain was too dark or too light to permit proper identification of the nuclei. During our prior immuno-histochemical fluorescence work on the aorta, we noticed that aortic elastins displayed a significant, broad-spectrum autofluorescence. We therefore decided to restrict the autofluorescent to one part of the spectrum and to use a suitable fluorescent tag for imaging the epitopes in another disjoint spectral region. This was done using the following method. The slides containing the samples were firstly incubated in 0.5 % Pontamine Sky Blue 6BX (Alfa Aesar, Haverhill, MA) for five minutes followed by a five minute washing in PBS (Cowen, Haven et al. 1985; www.uhnresearch.ca/facilities/wcif/PDF/Autofluorescence.pdf 2000).

For immunohistochemical study, the slides were then incubated in blocking solution (3% goat serum, 0.3%Triton-X, 20mM sodium phosphate, 0.9mM sodium chloride, 0.05% saponin) for 30 minutes followed by three washings in PBS. They were subsequently exposed to rabbit anti-rat AQP1 antiserum (category AQP11-A, Alpha Diagnostic International, San Antonio, TX [ADI]) diluted in PBS plus 3% goat serum, 0.2% bovine serum albumin (Sigma) in PBS for 18 –24 hours. After trying different concentrations, we settled on the primary antibody at a dilution of 1:500 (i.e. 2μg/ml)

because this concentration created the least amount of non- specific staining with the secondary antibody when analyzed.

Afterwards, the slides were washed in PBS three times and incubated with Alexa 488 conjugated goat anti-rabbit IgG (Molecular Probes, Carlsbad, CA) at a dilution of 1:50 in PBS for 90 minutes at room temperature. Samples were washed in PBS three times and mounted with Vectashield mounting media for fluorescence (Vector laboratories, Burlingame, CA). Coverslips were securely applied to the samples using clear nail polish. The samples were then kept in the dark to prevent damage to the Alexa 488 tag and subsequently viewed and captured using a Leica TCS SP2 AOBS confocal microscope.

Control Studies

There were two control experiments done in the immunohistochemical study. For the first control, PBS replaced the primary antibody and the experiment was conducted as mentioned before. For the second control, rat AQP1 control/blocking peptide (category AQP11-P Alpha Diagnostic International, san Antonio, TX [ADI]) was used. Excess blocking peptide was incubated with the primary antibody (50:1) and left for 90

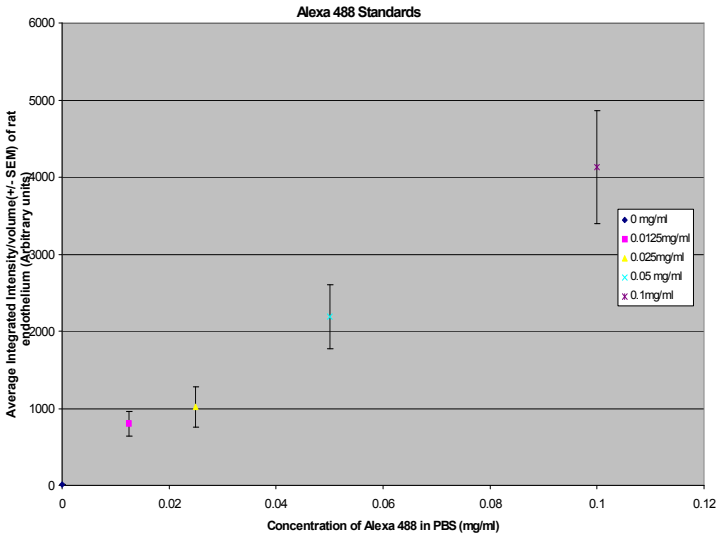

Figure 1: Demonstration of the linear range of integrated intensity/volume aortic endothelium against various concentration of Alexa 488

minutes at 6^{O}C. This mixture then replaced the primary antibody as previously mentioned in the other control and the immunohistochemical study done as before.

Confocal Microscopy and Image Analysis:

Laser Power Meter

Confocal microscopy was done using a Leica TCS SP2 AOBS confocal microscope. Several cautious preliminary steps were taken in order to be able to quantitatively compare confocal images taken from different samples. Firstly, before and during every confocal image acquisition, the confocal microscope's laser intensity was calibrated and the settings strictly maintained in order to make certain that each sample observed received the same level of laser power for the same amount of time. All other external conditions such as room temperature, humidity and stray lights etc were strictly monitored. The calibration of the microscope was done using a Coherent® Ultima LabMaster Power and Energy Dual-Channel Meter attached to a LM-2 silicon HD visible optical detector wand. A sample was placed on the microscope stage and the embedded tissue was brought into focus using the 40x PL APO N.A.1.25 oil immersion objective. The sample was then removed and replaced by the optical detector in the exact position over the objective. The 488nm Argon laser was then initiated and the detector was shifted around in order to find its "sweet spot," that is where the fullest intensity of the laser is felt. Both for different set of samples obtained after immunohistochemistry on different days and even for different samples from the same sample set, we adjusted the laser settings on the confocal microscope both before and periodically during the measurement procedure to obtain the same calibrated values on the laser meter for confocal scanning.

This was necessary since several factors such as temperature, humidity and stray lights can influence the intensity of the laser. The other settings on the confocal microscope were maintained for all samples as follows; scan-xyz, format-1024X1024, speed- 450Hz, average line-1, average frame-4, gain PMT1-725, gain PMT2-529, gain PMT3-0, gain PMT trans-152, offsetPMT1- -6%, offset PMT2-0%, offset PMT-0%, offset PMT trans-17, imageX-93.75imageY-93.75, pinhole (a.u.)-1.00airy, Objective-HCX Pl APO Cs 40x, Sequence- FITC Seq between lines and TRITC wide sequence and #of z-slices-50.

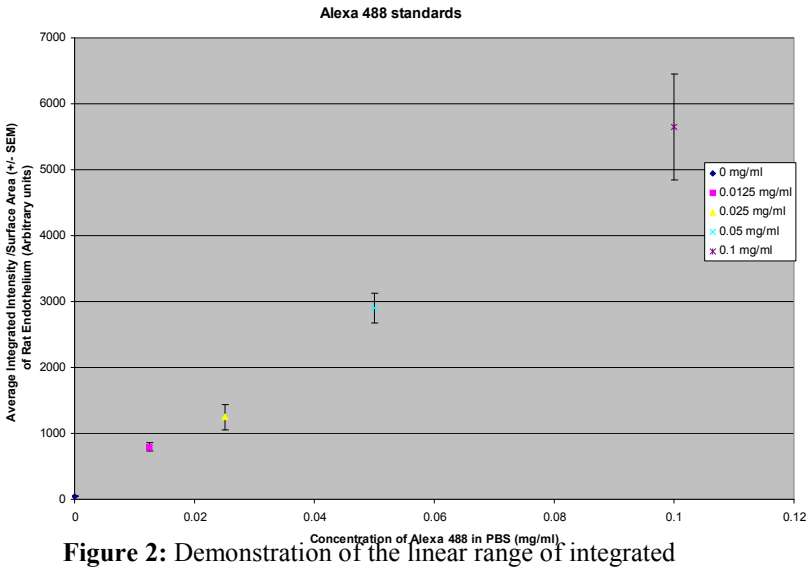

Figure 2: Demonstration of the linear range of integrated intensity/surface area aortic endothelium against various concentration of Alexa 488

Internal Standards

Internal standards were prepared in the following manner. Samples were prepared exactly as mentioned in

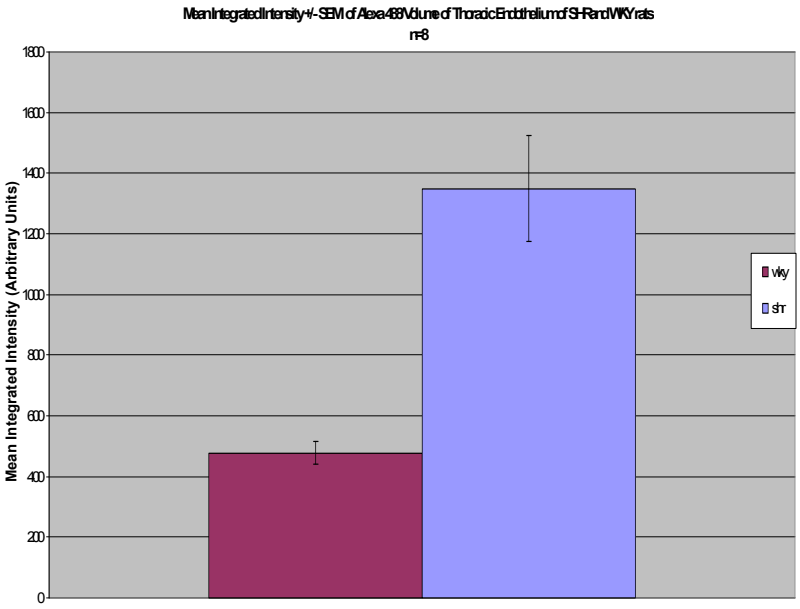

Figure 3: Mean integrated intensity/volume aortic endothelium for SHR and WKY rats

the methods section above except that we applied different known concentrations (0-0.1mg/ml in 0.02 mg/ml increments) of the secondary antibody/PBS onto individual slides containing tissue samples. We then applied coverslips and sealed them with clear nail polish. These standards were then subjected to the same confocal settings previously described using 488nm Argon laser. This ensured that the internal standards underwent the same process as the experimental samples.

Custom Software

The z slices of both the internal standards and those that were used for quantification in later studies were analyzed using a specially-coded custom software

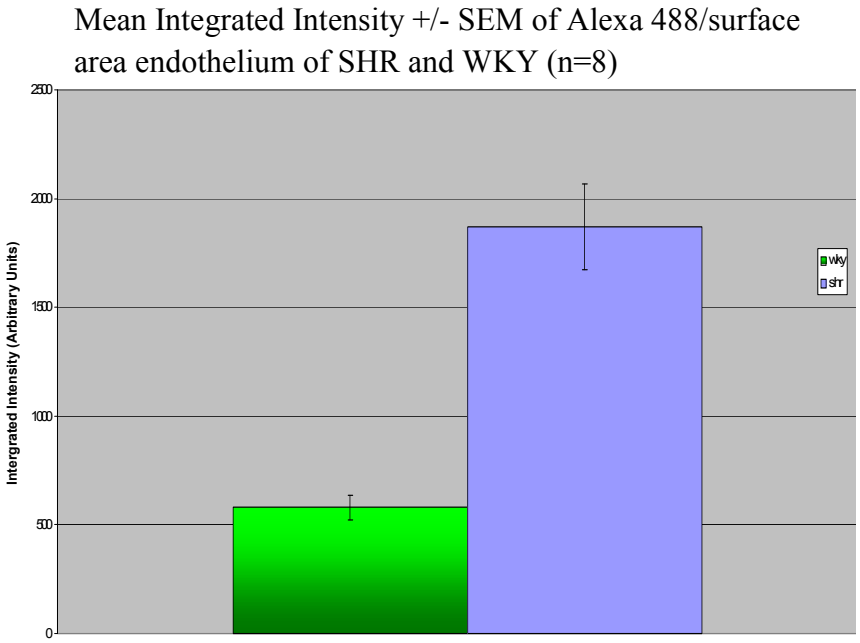

Figure 4: Mean integrated intensity/surface area endothelium for SHR and WKY rats

that uses active contours or snakes to find the boundaries of objects in an image (Kass, Witkin et al. 1998). This software tightly outlines and encloses the region, corresponding to the endothelium, of intense green staining beyond the IEL in each of the confocal sections/images of the confocal z-stack taken of the aorta. It then integrates the intensity of the Alexa 488 fluorescence enclosed in this region and calculates the perimeter and

area of the enclosed region. Simpson's rule is used to calculate integrated, the total surface area and the total volume of the z stack region of the intensity aortic endothelium. We thank Mr. Hadi Fadaifard and Professor George Wolberg, both of Department of Computer Science at City College of the City University of New York, for working with us on this program.

III. RESULTS

Figures1 and 2 demonstrate the reproducibility and strict linearity between concentration of Alexa 488 used for the standards and its fluorescent intensity obtained by the confocal microscope.

Figures 3 and 4, respectively, show the mean integrated intensity of Alexa 488 fluorescence per unit volume and unit surface area of the thoracic aortic endothelium of WKYs and SHRs. These figures show that the SHRs express over three times as many AQP1 as the WKYs. Below we analyze the consistency of this result with functional studies done by colleagues in my group.

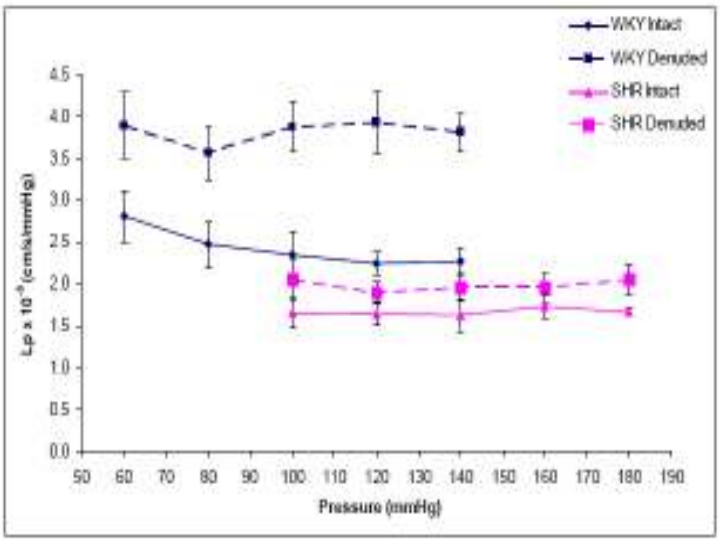

Figure 5:LpΔP of intact and denuded aorta from WKY and SHR rats.

IV. DISCUSSION

In this chapter we have shown a large difference in

AQP1 expression between the endothelial cells of the thoracic aortas of age-matched male WKY and SHR rats. What significance does the presence of AQP1 in these cells have? I begin by citing work from my labmates that substantiate a clear role for AQP1 in transport across the aortic endothelium. Dr. T. Nguyen in our group measured hydraulic conductivity (Lp) of matched pairs of BAEC monolayers *in vitro*, where one monolayer of each pair was treated with 25μM $HgCl_2$ and the other with a blank solution. The $HgCl_2$-treated monolayers showed an average drop of 22.1% ($p<0.05$) in Lp compared with control. Complementing this study, Dr. S. Russell, also in our group, showed that siRNA knockdown of AQP1 in BAEC monolayers, which produced ~70% knockdown by Western analysis, showed a 62 % drop in Lp compared with control. Both of these studies argue that AQP1 plays a role in hydraulic conductivity endothelial *in vitro*. Finally, Dr. T. Nguyen also measured Lp at 60, 100 and 140 mmHg first with intact endothelium, then after flushing with $HgCl_2$ to block endothelium aquaporins, and then again after endothelial denudation, all on the same vessel at all three pressures for n=6. Her data showed a sharp drop of ~1/3 in Lp_t at 60 mmHg. After an exhaustive set of controls, she concluded that, indeed, AQP1 played a significant role in vessel hydraulic conductivity. (Unfortunately, this effect is not simple, since her data also showed lesser drops of 11% and 5% both significant, at 100 and 140 mmHg respectively. The explanation of this variation of the percentage drop with pressure lies in the theory of intimal compaction under pressure loading and is the subject of a colleague, Shripad Joshi's, thesis, currently in progress. Its detail is beyond the scope of this present thesis. To summarize its basic idea, recall that the SI is a thin, very sparse region that compacts under pressure loading to a limiting value; this causes the endothelial cells to compress against the fenestral holes of

the IEL, partially blocking and impeding flow through them and thereby drastically reducing Lp_{e+i} (the Lp of both the combined resistances of the endothelium and intima) and therefore Lp_t (intact Lp values). The basic idea of Joshi's theory is that blocking endothelial AQP1s shifts a larger portion of the transmural pressure ΔP to the endothelial layer and compresses the SI at lower overall ΔP. Therefore, whereas without $HgCl_2$, the SI is not fully compressed until somewhere between 80 and 100 mmHg, with it, he suspects that the SI is already compressed at ΔP=60 mmHg.)

Now that these studies have established a functional role for AQP1 in the aortic endothelium, we address the question of whether our findings as to differential AQP1 expression for the SHR/WKY pair is consistent with these functional studies. Dr. T. Nguyen's results are shown in figure 5. First, consider the normotensive WKY rats. These experiments on intact and denuded WKYs exhibit the same qualitative trends observed in age matched SD rats (Shou, Jan et al. 2006). In particular, Lp of the intact vessel is highest at the lowest pressure (60mmHg) interrogated, then drops by (~12% $p<0.05$) for WKY rats from 60-80mmHg and remains pressure insensitive at least to 140 mmHg. This drop is smaller (27% ~12%) than found by Dr. T. Nguyen in SD rats. Denuded vessels show about double the Lp as the high-pressure intact values, and are pressure-insensitive over the entire 60-140 mmHg range. Intact WKY Lp values also show pressure insensitivity above 80mmHg, settling at ~$2.28\pm0.11\times10^{-8}$ $cm.s^{-1}.mmHg^{-1}$. Denuded values are about 36% larger (~$3.81\pm 0.32\times10^{-8}$ $cm.s^{-1}.mmHg^{-1}$ $p>0.05$) than the intact values over the entire range (60-140 mmHg). Dr. Nguyen also examined SHR Lp values over its physiological range, which is higher (100-180 mmHg). Both intact and denuded SHR curves are both pressure insensitive yielding values of

~1.67±0.14x10^{-8} cm.s^{-1}.$mmHg^{-1}$ and 1.99±0.18x10^{-8} cm.s^{-1}.$mmHg^{-1}$ respectively. This is likely because at the lowest pressure of 100 mmHg, the SHR's SI is likely already fully compressed. Equation 1 decomposes the resistivity (1/Lp) of the vessel wall, as is customary, as the sum of "resistances in series," corresponding to the resistances of its layers, as

$$\frac{1}{Lp_t} = \frac{1}{Lp_{e+i}} + \frac{1}{Lp_{m+I}} \tag{1}$$

where Lp_t and Lp_{m+I} represent the experimentally measured intact and denuded Lp values, respectively, Lp_{e+i}. Dr. Nguyen found that the SHRs exhibit an Lp_{e+i} of 10.92x10^{-8} cm.$s^{-1}$$mmHg^{-1}$ nearly double the 6.97x10^{-8} cm.s^{-1}.$mmHg^{-1}$ of the WKYs. This is consistent with our findings that SHR aortic endothelia express 3-4 times the AQP1s of WKY aortic endothelia. If we naively assume that Lp_{e+i} is simply the endothelial conductivity and ignore issues of intimal compaction and IEL fenestral blockage (Huang, Jan et al. 1998), the two Lp_{e+i} values and the difference of a factor of ~3.5 in AQP expressions between SHR and WKY aortic endothelium AQP1 concentrations allow us to estimate the Lp_j due to junctions and the Lp_{AQP} due to aquaporin1. Since conductances in parallel (junctions and AQP) add, we estimate Lp_j~5.39x10^{-8} cm.s^{-1}.$mmHg^{-1}$ and Lp_{AQP}~1.58 x10^{-8} cm.s^{-1}.$mmHg^{-1}$ for WKY and three times that for SHRs. This implies that AQPs account for ~22.7% of endothelial conductivity in WKYs and ~49.4% in SHRs. These numbers are just suggestive, since they

ignore issues of fenestral blockage, which we know to be important, and which would inclusion – a subject of theoretical work by a colleague (Shripad Joshi) in our research group, will change this calculation and its results completely.

The fact that SHR thoracic aortic endothelium expresses 3-4 times as much AQP1 as the same vessels from its normortensive WKY cousins suggests that a regulatory mechanism for endothelial AQP1 protein expression in response to chronic hypertension may exist. Although it appears that chronic pressure may be responsible for the upregulation of AQP1, one must still be careful in drawing this conclusion since these rats have been genetically bred to be chronically hypertensive. Several factors, whether genotypic, phenotypic or environmental can be at play to affect the upregulation of AQP1. For instance, it has been shown that although plasma calcium and magnesium levels are similar in these two strains of rats fed a normal chow diet, the SHRs exhibit lower levels of total plasma cholesterol and triacylglycerol (Yuan, Kitts et al. 1998). This makes it difficult to decouple chronic hypertension out of these variables and solely assume that it is responsible for the upregulation of the AQP1 proteins. We have recognized this problem and have decided to repeat this experiments with surgically, rather than genetically, induced chronically hypertensive rats to observe whether there will be any corroboration with our present results.

Before proceeding to this complementary study, we briefly examine a naive model for the lp of an individual AQP1 channel, whose details we leave for the appendix. The lp values obtained with this very simple, naïve (since it treats flow through an AQP1 pore by continuum methods) “unit operation” type model are between

$1.25*10^{-18}cm^5/N.s$ and $4.192*10^{-19}cm^5/N.s$ and the osmotic permeability values are between $1.814*10^{-14}cm^3/s$ and $6.084*10^{-15}cm^3/s$. Interestingly, as we shall see below, values from this naïve model are indeed similar to both experimentally-measured values and to very laborious molecular dynamics calculations. Molecular dynamics derived lp values for flow through single AQP1 are $2.0\pm0.3*10^{-17}$ $cm^5/N.s$ ($2.9\pm0.4*10^{-13}$ cm^3/s) and $9.5\pm0.7*10^{-18}$ $cm^5/N.s$ ($1.4\pm0.1*10^{-13}cm^3/s$) under different molecular dynamics conditions (Zhu, Tajkhorshid et al. 2002). Similar values have also been obtained for molecular dynamic simulations of osmotic flow through hexagonally packed carbon nanotubes, that $1.2*10^{-17}cm^5.N.s$ ($1.74*10^{-13}cm^3/s$) (Kalra, Garde et al. 2003). All these molecular dynamic simulation values are similar in magnitude to the experimental results of $8.06*10^{-18}$ $cm^5/N.s$ ($11.7\pm1.8*10^{-14}$ cm^3/s) for flow through a single aquaporin (Zeidel, Ambudkar et al. 1992; Zeidel, Nielsen et al. 1994) as measured in osmotic swelling experiments on erythrocytes. This experimentally-obtained value is considered the "gold standard" used for deducing the water flow rate through a single AQP1; it works out to be about $3*10^9$ water molecules per second per water pore. The magnitude of this number emphasizes the efficiency of water transport through AQP1 molecules

V. SUMMARY

Hypertension is a known risk factor for atherosclerosis and we believe that, at least in the absence of significant vessel wall remodeling, the higher the transmural pressure, the greater the convective macromolecular transendothelial transport. Due to the known

compressibility of the sparse arterial subendothelial intima (Huang, Jan et al. 1998) blood pressure changes and changes in the conductivities of wall layers can also have more indirect effects on artery wall mechanics and, subsequently on water and macromolecular transport in and through the wall. We investigate whether chronic hypertension conditions correlates with endothelial cell regulation of its AQP1 concentration. If that is indeed the case, then, given their water specificity, their presence in rat thoracic aortic endothelial cells and their capacity to very efficiently transport water, then endothelial cell aquaporins may be important in the pre-atherosclerotic processes.

We used male, normotensive Wistar Kyoto (WKY) rat and their hypertensive analogues, the Spontaneously Hypertensive Wister Kyoto rats (SHR) and quantitative immunohistochemistry coupled to confocal microscopy and image analysis to show that the hypertensive rat models express up to three times as many endothelial AQP1than the normotensives. Consistent with these findings are my colleague Dr. T. Nguyen's results of functional Lp studies that found that the SHRs exhibit an effective hydraulic conductivity, $Lp_{e+i,}$ of the endothelium plus the subendothelial intima, of nearly double that of the WKYs. We have also used a crude continuum (Unit Operations-type) approach to model flow through an aquaporin (clearly a non-continuum process). We have calculated lp values for individual aquaporins with this model that are very comparable, and at least as close as much more complex non-equilibrium molecular dynamics calculations, to results from osmotic swelling experiments in literature.

VI. APPENDIX

1. THEORY: FLUID FLOW THROUGH AN INDIVIDUAL AQUAPORIN CHANNEL

In this section, we formulate a simple mathematical model of the endothelium of its hydraulic conductivity in terms of fluid flow parameters for the aquaporins and the inter-endothelial cell junctions. This approach treats the water as a continuum that satisfies no-slip at the channel wall. It is unclear how to justify such an approach to describe single molecule flow through a channel. Right now, it is just a curiosity that is of interest because of how reasonable its results turn out to be.

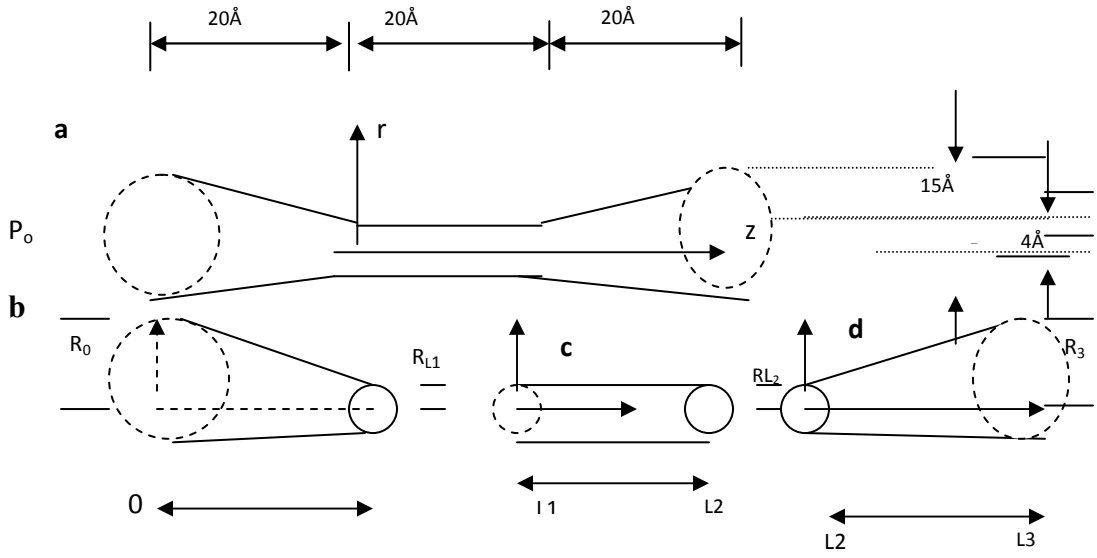

Figure 6: Model of aquaporin**:** a; total structure, b; converging cone, c; cylinder, d; expanding cone

Let us first look at flow through a single aquaporin channel. Based on X ray crystallography structural data for AQP1 obtained by (Sui, Han et al. 2001), the shape of the aquaporin resembles a reducing cone connected to cylinder followed by an expanding cone as shown in figures 6

We apply the Navier Stokes equation in cylindrical coordinates to the flow through the gradually reducing cone portion of the figure. Let the velocity u= (V_r,0,V_z). Assuming axisymmetry and steady state, we find the only remaining non-vanishing terms in the r and z components (equations 1 and 2) are

$$\rho\left[V_r\frac{\partial V_r}{\partial r}+V_z\frac{\partial V_r}{\partial z}\right]=-\frac{\partial \mathrm{P}^*}{\partial r}+\mu\left[\frac{1}{r}\frac{\partial}{\partial r}\left(r\frac{\partial V_r}{\partial r}\right)+\frac{\partial^2 V_r}{\partial z^2}-\frac{V_r}{r^2}\right] \tag{1}$$

$$\rho\left[V_r\frac{\partial V_z}{\partial r}+V_z\frac{\partial V_z}{\partial z}\right]=\frac{\partial \mathrm{P}^*}{\partial z}+\mu\left[\frac{1}{r}\frac{\partial}{\partial r}\left(r\frac{\partial V_z}{\partial r}\right)+\frac{\partial^2 V_z}{\partial z^2}\right] \tag{2}$$

Let R_z be the cone radius at z=0, L_1. Using the standard lubrication flow approximation ε: = (R_0-R_{L1})/L_1<<1, one can separate scales and, as in boundary layer theory, find $\partial P^*/\partial r=0$ to leading order in ε; therefore P is a function of z only to leading order in ε. One can follow this line of reasoning further or use the approach taken in the classic lubrication example of the rocker bearing problem (Batchelor 1999). As there, we assume that ε is sufficiently small so that the flow is locally Poiseuille (Navier-Stokes flow subject to a no-slip boundary condition at the channel wall), i.e., for α=O(1), over a region Δz~α(R_{L1}-R_0) <<L_1. (Note ε=0.275))

$$V_z(r,z)=\frac{\partial P^*}{\partial z}\frac{R(z)^2}{4\mu}\left(1-\frac{r^2}{R(z)^2}\right) \tag{3}$$

The average velocity (U(z)) is

$$U(z)=\frac{\int_{o}^{R(z)} V_z}{\int_{0}^{R(z)} rdr} rdr=\frac{\partial P^*}{\partial z}\frac{R(z)^2}{8\mu} \tag{4}$$

Therefore

$$V_z(r,z)\approx 2U(z)\left[1-\frac{r^2}{R(z)^2}\right] \quad . \tag{5}$$

Over longer z scales, R in (3) will vary with z and, as a result, so must $\partial P^*/\partial z$. Since the fluid is assumed incompressible, its flow rate Q, however, must be independent of z for all z, even for $\Delta z \sim L_1$, i.e.,

$$Q=\pi R(z)^2 U(z)=cons\tan t \text{ (Independent of z)} \tag{6}$$

$$Q=\pi R(z)^2\frac{\partial P^* R(z)^2}{8\mu\partial z}=\frac{\pi R(z)^4\partial P^*}{8\mu\partial z} \tag{7}$$

This yields an expression for how $\partial P^*/\partial z$ varies with z:

$$\frac{\partial P^*}{\partial z}=\frac{8\mu Q}{\pi R(z)^4} \tag{8}$$

To evaluate the Pressure

$$P_0-P_{L1}=\frac{8\mu Q}{\pi}\int_0^{L1} R(z)^{(-4)}dz \tag{9}$$

Assuming R varies linearly with z i.e.

$$R(z) = R_0 + \frac{(R_{L1} - R_0)z}{L_1} \tag{10}$$

one calculates

$$P_0 - P_{L1} = \frac{L_1}{3}\frac{8\mu Q(R_0^{-3} - R_{L1}^{-3})}{\pi(R_{L1} - R_0)} \tag{11}$$

For the middle, cylindrical portion of the channel, we neglect entrance and exit effects and assume Poiseuille flow, i.e., $V_z(r) = \frac{d P^* R_{L1}}{dz 4\mu}\left(1 - \frac{r^2}{R_{L1}^2}\right)$ (12)

$$P_{L1} - P_{L2} = \frac{8\mu Q(L_2 - L_1)}{\pi R_{L1}^4} \tag{13}$$

For the expanding cone, we have again checked that $\varepsilon' := (R_{L2}-R_{L3})/(L_3-L_2) << 1$ as well. (Note $\varepsilon' = 0.275$) In analogy to the converging case, R varies linearly with z and gives an expression for the expanding cone pressure drop, i.e.,

$$R(z) = \frac{(R_3 - R_2)}{(L_3 - L_2)}(z - L_2) + R_2 \tag{14}$$

$$P_{L2} - P_3 = \frac{\frac{1}{3}(L_2 - L_3)\left(R_3^{-3} - R_2^{-3}\right)8\mu Q}{\pi(R_3 - R_2)} \tag{15}$$

Combining the results in all three regions gives a total pressure drop across an AQP1 channel of

$$(P_0 - P_{L1}) + (P_{L1} - P_{L2}) + (P_{L2} - P_3) = P_0 - P_3 = \Delta P \quad (16)$$

.

From Starlings Law

$$Q = Lp\Delta P \quad . \quad (17)$$

Therefore

$$Lp = \frac{3\pi}{8\mu}\left[\frac{(R_0^{-3} - R_{L1}^{-3})L_1}{(R_{L1} - R_0)} + \frac{3(L_2 - L_1)}{R_{L1}^4} + \frac{(L_2 - L_3)(R_3^{-3} - R_2^{-3})}{(R_3 - R_2)}\right]^{-1} \quad (18)$$

The viscosity of water is $6*10^{-8}$ Ns/cm^2. For one channel, $R_0 = 7.5*10^{-8}$ cm and $R_{L1} = 2.0*10^{-8}$ cm. We thus calculate the hydraulic conductivity (lp) for one aquaporin tetramer where $Lp_{AQP1} = 4.23*10^{-18}$cm^5 /N.s. If instead, we assume that the entire channel is cylindrical and of length $60*10^{-8}$ cm with R~ $2*10^{-8}$cm and if one just simply invokes the equation for steady state Poiseuille flow, one finds $Lp_{AQP1} = 1.75*10^{-18}$cm^5 /N.s, a far lower result corresponding to a far longer, narrow channel, rather than a short narrow channel between converging and diverging cones. By comparison, the Lp values obtained from experiment are $8.06*10^{-18}$ cm^5/N.s (11.7±1.8

$*10^{-14}$ cm^3/s) for flow through a single aquaporin (Zeidel, Ambudkar et al. 1992; Zeidel, Nielsen et al. 1994) and from molecular dynamics are $2.0\pm0.3 *10^{-17}$ $cm^5/N.s$ ($2.9\pm0.4* 10^{-13}$ cm^3/s) and $9.5\pm0.7*10^{-18}$ $cm^5/N.s$ ($1.4\pm0.1*10^{-13} cm^3/s$) under different molecular dynamics conditions (Zhu, Tajkhorshid et al. 2002). Clearly, the model with converging and diverging cones and the Poisseuille flow model sandwich the experimental and MD results. That these results are so reasonable is surprising, since they are very rough continuum models, an approach that is hard to justify from first principles for a flow of single molecules through a channel.

Let P_f be the usual *osmotic permeability*, R be the ideal gas constant ($841.935 cm.N.mol^{-1}.K^{-1}$), T the absolute temperature and Vw the molar volume of water ($18 cm^3/mol$). P_f is related to Lp by

$$Pf = \frac{RT}{V_w} Lp \quad . \qquad (19)$$

A comprehensive understanding of this equation can be found in (Zhu, Tajkhorshid et al. 2002). The Lp values from our model translate to osmotic permeability values of $6.17* 10^{-14} cm^3/s$ for the model with converging and diverging cones and $2.53*10^{-14} cm^3/s$ for simple Poisseuille flow. We can then calculate the number of water molecules passing through each water pore per second using the following equation

$$\frac{Q}{s} = \frac{Pf}{V_w} NA \qquad (20)$$

where Q is the number of molecules of water passing per unit time, and N_A is Avagadro's number ($6.023*10^{23}$). Using the osmotic permeability values obtained from our converging- diverging model, we obtain values of $2.06*10^{9}$ surprisingly close to the $3*10^{9}$ expected value.

2. THEORY. FLOW THROUGH A SERIES/PARALLEL ARRANGEMENT OF AQUAPORIN-1 CHANNELS AS A MODEL FOR FLOW THROUGH AN ENDOTHELIAL CELL.

We model the luminal cell membrane of an endothelial cell as an array of x AQP1s in parallel and its abluminal cell membrane as y AQP1s in parallel. We assume that the luminal membrane is in series the abluminal side of the endothelium. Linear conductivities in parallel add whereas the inverses of linear conductivities in series add. If we ignore any intracellular AQP1s, this elementary argument leads to an expression for the hydraulic conductivity of a single cell as

$$Lp_{\sin glecell} = \frac{1}{\frac{1}{xlp_{lu\min alaqp1}} + \frac{1}{ylp_{ablu\min alaqp1}}} \quad . \qquad (21)$$

Assuming the endothelium has q cells in parallel with q-1 junctions, its hydraulic conductivity is

$$Lp_{endothelium} = q\left[\frac{1}{\frac{1}{xlp_{lu\min alaqp1}} + \frac{1}{ylp_{ablu\min alaqp1}}}\right] + \left(q-1\right)\left[lp_{junction}\right] \qquad (22)$$

To get x, y and q, we will attempt to use some of the various quantitative results described in this thesis. We can use the fact that conductances in parallel add to calculate the Lp of the endothelium due to aquaporins and junctions in parallel. We have already shown that $Lp_{junctions(WKY)}$ ~$5.39x10^{-8}$ $cm.s^{-1}.mmHg^{-1}$ ($1.94x10^{-8}$ cm^{-3} s^{-1} $mmHg^{-1}$)and $Lp_{AQP1(WKY)}$~$1.58 x10^{-8}$ $cm.s^{-1}.mmHg^{-1}$ ($0.56x10^{-8}$ $cm^3.s^{-1}.mmHg^{-1}$) Since $Lp_{AQP1(WKY)} = n_i lp/m$, we find that n_i/m ~ $1.29x10^{11}$ AQP/cm^2~$7.7x10^5$ AQP/cell-AQP-layer~3.85 times the estimate for the number of AQP1 in red blood cells (~$2x10^5$) (Zeidel, Ambudkar et al. 1992). If we take m=2, that is luminal and abluminal, we find that each layer has ~ $3.85x10^5$ AQP1. We must note that the ratio of the enface surface area of RBC:EC is $135\mu m^2$:$520\mu m^2$(Chen, Jan et al. 1997), therefore the estimate for AQP/layer is pretty comparable. For the hypertensive SHRs, we multiply by a factor of 3.5x.

CHAPTER 4: AQUAPORIN-1: ITS QUANTIFICATION IN ARTERIAL ENDOTHELIUM OF 2-KIDNEY 1-CLIP GOLDBLATT RAT MODEL AND HOW THESE CHANGES WITH CHRONIC HYPERTENSION- WITH RELEVANCE TO EARLY ATHEROGENESIS

I. INTRODUCTION

Atherosclerosis is responsible for over 50% of all deaths in the US and the Western world. About two thirds of these deaths are caused by heart attacks as a result of blood clots of one or more coronary arteries. The other one third are caused by clots in vessels of other organs, especially the brain, which results in strokes, the kidneys, liver, gastrointestinal tract, limbs, etc (Guyton and Hall 2000).

Atherosclerosis is a progressive systemic pathological condition of large and intermediate sized arteries. The earliest events involve the passage, deposit and accumulation of cholesterol from the blood, across the endothelium and into the subendothelial intima of these vessels. This build up of cholesterol deposits eventually grows and coalesces, leading to the complicated process of atheromatous plaque (atheroma) development. These plaques or lesions are typically present as asymmetric focal thickenings of the intima and can become large enough to bulge into the arterial lumen, leading to stenosis and reduction of blood flow in these vessels. Atheromas are generally composed of blood-borne inflammatory/immune cells, vascular endothelial and smooth muscle cells, connective tissues, lipids and other debris. The precursors of atheromas are generally

fatty streaks, which are sites of accumulation of lipid droplets and immune cells (Duff and Mc 1951; Guyton and Hall 1996; Hansson, Robertson et al. 2006).

Data obtained from clinical (Kannel, Neaton et al. 1986; Stamler, Neaton et al. 1989), pathological and experimental studies have shown than hypertension is a major risk factor for the development and progression of atherosclerosis. Unfortunately, the mechanisms by which this occurs are poorly understood, a situation that can lead to conflicting interpretations of or apparent inconsistency among experimental results.

Postmortem pathology studies done by several authors have found that, at death, atherosclerosis of the major arteries is more severe in hypertensive humans than in normotensive subjects (Bell 1928; Murphy 1932; Clawson 1939; Davis and Klainer 1940; Wilkins, Roberts et al. 1959). Experimental studies done by Hollander et al found that primates made hypertensive by aortic coarctation and fed a high cholesterol diet developed severe coronary atherosclerotic disease with fibrous plaque formation resulting in over 60% luminal narrowing of the major coronary arteries and their extramural and intramural branches. Normotensive primates however, fed the same diet developed a milder form of atherosclerosis of only the major coronary arteries resulting in 12% luminal narrowing. When the hypertensive animals were fed a low cholesterol diet however, they did not develop complicating atherosclerosis but did develop focal intimal lesions (Hollander 1976).

Mc Gill et al examined the relationship of hypertension and plasma rennin activity to atherosclerosis in hyperlipedemic baboons. They surgically induced renal artery stenosis to cause hypertension and elevate plasma rennin activity in these animals. This technique

results in the well-known 2-kidney, 1 clip (2K1C) Goldblatt animal. They also used cellophane wrapping of both kidneys (bilateral perinephritis) that also induces hypertension but does not change plasma rennin activity. They found that both groups exhibited significantly greater atherosclerotic lesions in the abdominal aorta, brachial, iliac, femoral and carotid arteries than the control group (McGill, Carey et al. 1985). Using techniques similar to those of Mc Gill et al, Chobanian et al induced chronic hypertension in Wantanabe Heritable Hyperlipedemic (WHHL) rabbits using the one kidney, one clip (1K1C) Goldblatt method. This involves compressing one renal artery and the removal of one of the kidneys. Although the systolic blood pressure in these animals increased significantly compared to the sham operated animals, their body weight, heart rate, serum cholesterol and serum triglyceride remained unaffected. They found that the size of the aortic atherosclerotic lesions was increased after only 2-3 months of hypertension compared with the controls. At three months after the surgery, the surface area of the descending aorta was covered by lesions that averaged 77± 4.4% in the Goldblatts compared with 16± 3.3% ($p<.00001$) in the shams. At six months, these numbers were 62 ± 8.2% and 30± 5.3% ($p<0.01$), respectively (Chobanian, Lichtenstein et al. 1989).

Deming et al also induced chronic hypertension in rats using two different methods. The first method used a desoxycorticosterone and salt treatment (DOC-salt); the second was the 1K1C Goldblatt technique. They found that both of these methods not only increased the level of hypercholesterolemia and hyperlipemia in these animals, but also caused these animals to exhibit a greater degree of atherosclerosis than normotensive ones (Deming, Mosbach et al. 1958).

These results suggest that there may exist a relationship between chronic high blood pressure and the severity of atherosclerosis, but such a relation is not yet understood. Three possible explanations that have been proposed for this correlation are: 1) Hypertension accelerates or makes one susceptible to atherosclerosis. 2) Hypertension and atherosclerosis share a common pathological mechanism. 3) Atherosclerosis makes one susceptible to developing hypertension (Doyle 1992).

Several ultrastructural alterations of blood vessels have been found to be common to both hypertensive and atheriosclerotic animal models and, as such, give some credence to the belief that hypertension and atherosclerosis share similar pathological mechanisms. Most of the work done using animal models has found that these changes are confined to the intimal and medial regions of these vessels and mainly affect the morphology and permeability of the endothelial cells and the bulkiness of the smooth muscle cells. In the (DOC-salt) rats, it was found that after 1 month, significant changes such as increased height of endothelial cells, the presence of cells in the normally cell-free subendothelial intima and endothelial cell extensions and increased amounts of collagenous extracellular materials in the subendothelial zone all caused multiple focal elevations of the intima that varied in size and shape. Similar changes were also seen in the 18 week old spontaneously hypertensive rats (SHR) (Haudenschild, Prescott et al. 1980). Arteries taken from rats with experimental renal hypertension have also shown increased permeability to colloidal particle of carbon, the plasma protein fibrinogen and cells such as platelets and erythrocytes. This elevated permeability has been attributed to changes in the endothelial linings of these vessels, where discontinuities have been found to vary from separations of endothelial cell junctions to area denuded of one to several

endothelial cells (Wiener, Lattes et al. 1969). Smooth muscle hypertrophy i.e. the increase in cell numbers, has been implicated in the thickening of the medial region of arteries seen in SHRs during vessel remodeling. These cells also appear to migrate from the media into the subendothelial intima. With these increases in medial thickness and connective tissue deposition, vessel walls generally thicken and their resistances to pressure-driven transmural water flow increase (Wiener, Loud et al. 1977; Warshaw, Mulvany et al. 1979; Owens, Rabinovitch et al. 1981; Chobanian 1988).

All of these changes that occur to the vessels during hypertension are also seen during the development of atherosclerotic lesions. However, lipid deposition observed in the subendothelial intima does not occur unless the blood plasma becomes hyperlipidemic (Chobanian 1983).

Several groups have been particularly interested in the elevated permeability of atherosclerosis-prone vessels to blood-borne lipoprotein cholesterol and the pathways afforded for these macromolecules to penetrate through the endothelium. As such, numerous permeability studies have employed several different large tracer molecules of various sizes. Lin et al investigated macromolecular leakage in rat thoracic aortas by injecting rats with both a 6nm diameter Evan Blue Albumin (EBA) and the 22nm Lucifer Yellow Low Density Lipoprotein (LY-LDL) preparation, allowing these tracers to circulate for three to five minutes before sacrificing the rats. Their thoracic aortas were then scanned and the dividing cells identified by hematoxylin staining. They found that, although mitotic cells are very rare (1.4 in 10^4), 99% of these cells were associated with EBA leakage and 80% with (LY-LDL) conjugate leakage. These leaks, however, only account for 30% of all leakage found when EBA, and 45% when LY-LDL, was used

(Lin, Jan et al. 1988; Lin, Jan et al. 1989). Chen et al also conducted similar permeability studies and found that when the smaller sized (4-5nm) horseradish peroxidase (HRP) molecule was used, 90-100% of all mitotic cells showed junctional leakage, but these cells accounted for only between 3.9-8.6% of all HRP leaks (Chen, Jan et al. 1997). Truskey et al. also investigated the association of mitotic cells with macromolecular leakage in rabbit aorta. They found that 25% of all mitotic cells exhibited higher ^{125}I-LDL leakage and permeability than non-mitotic cells (Truskey, Roberts et al. 1992). Lin et al conducted similar experiments to account for non-mitosis-related macromolecular leakage. They found that, although dead or dying cells are also infrequent (0.48% in 12 rats), 63% of them are associated with EBA leakage (Lin, Jan et al. 1990). In summary, these studies show that macromolecules do not cross the endothelia of these atherosclerosis-prone vessels uniformly. Rather, much of this transendothelial penetration occurs through very rare, focal endothelial leaks, some of which are associated with transient leaky junctions of endothelial cells that are either dying or dividing.

Chuang et al conducted time dependant studies of the growth of HRP and EBA leakage as a function of the circulation time between these intravenous tracer injection and animal sacrifice. They found that both tracers showed similar trends, that is, the observed tracer spot sizes increased rapidly with increasing circulation time. In the case of the HRP, these spots became nearly steady at about 250μm diameter at about 4 minutes circulation time. The very rapid macromolecular spot growth and the achievement of a nearly steady spot size both suggest that these tracers spread predominantly through tracer advection by a pressure-driven transmural water flow, rather than simply by diffusion, which would be far slower than observed (Chuang, Cheng et al. 1990).

These tracer studies galvanized the search for mathematical models to explain macromolecular transport into the artery wall. Huang et al. was able to successfully model this transport. Their model assumes that transmural pressure drives the liquid component of the blood (mostly water and small solutes) through both the (far more numerous) normal and the (rare) leaky junctions of the vessel endothelium. This fluid advects macromolecules through the leaky junctions of the endothelium into arterial walls where they can bind to extracellular matrix to form atherosclerotic lesions. Fluid entering via these localized leaks subsequently spreads away from the leak parallel to the endothelim in the subendothelial intima before seeping through the fenestrae of the IEL and into the media. Most of the transmural flow is, however, through the far more numerous normal endothelial junctions. This flow dilutes the local LDL concentration of the subendothelial intima and greatly accelerates its flushing into the deeper media. Clearly water transport is critical in modulating the macromolecular transport of cholesterol from the blood into the arterial wall and the investigation of the convective fluid transport is central to the greater understanding of the arteriosclerotic process.

During the last two decades, Agre and coworkers while attempting to isolate a 32kDa Rh polypeptide from erythrocytes also identified, purified and partially characterized an abundant 28kDa novel integral membrane protein from them and the renal tubules of kidneys. This 28kDa protein was mistakenly believed to be a breakdown product of the 32kDa protein. (Agre, Saboori et al. 1987; Denker, Smith et al. 1988; Saboori, Smith et al. 1988). The protein was later named CHIP28 (channel –like integral membrane protein of 28Kda) (Preston and Agre 1991) but subsequently called aquaporin-1(AQP1). Since their discovery, an entire family of aquaporins has been identified and characterized in

several diverse tissues in animals (AQP0-12) such as the testes, brains, kidneys, eyes, salivary and tear glands and plants. (Brown, Katsura et al. 1995; Ishibashi, Kuwahara et al. 1997; Ishibashi, Kuwahara et al. 1997; Connolly, Shanahan et al. 1998; Ishibashi, Kuwahara et al. 1998; Koyama, Ishibashi et al. 1998; Yasui, Kwon et al. 1999; Hatakeyama, Yoshida et al. 2001; Itoh, Rai et al. 2005; Morishita, Matsuzaki et al. 2005). Aquaporins are highly specific for water transport and prevent other small molecules, solutes and ions from crossing the membrane such as hydroxide (OH^-) ions, ammonia (NH_3) and urea. (Zeidel, Nielsen et al. 1994; Agre, Lee et al. 1997)

In chapter two, we used immunohistochemistry and confocal microscopy to identify and show the existence of AQP1 on the endothelial cells of rat aorta. In chapter 3 we were able to demonstrate that the endothelial cells of male SHR thoracic aortas express three to four times as many AQP1 than the corresponding cells of their age-matched normortensive WKY cousins. Hydraulic conductivity studies from our group on both endothelial cell monolayers in culture and on whole vessels *ex vivo* show that these AQP1 also function as water transport pathways. Our general goal in this chapter is to repeat the work done in chapter 3 using different rat models, the 2K1C Goldblatt rat that avoids the use of a genetic variant to induce hypertension. We use the male 2K1C Goldblatt Sprague-Dawley rat and age-matched controls (normotensive with no operation, those with sham operations and 2K1Cs with blood pressure controlled to normal pharmacologically) to investigate whether the endothelium can actively regulate its AQP1 expression in response to chronic changes in transmural (blood) pressure. Clearly, such changes may be relevant to and impact transendothelial transport process.

II. METHODS

Goldblatt Surgical Procedure:

Five weeks old healthy male Sprague Dawley rats (SD) were made hypertensive by using 1% sodium pentobarbital (Abbot Laboratories, North Chicago, IL; 30mg/1000g i.v.). The stomach regions were cleanly shaved and povidone iodine applied liberally over the shaved areas. Alcohol swabs were then used to remove the iodine and to further

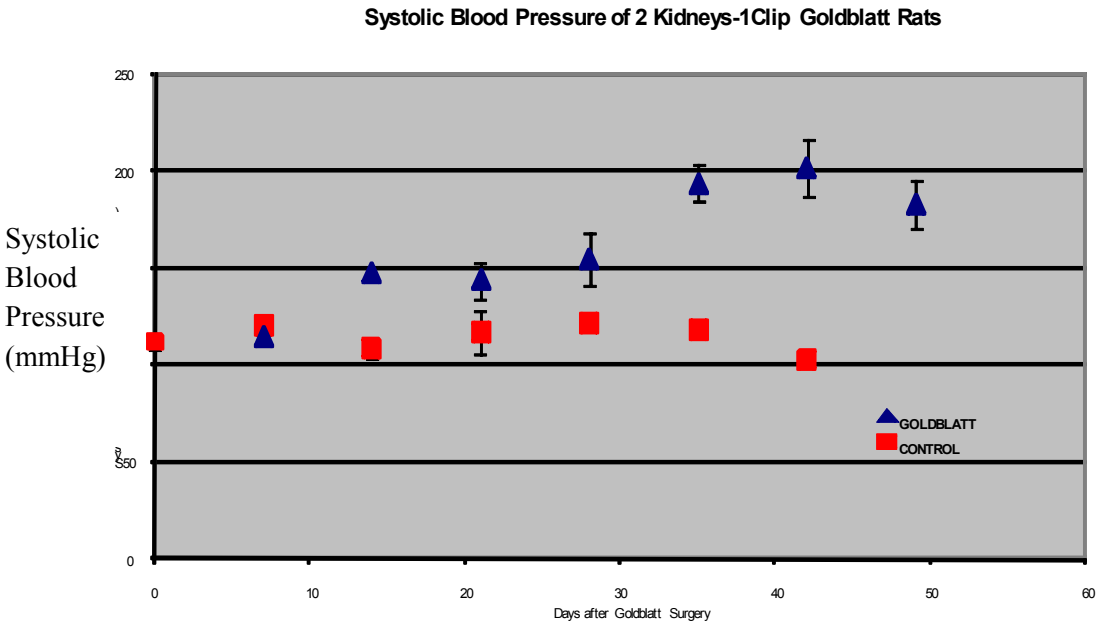

Figure 1: Systolic blood pressure time course in 2K1C rat and control non-clipped rats using the tail cuff method. $p<0.05$, Values are means± SEM

sterile surgical pads on heated beds kept at 37^{O}C and fabricated to our specifications. The right kidneys were located by touch and isolated. Surgical pads were secured to the stomach of these rats and a small slit made in the pad to expose the isolated kidney. A small semi-circular incision was made into the skin of the rats and the muscle and adipose tissue dissected out to isolate and expose the right kidney. The renal artery was

located and separated from the renal vein and a 20μm silver clip secured to this artery. The organ was returned to its original position in the rats' body and the muscles and skins sutured together. The areas were sterilized with bezoin tincture and an antibiotic ointment. 0.1cc of buphrenophine hydrochloride analgesic was injected into the femoral muscles and the animals left in a warm area to recover. The analgesic regimen was continued every twelve hours until the animal appeared to have recovered fully. Sham operations were also done in the exact fashion except that no clips were used.

Tail Cuff Blood Pressure measurements (non-invasive):

Rats were removed from the animal facility and kept in a quiet, dark room for about 1 hour in order to acclimatize them to the new room conditions. The rats, while conscious, were then placed in a restrainer and foam cushion material added to the restrainer to give the animals a cozy, snug fit. The tail cuffs were placed on the tails of the rats and the rats warmed to ~40^{O}C. The tail cuff pressure measurements were monitored using a Non-invasive Blood Pressure (NIPB) system attached to a Powerlab module (ADInstruments, Colorado Springs, CO) until stable readings were achieved. Figure 1 shows the effect of renal artery constriction using a 20μm internal diameter (I.D) clip on systolic blood pressure ± SEM after Goldblatt surgery on SD rats. Comparisons between these means were tested for significance using the student's *t* test ($p<0.05$). Rats became hypertensive ~150mmHg within two weeks after surgery and become fully hypertensive >200mmHg between five to six weeks after the operation. Sham operated controls and other controls in which no operations were done remained ~120mHg.

Captopril control animal:

Hypertensive Goldblatt (~150mmHg, systolic blood pressure) rats were kept in the

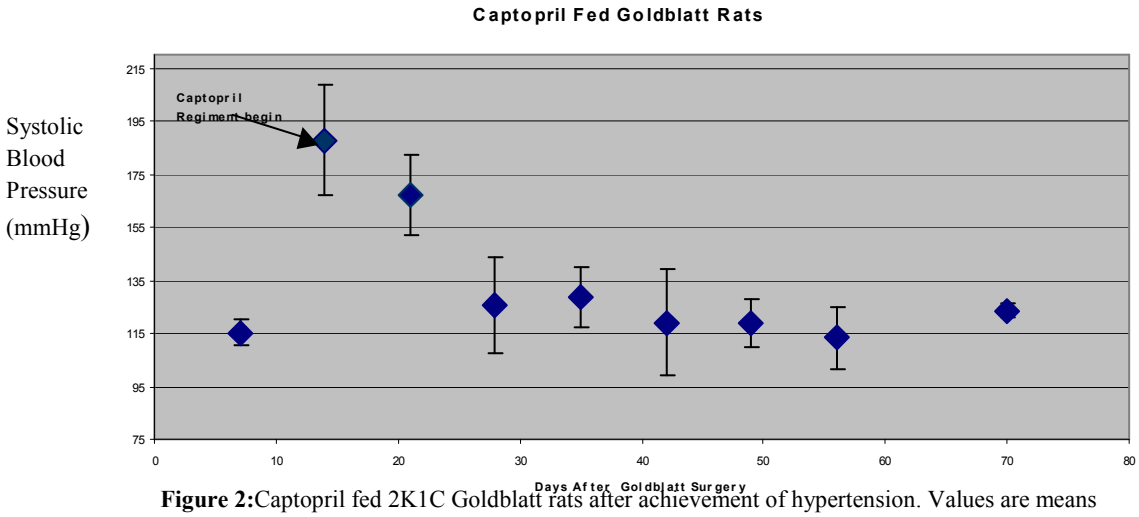

Figure 2: Captopril fed 2K1C Goldblatt rats after achievement of hypertension. Values are means ± SEM.$p<0.05$

animal facility with a light dark cycle of 12/12 hrs at a constant temperature of $22\pm1^{O}C$. Food pellets and Captopril solutions were available *ad libidum*. The rates of systolic blood pressure reduction in the individual rats used in this study varied and because it was important to have all the rats aged-matched at the time of sacrifice, the Captopril dosages given to these controls were adjusted accordingly between 1-8mg Captopril/15ml H_2O to ensure that their systolic blood pressure decreased to ~120mmHg within the time frame available. This progression in systolic blood pressure reduction in response to Captopril treatment can be seen in figure 2.

Quantitative Immunohistochemistry*:*

An immunohistochemistry study was performed on the aortas of young healthy male Sprague-Dawley rats made hypertensive by the Goldblatt procedure. 2K1C Goldblatt rats with systolic blood pressure 1) at ~150mmHg; 2) greater than 200mmHg; 3) that had reverted to normotensive values (~125mmHg) with Captopril treatment; 4) that remained normotensive because they had undergone control sham operations; and 5) those that were normotensive because they had not been operated on were used in this study. The rats were anesthetized with 1% sodium pentobarbital (Abbot Laboratories, North Chicago, IL; 30mg/1000g i.v.). The left femoral vein was located and cannulated by using PE50 polyethylene tubing attached to two syringes, one containing excess sodium pentobarbital and the other containing 0.3 ml of heparin (5000USP unit/ml; China Chemical &Pharmaceutical, Tapei, R.O.C). The carotid artery was also cannulated with PE50 polyethylene tubing connected to two pressurized syringes; one containing 60ml PBS with 0.3ml heparin, the other containing Accustain Bouin's fixative (Sigma Chemical, St. Louis, MO). The trachea was then intubated and mechanically ventilated. The rat was perfused through the femoral vein with the heparin, immediately followed by an overdose of sodium pentobarbital through the same vein to stop the heart. The carotid artery was perfused with the PBS/Heparin solution at a pressure of 70 mmHg until the efflux from the femoral arteries appeared clear. The perfusate was switched to the Bouin's solution at the same pressure with the femoral arteries serving as exit points. The abdomen was opened by a midline incision and the aorta removed and placed in the fixative for one hour. After the aorta was removed from the fixative, the connective tissue, including the adventitia, was carefully removed under a dissecting microscope

with fine forceps. The aorta was sectioned into several segments. These segments were washed in 70% alcohol plus several drops of ammonium hydroxide until all the yellow color disappeared. The segments were placed in 30% sucrose and left overnight at 4^{o}C. Subsequently, the excess solution was absorbed away and the pieces embedded in O.C.T (Optimal Cutting Temperature compound Tissue- Tek, Sakura Finetek, Torrance, CA). The pieces were then sliced in a cryostat (Microtome Cryostat Cryostar HM 560 MV); (10-µm- thick specimens). The specimens were collected on Superfrost Plus slides (Fisher Scientific, Pittsburgh, PA). To view the nuclei of the individual cells in the specimen, the slides were stained with Hematoxylin solution, Gill #2 (Sigma) according the following method (Presnell and Schreibman 1979). The sections were rehydrated with two changes of five minutes each of 100% alcohol followed by 70% alcohol, followed by five minutes of running water. The slides were then dipped ten times in 2% Hematoxylin solution for two minutes each. This was followed by dips in water until the water looked clear. The slides were dipped in 0.3% ammonium hydroxide and rinsed twice again for one minute in water. The blue intensity was then checked under a microscope and the procedure repeated if the stain is too dark or too light to allow permit proper identification of the nuclei. From our prior fluorescent immuno-histochemical work on the aorta, we noticed that the elastin component of the aortic wall exhibited a significant broad-spectrum autofluorescence. We restricted the autofluorescent to one part of the spectrum and to use a suitable fluorescent tag for imaging the epitopes in another region. This was done using the following method (Cowen, Haven et al. 1985; www.uhnresearch.ca/facilities/wcif/PDF/Autofluorescence.pdf 2000) This procedure required incubating the slides containing the samples in 0.5 % Pontamine Sky Blue

6BX(Alfa Aesar, Haverhill, MA) for five minutes followed by washing for five minute in PBS. For the immunohistochemical study, the slides were then incubated in blocking solution (3% goat serum, 0.3%Triton-X, 20mM sodium phosphate, 0.9mM sodium chloride, 0.05% saponin) for 30 minutes followed by three washing in PBS. They were subsequently exposed to rabbit anti-rat AQP1 antiserum (category AQP11-A, Alpha Diagnostic International, san Antonio, TX [ADI]) diluted in PBS plus 3% goat serum, 0.2% bovine serum albumin (Sigma) in PBS for 18 –24 hours. After trying different concentrations, we settled on the primary antibody at a dilution of 1:500 (i.e. 2μg/ml) based on this concentration creating the least amount of non- specific staining with the secondary antibody. The slides were then washed in PBS three times and incubated with Alexa 488 conjugated goat anti-rabbit IgG (Molecular Probes, Carlsbad, CA) at a dilution of 1:50 in PBS for 90 minutes at room temperature. Samples were washed in PBS three times and mounted with Vectashield mounting media for fluorescence (Vector laboratories, Burlingame, CA). Coverslips were securely applied to the samples using clear nail polish. The samples were then kept in the dark to prevent damage to the Alexa 488 tag and subsequently viewed and captured using a Leica TCS SP2 AOBS confocal microscope.

Control Studies

There were two control experiments done in the immunohistochemical study. For the first control, PBS replaced the primary antibody and the experiment was conducted as mentioned before. For the second control, rat AQP1 control/blocking peptide (category AQP11-P Alpha Diagnostic International, san Antonio, TX [ADI]) was used. This

blocking peptide was incubated in an excess of the primary antibody (1:50) and left for 90 minutes at 6^{O}C. This mixture then replaced the primary antibody as in the other control and the immunohistochemical study done as before.

Confocal Microscopy and Image Analysis:

Laser Power Meter

Confocal microscopy was done using a Leica TCS SP2 AOBS confocal microscope. Several cautious preliminary steps were taken in order to properly be able to quantitatively compare confocal images from different animals, different sections of the same aorta and measurements taken at different times or on different days. Firstly before and during every confocal image acquisition, the confocal microscope and its lasers were calibrated and the intensity and settings strictly maintained in order to make certain that each sample observed received the same level of laser power for the same amount of time. All other external conditions such as room temperature, humidity and stray lights etc were strictly monitored. The calibration of the microscope was done using a Coherent Ultima LabMaster Power and Energy Dual-Channel Meter attached to an LM 2 silicon HD visible optical detector wand. A sample was placed on the microscope stage and the embedded tissue was brought into focus using the 40x PL APO N.A.1.25 oil immersion objective. The sample was then removed and replaced by the optical detector in the exact position over the objective. The 488nm Argon laser was then initiated and the detector was shifted around in order to find its "sweet spot," that is where the fullest intensity of the laser is felt. For each different set of samples obtained after immunohistochemistry on

different days, and even for the same set of sample undergoing confocal scanning, the laser settings on the confocal microscope were adjusted periodically to obtain the same calibrated values on the laser meter. This was necessary since several factors such as temperature, humidity and stray lights can influence the intensity of the laser.

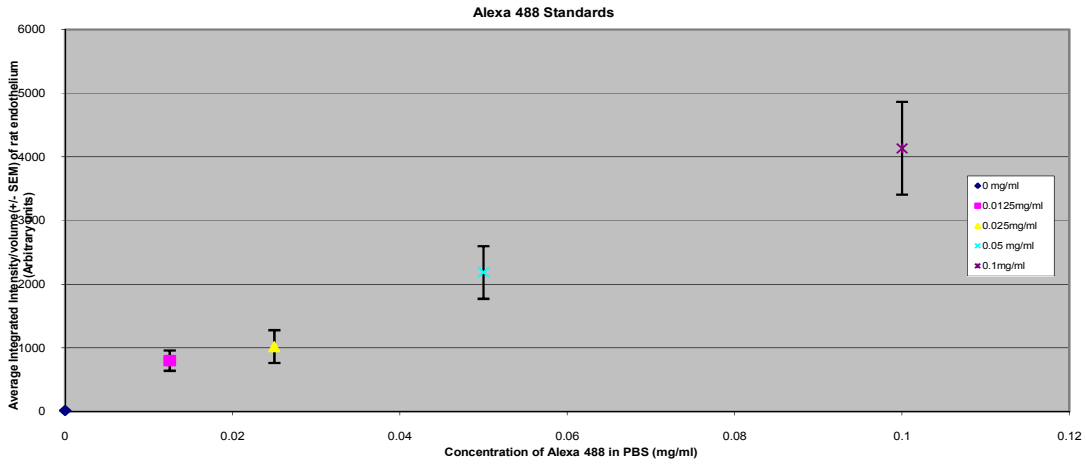

Figure 3: Demonstration of the linear range of integrated intensity/volume aortic endothelium against various concentration of Alexa 488**.** Values are means± SEM. $p<0.05$

The other settings on the confocal microscope were maintained for all samples as follows: scan-xyz, format-1024X1024, speed- 450Hz, average line-1, average frame-4, gain PMT1-725, gain PMT2-529, gain PMT3-0, gain PMT trans-152, offsetPMT1- -6%, offset PMT2-0%, offset PMT-0%, offset PMT trans-17, imageX-93.75imageY-93.75, pinhole (a.u.)-1.00airy, Objective-HCX Pl APO Cs 40x, Sequence- FITC Seq between lines and TRITC wide sequence and #of z-slices-50.

Internal Standards

Internal standards were prepared for absolute quantitative analysis of AQP1

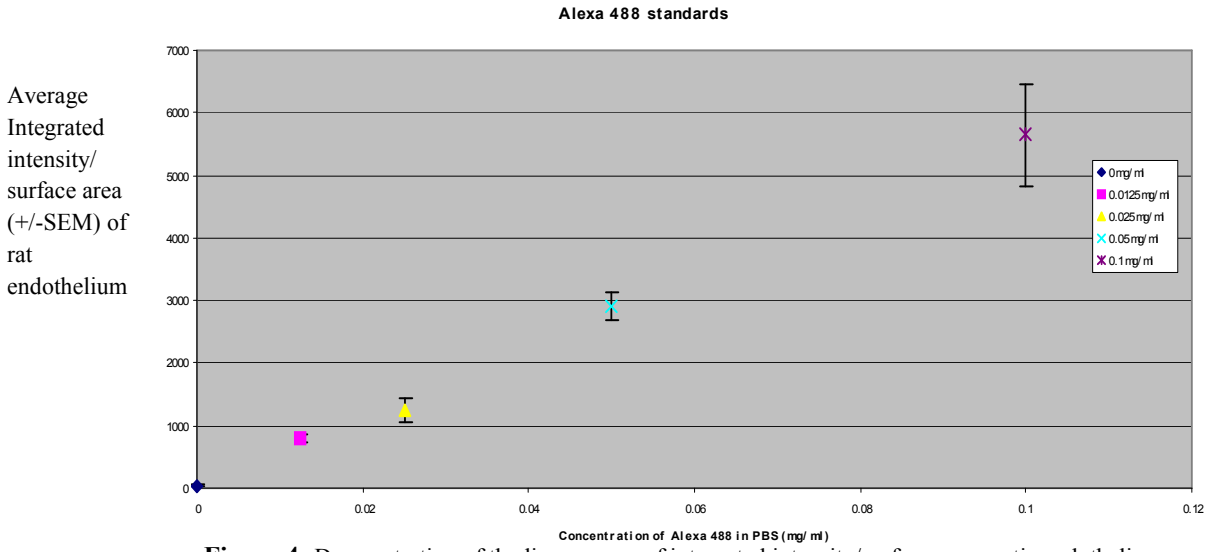

Figure 4: Demonstration of the linear range of integrated intensity/surface area aortic endothelium against various concentration of Alexa 488. Values are means± SEM. $p<0.05$

secondary antibody concentrations in the following manner. Samples were prepared exactly as mentioned in the methods section, except that different concentrations (0-0.1mg/ml) of the secondary antibody were left on individual slides containing tissue samples. Coverslips were applied and then sealed with clear nail polish. These standards were then subjected to the same confocal settings previously described using the 488nm Argon laser. This ensured that the internal standards underwent exactly the same procedure as the experimental samples. Figures 3 and 4 demonstrate a strict linearity between concentration of Alexa 488 used for the standards and its fluorescent intensity

per unit volume and area of endothelium respectively obtained by the confocal microscope.

Custom Software

The z slices of both the internal standards and those that will be used for quantification in later studies were analyzed using a specially-coded custom software that uses active contours or snakes to find the boundaries of objects in an image (Kass, Witkin et al. 1998). This software tightly outlines and encloses the region corresponding to the endothelium, of intense green staining beyond the IEL in each of the confocal sections/images of the confocal z-stack taken of the aorta. It then integrates the intensity of the Alexa 488 fluorescence enclosed in this region and calculates the perimeter and area of the enclosed region. Simpson's rule is used to calculate integrated intensity, the total surface area and the total volume of the z stack region of the aortic endothelium. We thank Mr. Hadi Fadaifard and Professor George Wolberg both of Department of Computer Science at City College of the City University of New York for working with us on this program.

Statistics

Paired students t-tests were used to compare Alexa 488 mean integrated intensity per unit volume and per unit surface area values for Goldblatts and for the various controls. $P<0.05$ was used as the criterion for statistical significance. Values are means ± (SEM).

Absolute AQP1 Values

As shown in the appendix, a back of the envelope calculation estimates the AQP1 concentration per unit surface area of the endothelium of the SD rats controls used in this study as ~2826/μm^2. Based on the manufacturer's advice of both the primary (rabbit anti-rat AQP1 antiserum) and secondary (Alexa 488 conjugated goat anti-rabbit IgG) antibody binding, it was accepted from the manufacturer of the antibodies that the primary antibody binds to both the AQP1 and the secondary antibody in a one to one ratio. Based on these manufacturer's reported binding ratios, AQP1 concentration values based on Lp data and the internal standards that show a linear relationship between the secondary antibody concentration and Alexa fluorescence, the absolute AQP1 concentrations as a function of pressure can be predicted.

III. RESULTS

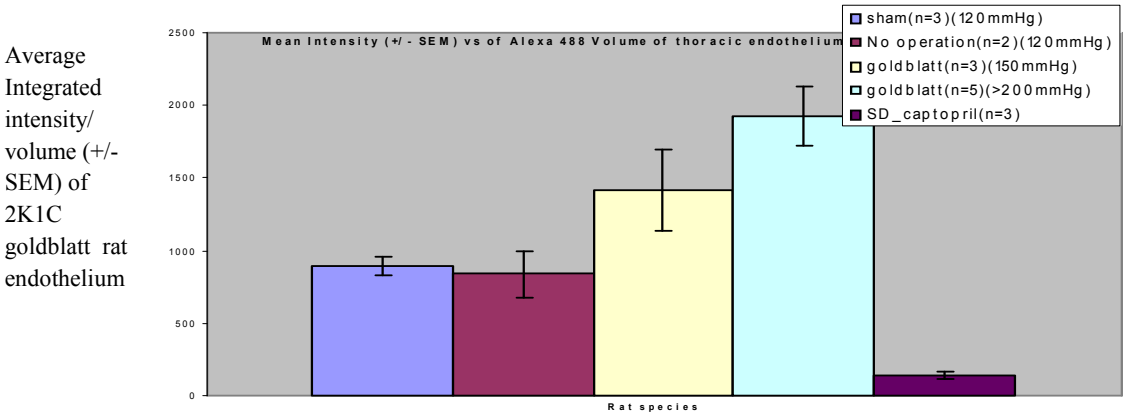

Figure 5: Mean integrated intensity/volume of aortic endothelium for 2K1CGoldblatt rats with systolic blood pressure at ~150mmHg, >200mmHg, those reverted to normotensive values (~125mmHg) with antihypertensive captopril treatment and control sham operated and non-operated rats. Values are means ± SEM. ($p<0.05$)

The systolic blood pressures of about 60% of the 2K1C rats used in this study were typically elevated (~140mmHg) between two to three weeks after surgery. This is similar to results seen by other investigators using similar sized clips (Owens and Schwartz

1983). These animals became fully hypertensive (<200mmHg) between five to six weeks after surgery as shown in figure1. Animals reverted to normotensive systolic blood pressure values (~120mmHg) between 2-4 weeks when subjected to Captopril treatment after elevated hypertensive values of 140mmHg. Figures 5and 6 respectively show the mean integrated intensity of Alexa 488 fluorescence per unit volume and per unit surface area of the thoracic aortic endothelium for each of the following sets of rats: 1) 2K1C Goldblatt rats with systolic blood pressure at ~150mmHg, n=3; 2) 2K1C Goldblatt rats with systolic blood pressure at >200mmHg, n=5; 3) 2K1C Goldblatt rats with systolic blood pressure reverted to normotensive values (~125mmHg) with treatment with the antihypertensive captopril, n=3; and 4) rats that had undergone control sham operations and age-matched rats that had not undergone any operation, n=5. Note that group 4 lumps two sets of rats together. This is because the sham-operated rats show very similar AQP1-values as the non-operated rats in these figures. Based on a rough back of the envelope calculation as shown in the appendix using Lp measurements conducted in our lab,

Average Integrated intensity/ surface area (+/-SEM) of 2K1C goldblatt rat endothelium

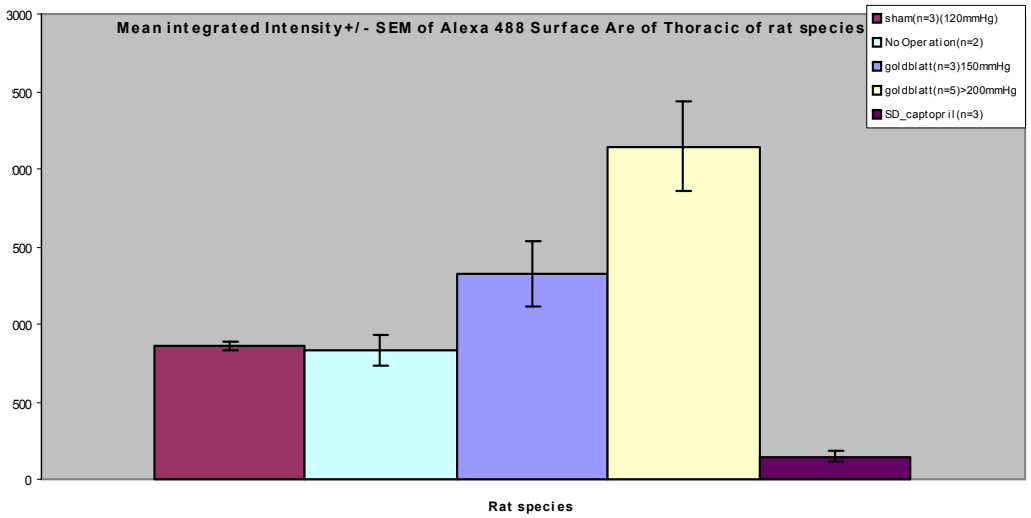

Figure 6: Mean integrated intensity/surface area of aortic endothelium for 2K1CGoldblatt rats with systolic blood pressure at ~150mmHg, >200mmHg, those reverted to normotensive values (~125mmHg) with antihypertensive captopril treatment and control sham operated and non-operated rats. Values are means± SEM. ($p<0.05$)

Rat	AQP1x10^{12}/surface area endothelium (cm^2)	AQP1x10^{14}/volume endothelium (cm^3)
Sham / No Operation	0.3 / 0.3	4.55/4.28
2K1C (~ 150mmHg)	0.48	7.22
2K1C (>200mmHg)	0.78	9.83
Captopril treated	0.05	0.68

Table 2: Estimated Absolute AQP1 values for different rat models

manufacturer's reported antibody binding and the internal standards shown in this thesis, we have been able to estimate the concentration of aortic endothelial AQP1 found in the sets of rats used in this study. These are shown in table 1.Two weeks after the Goldblatt surgery, the blood pressure in the 2K1C Goldblatt rats increases to ~150mmHg and there is an increase in Alexa 488 mean integrated intensity of up to 59± 28% per unit surface area and 59±32% per unit volume endothelium over the controls. At blood pressures

greater than 200mmHg, approximately six weeks after the operation, the Alexa 488 mean integrated intensity increases by 62±27 % per unit surface area and 36±24% per unit volume over the 150mmHg blood pressure animals. Interestingly, the captopril-treated hypertensive rats however, show Alexa 488 mean integrated intensity values that are not just not elevated relative to, but in fact significantly lower than the shams and the non-operated rats. These values are 134 ±36 per unit volume and 147 ± 35 per unit surface area. See discussion on this point.

Quantitative Immunohistochemistry vs 2D SDS-PAGE/Western Blot

Several methods are presently in use to separate, detect and quantify proteins. Those for separation include several chromatographic methods (affinity chromatography, ion-exchange chromatography, reversed phase chromatography), ultracentrifugation and gel electrophoresis. These are then coupled several detection techniques, such as Western blots where the protein of interest can then be analyzed quantitatively. Of the aforementioned techniques, gel electrophoresis, the most common type being 2D SDS-PAGE/ Western Blot, remains the most established universal method of choice (Issaq, Conrads et al. 2002). Quantification analysis using Western blots and immunohisto-chemistry is identical in nature. With Western blot, proteins are first separated during the 2D SDS-PAGE stage in a gel matrix based on their isoelectric points and masses. They are then transferred as bands to an absorbent membrane, the most common being PVDF and nitrocellulose, where molecular probes such as antibodies can detect their presence. Subsequently images of these bands, obtained from a secondary antibody, conjugated to a photoluminescent marker, can be captured and the proteins quantified based on their

densitometric difference and comparison with standard molecular weight markers (Kurien and Scofield 2003). In a similar vein, as previously shown, confocal images of immuno-tagged proteins that undergo the identical immunohistochemistry processes can also be quantified based on their intensity levels.

Although 2D SDS PAGE/western blot is the "gold standard" for quantifying proteins, it does have some inherent disadvantages that we took into consideration in deciding on our method of choice. Western blots efficiency are affected by two main factors, one being the elution efficiency of a protein from the gel matrix to the nitrocellulose membrane and the other being the efficiency at which the protein binds and remains on this membrane. Several modifications such as pressure double blotting, tissue printing and electro double blotting have been used to address these problems and improve this technique; however, they add to the complexity of the (Kurien and Scofield 2003). A second issue that became relevant to us, was the concentration of protein commonly used in the 2D SDS-PAGE/ Western Blot method. A review of the literature showed a wide range of cell concentrations (10^6 to 10^9 cells) used for this method (Burnette 1981; Hall, Ostedgaard et al. 1998; Barton and Medzhitov 2002). Based on this, we calculate (based on a rat aorta's inner diameter of 2mm, with 500 μm^2 EC's)(Pereira, Bezerra et al. 2004; Shou, Jan et al. 2006) that each vessel has ~ 300,000 EC and taking into consideration that there will be EC loss during cell harvesting, we will need a minimum of at least five aortas per data point if we were to use this technique; which amounts to an unreasonably large number of animals. In our opinion, this would pose ethical issues.

Another matter of concern for us was the type of information that we were interested in extracting from our chosen method. In addition to investigating the difference in aortic

endothelial cell AQP1 expression between chronically hypertensive and normortensive models, we would also like to examine the statistical distribution of measurements in different regions, chosen randomly, of a single animal's thoracic aorta and between animals that underwent the same treatment. The Western blot preparation pools a large number of cells, lyses them and quantifies the protein in the lysate. As such, it does not provide this information on regional variation. Moreover, it is well-known (and we have confirmed above) that aortic smooth muscle cells (SMCs) express AQP1 avidly. As such, when removing the endothelial cells from the test rat aortas, one must be extremely careful to completely segregate out all SMCs from the endothelial cell preparation, because even a small number of residual SMCs can contaminate the AQP1 expression results. Finally, as noted, we are interested in verifying the plausibility of AQP1 forming a pathway for water transport through an endothelial cell, which requires us to see if and how AQP1 is distributed through the endothelial cell, e.g., if it is present on both the luminal and abluminal cell membranes. Clearly this information is not available from the lysate. In contrast, *in situ* immunohistochemistry, avoids the SMC contamination information and lends itself to the AQP1 spatial distribution, since one can look at regions of just a few cells, one can spatially map the AQP1 concentration in three-dimensions and can easily ascertain that one is indeed measuring the AQP1 content of an endothelial cell. We therefore opt from quantitative immunohistochemistry, rather than separation followed by Westerns.

Figures (1-5) show histograms of the aortic Alexa 488 intensity per unit area of rat thoracic aortic endothelium. Each figure represents six regions/confocal stacks per rat times the number of rats of the given species and pressure used at the given conditions,

for the various rat model used. These are indicative of the distribution of AQP1 concentration and distribution. Figures 6 and 7 show two such distributions for individual rats. First notice that these latter two figures are classic in shape, whereas the pooled data in figures 1-5 have a pronounced skewness, with a concentrations of points about a mean, augmented by a tail of points of higher total intensity. Table 2 summarizes the statistical data for the histograms in Figures 1-5. All the data show positive skewness with the bulk of distribution concentrated on the left the figures (1-5), with the partial GBs having the highest right skewedness, followed by the non operated SD's, WKYs, SHRs and fully GBs. Such distributions are reminiscent of what one sees in quantitative stereology (Underwood 1970; Wiebel 1980). In those cases, one looks at random thin sections of the IEL and at the distribution of fenestral lengths found in those sections. Since the fenestral holes can vary in size and since each fenestral hole intersected by each section is a random chord through that hole which is unlikely through its diameter, one needs some theory to extract the likely distribution of actual fenestral hole diameters. As it turns out the distribution of these chord lengths has a shape similar to that found in Figures 1-5. Perhaps there is an analogy between the random sections in their work and the random regions of the thoracic aorta chosen here, and of the individual fenestral holes there and the individual animals here? Clearly such an analogy, if reasonable, still needs to be fleshed out.

As noted already, the means indicates that the SHRs appear to express ~ three times the amount of AQP1 as the WKY's., whereas the fully Goldblatts express up to two and a half times the non-operated Sprague Dawleys. The partial Goldblatts show an

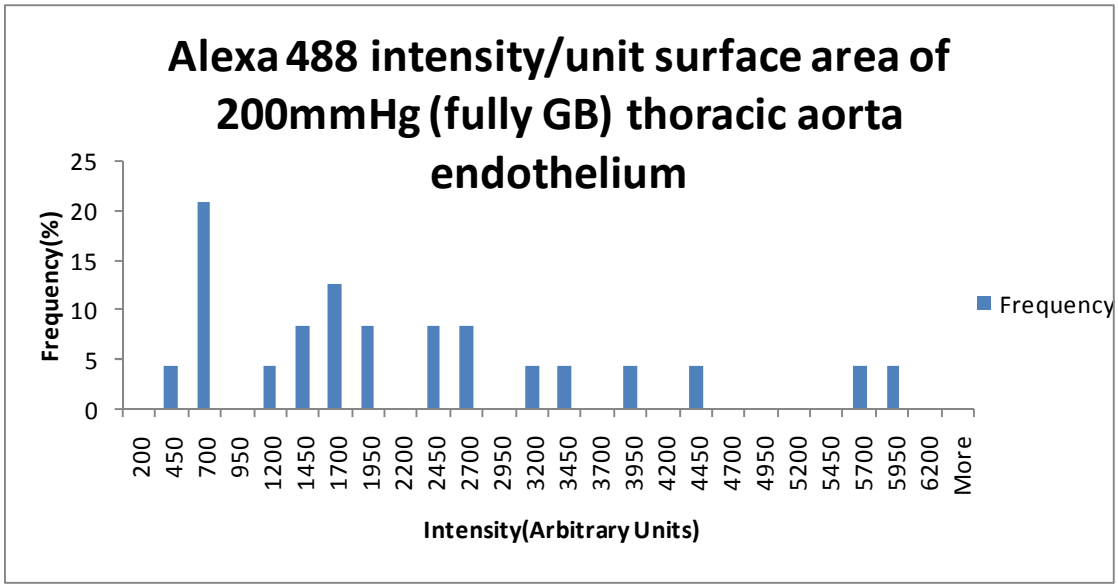

Figure 7: Histogram of Alexa 488 intensities/unit surface area of fully Goldblatt SD rat thoracic aorta whole endothelium for 6 regions in 4 rats each

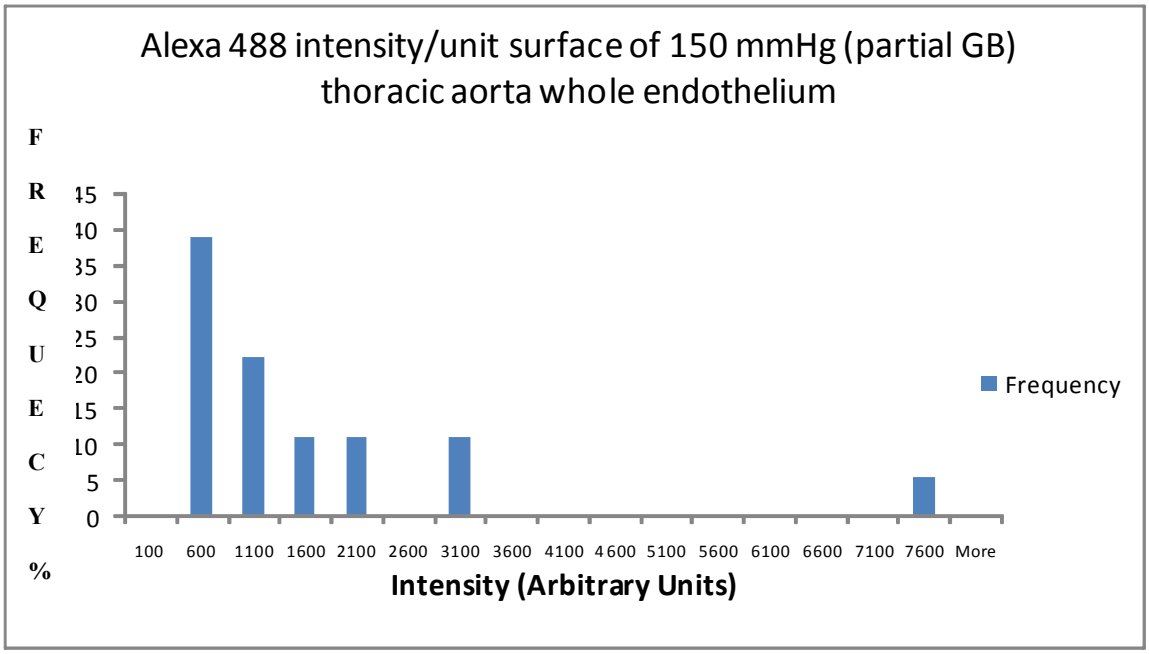

Figure 8: Histogram of Alexa 488 intensities/unit surface area of partial Goldblatt SD rat thoracic aorta whole endothelium for 6 regions in 3 rats each

intermediate expression between the controls and the fully Goldblatt animals. The SEMs of all means for the data reported are quite reasonable.

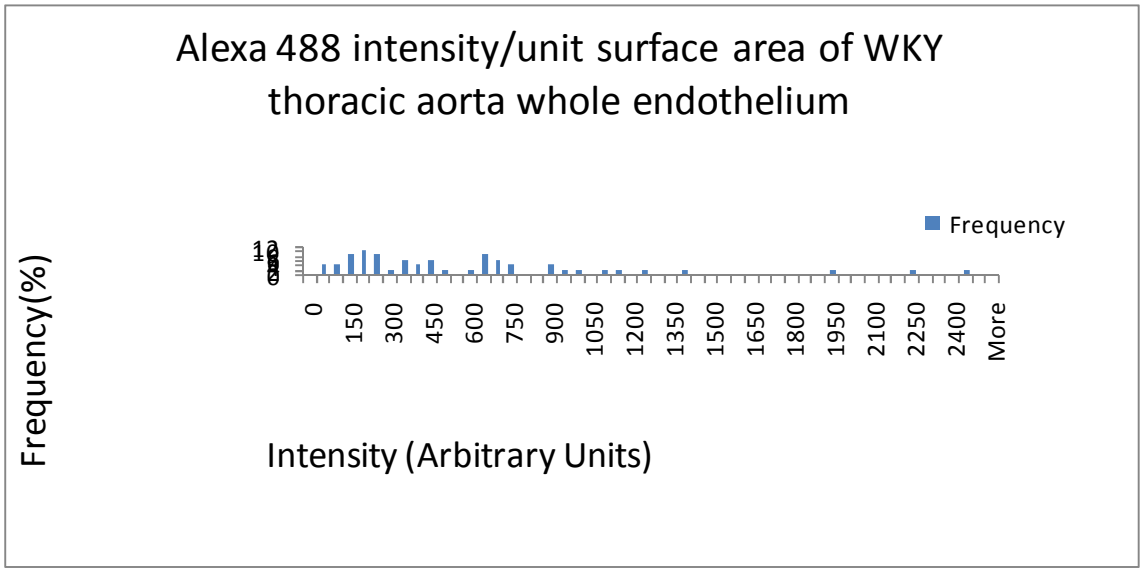

Figure 9: Histogram of Alexa 488 intensities/unit surface area of WKY rat thoracic aorta whole endothelium for 6 regions in 8 rats each

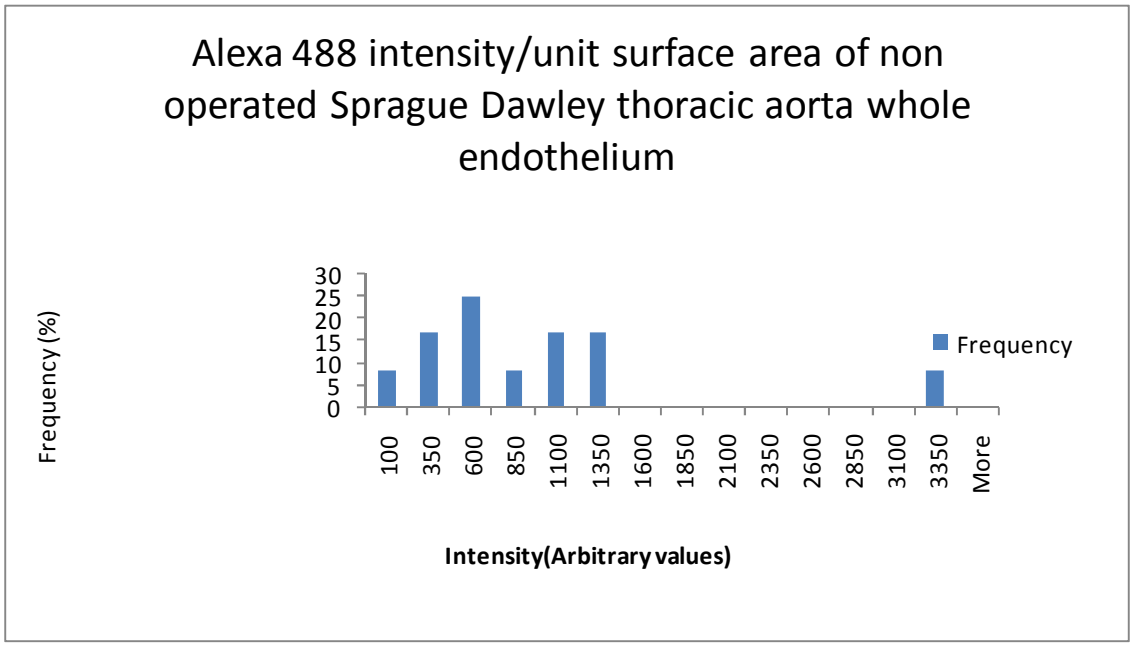

Figure 10: Histogram of Alexa 488 intensities/unit surface area of non- operated rat thoracic aorta whole endothelium for 6 regions in 2 rats each

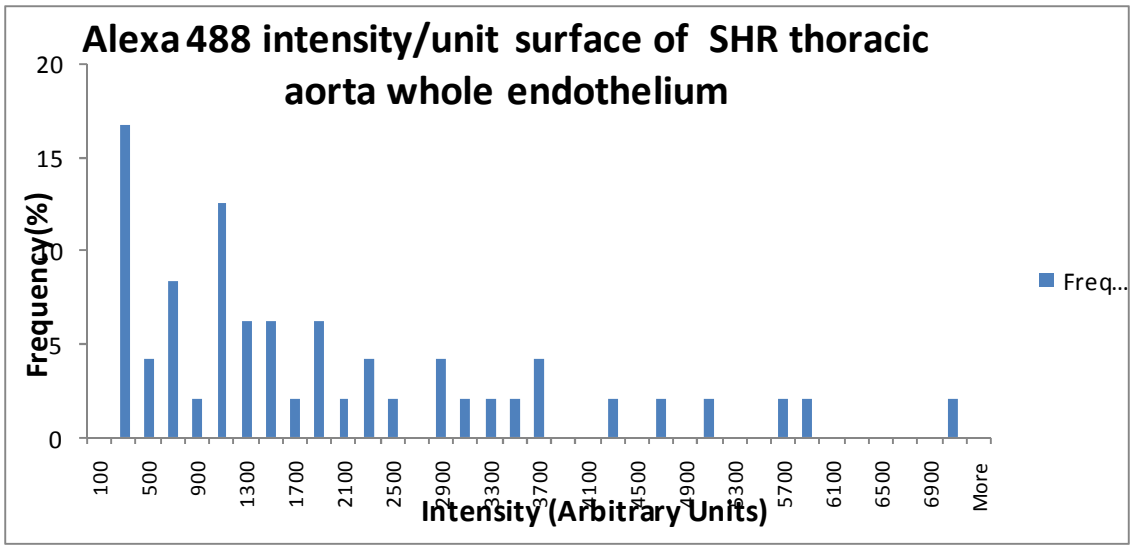

Figure 11: Histogram of Alexa 488 intensities/unit surface area of SHR rat thoracic aorta whole endothelium for 6 regions in 8 rats each

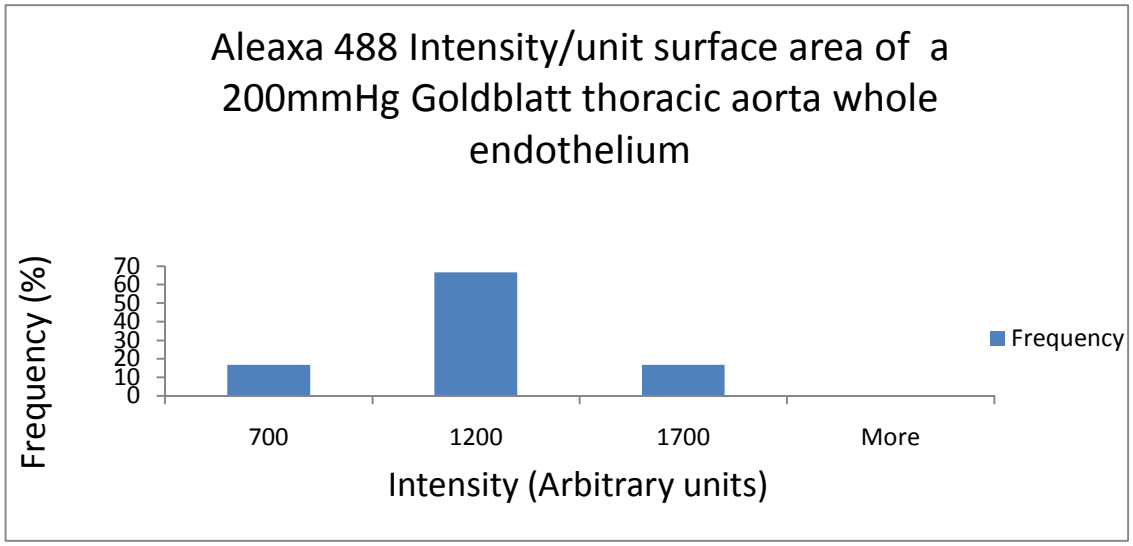

Figure 12: Histogram of Alexa 488 intensities/unit surface area of one fully GB thoracic aorta rat whole endothelium for 6 regions

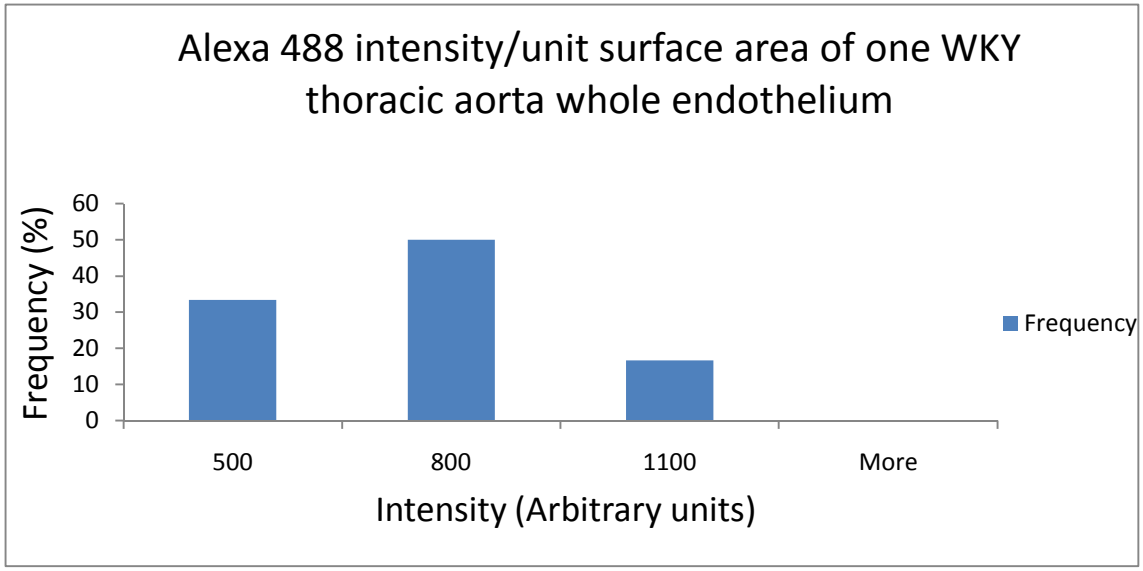

Figure 13: Histogram of Alexa 488 intensities/unit surface area of WKY thoracic aorta rat whole endothelium for 6 regions

Statistics	Rat Models [# of rats] **[#of regions x # of rats]**				
	SHR n=8 **48**	WKY n=8 **48**	Fully GB n=4 **24**	Partial GB n=3 **18**	Non Op SD n=2 **12**
Mean	1870	579	2145	1348	833
SEM	241	78	315	387	241
Skew	1.27	1.79	1.01	2.86	2.17

Table2: Statistics showing mean, SEM and skewness of Alexa 488 intensities/unit surface area of several different rat thoracic aorta rat whole endothelium.

IV. DISCUSSION

Pressure-driven transmural water transport advects LDLs from the blood across the endothelium, spreads them out and dilutes and flushes them from the subendothelial intima. These latter processes likely directly drastically slow the kinetics of their binding and accumulation to SI ECM. The nature of this convective water flux is therefore critical to the prelesion events of atherosclerosis and our focus is on the potential role of a water-specific (Fushimi, Uchida et al. 1993; Zeidel, Nielsen et al. 1994; Mulders, Preston et al. 1995; Raina, Preston et al. 1995; Ishibashi, Kuwahara et al. 1997; Nielsen, King et al. 1997; Ishibashi, Kuwahara et al. 1998; Beitz and Schultz 1999; Koyama, Yamamoto et al. 1999) AQP1-mediated transcellular pathway that complements the well-documented paracellular route.

In chapter 2, we showed that the thoracic aortic endothelial cells of several species of rats express AQP1 and do so throughout their ECs. Complementary studies in our group showed that blocking or knocking down AQP1 expression in these cells reduces both monolayer and whole vessel hydraulic conductivity. In chapter 3, we quantified and investigated the distribution of AQP1 in normotensive Wistar Kyotos (WKY) and in their genetically hypertensive variant SHRs. We found that SHRs express 3-4 times as much AQP1 as their normotensive cousins. Here we investigate if the rat aortic endothelium can actively upregulate its expression of AQP1 in response to changes in chronic transmural pressure, as induced by chronic hypertension by using the non-genetically modified normotensive and 2K1C male Sprague-Dawley rats. First, figures 3 and 4 establish that our immunohistochemistry is indeed quantitative. Moreover, it allows us to convert arbitrary fluorescence units into absolute concentrations of the fluorophore

Alexa-488, which tags our AQP1 secondary antibody. To convert this value to absolute AQP1 values we have used various conversion factors provided to us by the manufacturer of the antibodies. The aggregate result is fluorescent unit/AQP1/volume endothelium: fluorescent unit/AQP1 surface area endothelium is 1:0.3.

Figure 1 show the progression of rat blood pressure as a function of time after the Goldblatt procedure compared with that of sham animals. It shows that the blood pressures (BP) of Goldblatts increase from normal to fully elevated over approximately a period of six weeks. This characteristic time scale of BP changes is far longer than the characteristic time scale (10' s of days) of protein turnover (Walsh and Wright 1995). Thus one would expect the AQP1 number at any given BP to be the rat's quasisteady value consistent with that chronic BP. Figures 5 and 6, the per unit volume and per unit area AQP1 concentrations at different chronic rat BPs, are our main results of this section. Comparing the first three bars, normotensive, partially elevated and fully elevated BP, we find these numbers show a clear trend of increasing AQP1 numbers as a function of increasing chronic BP, with rats whose systolic BP over 200mmHg expressing over twice the AQP1s per unit volume as the normotensive ones. The Goldblatts with systolic blood pressure over 200mmHg express about 1.3 times as many AQP1 per unit volume as the SHRs. This may have at least two causes. First there is the obvious difference in strain of rat, and each strain may exhibit slightly different AQP1 concentrations at similar BPs. The second is that the systolic blood pressure of the age-matched SHRs used in this study was about 175mmHg, which is lower than the >200mmHg of the 2K1C Goldblatt SD rats. From the linear regression of figure 4, the predicted AQP1 value for 2K1C Goldblatt SD rats at 175 mmHg is

$0.62x10^{12}$AQP1molecules/ surface area (cm^2) of endothelium, which is quite similar to the actual value of $0.46x10^{12}$AQP1molecules/ surface area (cm^2) of endothelium for the SHR. Interestingly, our observed AQP1 increase in the SD/ SD-Goldblatt system was a factor of 2.5, very similar to the 3-4 factor observed in the WKY/SHR system. As a further control in addition to the shams and the rats that did not undergo any operation at all, we also chemically reverted 2K1C SD-Goldblatts whose systolic BP had already risen to a ~150mmHg and clearly showed (Figure 2) that they were on track to become fully hypertensive back to normotensive values using the antihypertensive drug captopril (Kopecky, Thomas et al. 1987). Interestingly, these rats showed AQP1 values that not only were not elevated, but were actually even *lower* than the other normotensive controls. This suggests that the drug itself may have a direct effect on the AQP1 expression, independent of its BP control. After an extensive literature search, we found that another ACE inhibitor decreases AQP1 expression (Imai, Nakamoto et al. 2001). Since diuretics, by directly affecting water retention, conceivably might also directly affect AQP1 expression, we are in the process of redoing these controls using two candidate drugs, one of which is a beta blocker. Beta blockers work by a completely different mechanism that affects the intensity of heart pumping, rather than on water transport. It is therefore conceivable that it may not directly affect AQP1 expression, except via its affect on BP.

Assuming this control is successful, we shall conclude that the rat thoracic aortic endothelium indeed actively upregulates its AQP1 expression in response to chronic hypertension.

It has been well established that susceptible vessels undergo remodeling in response to the onset of hypertension. This remodeling involves the hypertrophy of smooth muscles cells of the media of arteries resulting in medial thickening. It also involves the proliferation of these cells into the intimal layers of these vessels where lesions are known to be formed (Wolinsky 1972; Owens, Rabinovitch et al. 1981; Owens and Schwartz 1983; Mulvany 1993; Mulvany 1993).These morphological changes probably occurs in these vessels to resist the greater pulsatile forces and as a result of this increased vascular resistance it is believed that it also helps to continue to maintain the hypertensive state (New, Chesser et al. 2004). It has also been well documented that a variety of cell types including SMCs and ECs of these arteries produces nitric oxide (NO) from L-arginine (Palmer, Ashton et al. 1988). NO has also been implicated in the inhibition of SMC proliferation, contractibility and medial thickening (Garg and Hassid 1989; Rudi and Alexander 1990; Hansson, Geng et al. 1994; Yasa, Kerry et al. 1999) as seen in vessel remodeling during hypertensive conditions. It has also been observed that NO produced by EC has an inhibitory effect on the NO produced by SMC (Lopez Farre, Mosquera et al. 1996).The pathways by which NO is transport across cell membranes have not been fully elucidated and it has generally been accepted that it freely diffuses across them without the need for a specific transporter. Herrera et al, however confirmed that AQP1 in addition to being a water pore, also transports NO (Herrera, Hong et al. 2006). These findings do have huge implications on our work. Firstly if the endothelium does in fact upregulate its AQP1 in response to chronic BP and since Lp studies confirm their functionality, we should expect that Lp_{e+I} in the hypertensive rats to be higher than the normotensive animal since there will be more EC water pores available in the

hypertensive animal for transendothelial water flow. This has been confirmed by Dr. Nygugen in our lab and shown in table 3.

Lpe+i x 10^{-8} cm/s/mmHg			
	n	100 mmHg	140 mmHg
SD-2K1C	6	4.49 ± 1. 83	5.66 ± 2.31
SD Normotensive	6	3.97 ± 0. 34	4.61 ± 0.58

Table 3: A comparison of the endothelial conductivity (Lpe+i) in normotensive (Sprague Dawley (SD)) and hypertensive rat (SD-2K1C). Values are means± SEM. $p<0.05$

Because vessel remodeling during hypertensive conditions affects the filtration properties on the vessel wall by increasing its hydraulic resistance, we hypothesize that the vessels attempts to oppose this effect by upregulating its AQP1 expression in order to increase the transmural transport of water. This enhanced water transport can have serious implications for early atherosclerosis since it can have either of two competing effects. Firstly, it can dilute the local LDL concentration at leakage sites and also wash them from the intima and secondly, it can also enhance binding of the LDL to the ECM by spreading them out in the subendothelial endothelium as mentioned above. AQP1 upregulation can also potentially increase NO transport, which as mentioned before should hinder the deleterious effect of vessel remodeling such as SMC proliferation, hypertrophy and contractability. Since the onset of hypertension causes an increase in pressure that compresses the intima, the enhanced expression of EC AQP1s recognized during this condition also increases the available pores available for water transport. This

enhancement works to inhibit this pressure build up by decreasing the force per unit area on the endothelium thus relieving the endothelium of the pressure effects such as the compaction of the intima and the blockage of the fenestral holes. It is conceivable to believe that when faced with the hypertensive state, the vessel attempts to homeostatically revert to its original compacted intimal state as was in the normotensive environment. Chronic hypertension and protein regulation as we have mentioned, occurs with different characteristic time scales with the latter occurring at a much faster pace than the former. This motivates us to use existing or attempt to discover the underlying biological mechanisms to explain this phenomenon. In the following chapter we will attempt to build a simple steady state kinetic model using these mechanisms. If this model is successful, we should be able to predict both new and useful steady state and dynamic information under different pressure conditions

V. SUMMARY

Hypertension is a known risk factor for atherosclerosis and it is reasonable to suspect that, in the absence of extensive vessel wall remodeling, the higher the transmural pressure, the greater the convective macromolecular transendothelial transport. In Chapter 3 we showed that the aortic endothelial cells of chronically hypertensive express far more AQP1 than those of their normotensive cousins. In order to eliminate the possibility that this change in aquaporin number was a direct effect of the genetic differences between the variants and not due directly to their difference in chronic transmural pressure, we have repeated this study using non- genetically modified

chronic hypertensive rat model and controls. Again, the goal is to investigate whether chronic hypertension can cause an upregulation of endothelial AQP1 concentration. Our longer term goal is to attempt to understand AQP1's possible functional role in the atherosclerotic process.

We used 2K1C Goldblatt rats with systolic blood pressure 1) at ~150mmHg (labelled "partial GBs"); 2) greater than 200mmHg ("fully GB"); 3) that had reverted to normotensive values (~125mmHg) due to treatment with Captopril; 4) that remained normotensive because they had undergone only control sham operations; and 5) those that were normotensive because they had not been operated on. We analyzed the abdominal aorta of each animal using quantitative immunohistochemistry coupled to confocal microscopy and image analysis. This study showed a clear trend of increasing AQP1 numbers with increasing chronic BP. Comparing different rat strains, we find that the Goldblatts with systolic blood pressure over 200mmHg express about 1.3 times as many AQP1 per unit volume as the SHRs. We found that aortic ECs from SD-Golblatts expressed 2.5 times AQP1 as do those of normotensive SDs, very similar to the 3-4 factor that we observed in the WKY/SHR system. Histograms of the aortic Alexa 488 intensity per unit area of rat thoracic aortic endothelium were constructed for individual and pooled rat data and statistical analyses done on them. All the pooled data showed positive skewness with the bulk of distribution concentrated on the left of the histograms. The partial GBs having the highest right skewedness, followed by the non-operated SD's, WKYs, SHRs and fully GBs. This gives us an idea of the lack of symmetry of their distribution, hence the deviation of the data from the mean.

APPENDIX

Based on the standard assumption that the vessel layer resistance (1/Lp) add as does linear resistances in series (Tedgui and Lever 1984):

$$\frac{1}{Lp_t} = \frac{1}{Lp_{e+i}} + \frac{1}{Lp_{m+I}}$$

We are able to extract the contribution of the endothelium $1/Lp_{e+I}$ to the total resistance $1/Lp_t$. $1/Lp_{m+I}$ is the contribution of the resistance due to the media and the IEL. Dr. Tuevi Nguyen from our lab, measured LpΔP of the thoracic aortic endothelial AQP1 of male SD rats. She then took these vessels and blocked the AQP1 using $HgCl_2$ and again measured their Lp. It is assume that water is transported transendothelially through junctions and AQP1s, however when these vessels are incubated in $HgCl_2$ and the AQP1 blocked, water is expected to only travel through the junctions of the endothelium. We can use this difference i.e $Lp_{e+i}\Big|_{unblocked}$ - $Lp_{e+i}\Big|_{blocked}$ to get the contribution due to the AQP1. From her work,

$Lp_{e+i}\Big|_{unblocked} = 2.5 * 10^{-8}\ cm^3\ s^{-1}\ mmHg$

$Lp_{e+i}\Big|_{blocked} = 1.2 * 10^{-8}\ cm^3\ s^{-1}\ mmHg$

$Lp_{AQP1} = 1.3 * 10^{-8}\ cm^3\ s^{-1}\ mmHg$

Since Lp_{e+I} ~Lp_e (relaxed intima)~ Lp_{e+I}(60mmHg) and the luminal and abluminal layers of the EC are in series and these resistances (1/Lp) add in series, we can use this to calculate the AQP1 on both layers as

$$\frac{1}{Lp_e} + \frac{1}{Lp_{lu\min al}} + \frac{1}{Lp_{ablu\min al}}$$

$$Lp_{lu\min al} = Lp_{ablu\min al} = 2.6\text{x } 10^{-8} \text{ cm}^3\text{s}^{-1}\text{mmHg}$$

As explained previously in chapter 2 $Lp_{AQP1(SD)} = n_i lp/m$, we find that n_i/m ~ $0.3\text{x}10^{12}$AQP/cm^2~12-14x10^5 AQP/cell-AQP- layer~4-5 times the estimate for the number of AQP1 in red blood cells (~2x10^5) (Zeidel, Ambudkar et al. 1992). If we take m=2, that is luminal and abluminal, we find that each layer has ~ 6-7x10^5 AQP1. We must note that the ratio of the enface surface area of RBC:EC is 135μm^2:520μm^2(Chen, Jan et al. 1997), therefore the estimate for AQP/layer is pretty comparable. Rat aortic cell volume has been estimated to be ~3500μm^3 (Armitage, Lakasing et al. 2005). We can now use this information to convert per volume units to absolute values as shown in table 1.

CHAPTER 5: A KINETIC MODEL OF AQUAPORIN-1 EXPRESSION AND REGULATION

I. INTRODUCTION

The *central dogma* as expressed by Francis Crick several decades ago has remained one of, if not the most important fundamental principles in, modern day molecular biology. It states that DNA produces RNA (transcription), which, in turn, codes for protein production (translation), but not the other way around (Crick 1958; Crick 1970). The DNA (genotype) that one inherits is eventually converted to the proteins that depict the observable characteristics or traits (phenotype) of the organism with, RNA serving as an intermediate. This idea, however, has had its challenges with the discovery of reverse transcriptase, which produces DNA from an RNA template (Temin 1976; Baltimore 1995). All somatic cells contain two complete sets of the genome that is the hereditary information encoded in DNA needed for producing all the proteins the cell needs (Brown and Brown 2002). Not all proteins are required at all times; therefore it becomes critical to explore how selective gene expression is regulated in order to control this function. The fundamental role of transcription, the production of RNA from DNA, in the gene expression process, also brings to bear the tantalizing possibly of it serving as a regulatory point for the control of gene expression in response to certain signals. This does not contradict data that suggest that several downstream regulatory points such as the rate of mRNA transport from the nucleus to the cytoplasm, the stability and frequency of translation in the cytoplasm and other post-translational regulatory mechanism may also exist (Darnell 1982).

Several authors as discussed below have studied the transcription mechanism as a control point for gene expression. Odom et al identified transcription factors HNF4α, HNF1α and HNF6 that occupy target genes in tissue culture of both human liver hepatocytes and pancreatic islets cells using genome-scale location analysis. They found that the genes that are complexed with these factors encode products that are widely important to the normal biochemical functioning of the cells of both of these organs. They concluded that these factors form regulatory networks and mutations among them can affect hepatic functions such gluconeogenesis and pancreatic functions resulting in diabetes mellitus (Odom, Zizlsperger et al. 2004).

The direct and indirect connections made between sensory and motor neurons are known to play an extremely important role in the control of motor skills functions (Shinoura, Suzuki et al. 2005). Arber et al used wild type mice and identified the transcription factor ER81, expressed by these two types of neurons. They then used mutated ER81 mice and studied the effect of this gene on the connectivity of these neurons, from whence the motor coordination of these animals arises. They found that, although these mutated animals' neurons develop normally, they experience a gross reduction in the connections between their neurons and these animals suffer from severe motor discoordination (Arber, Ladle et al. 2000). Prion proteins are widely expressed in several diverse tissues. Prion diseases are believed to result when these proteins form misfolded pathogenic variants, which results in a decreased α-helical and an increased β-sheet content (Uversky and Fink 2006). Copper has been shown to regulate the expression of prion proteins in rat primary hippocampal and cortical neurons (Varela-Nallar, Toledo et al.

2006). Prion proteins bind to copper with high affinity and a functional role has been suggested for this observation (Jackson, Murray et al. 2001).

Bellingham et al identified and studied the transcription factors SP1and Metal Transcription factor-1 and their effect on regulating human prion gene expression during copper homeostasis. They found that, in the presence of extracellular copper that can be toxic to cells, these proteins become upregulated. This finding supports a regulatory role for these factors, which suggests potential therapeutic approaches to the prevention of this disease (Bellingham, Coleman et al. 2009). Over the years, several general frameworks have been proposed to mathematically model gene expression. Some of the more common approaches include Boolean networks, the Bayesian networks, logical networks and ordinary differential equations (ODEs) models. For a review see (de Jong 2002). Chen, He et al (1999) used ODEs to model gene expression from a set of hypothetical temporal data. They used kinetic equations to model both the transcription (DNA to mRNA) and translation phases (mRNA to Protein). They also incorporated a feedback loop from the translation products back to transcription and a degradation rate for proteins and mRNA. They used two methods to construct their model, one being the Minimum Weights Solution to Linear Equations (MWSLE) and the other, a Fourier Transform for Stable System (FTSS). They found that the MWSLE does not contain a time delay between transcription and translation, and this drastically simplified the problem. In fact, even when they incorporated such a delay, no additional interesting conclusions emerged. They found that the FTSS was limited by the fact that it assumes gene expressions are periodic in all cell cycles; this assumption however does not hold for all genes(Chen, He et al. 1999).

Veflingstad and Plahte (2007) used sigmoidal functions to model steady state protein expression levels. This is known as the steep sigmoidal approach. They postulated that the concentration level of a gene's transcription factors is the point at which regulatory processes ratchet a gene's activity up or down. Their model assumes that gene and protein levels are continuous and that there is a maximum saturation gene expression level. Their model incorporates three feedback loops, two of which are autoregulatory. They state that their results simplify the search for steady state solutions and also emphasizes the necessity of feedback loops in order to account for the dynamics of the system(Veflingstad and Plahte 2007).

Hargrove and Schmidt (1989) constructed a simple two-compartmental mathematical model to show the effects that changing the degradation and synthesis rates of hypothetical mRNAs and protein would have on the final concentration of the proteins. This model relates the kinetics of mRNA synthesis and degradation to protein synthesis in non-dividing cells. Their model predicts that the steady state concentration of the protein is equal to the product of the rate constants of the mRNA and protein synthesis divided by the products of the rate constants of their degradations. It also predicts that the rate at which a protein concentration changes also depends on these two degradation constants. Finally it shows that the relative rates of mRNA transcription and translation and the comparative stability of the mRNA and protein contribute equally to the concentration of gene products in cells (Hargrove and Schmidt 1989).

In chapter 4 we quantified, investigated and presented the results of the distribution of thoracic endothelial AQP1 in young healthy male Sprague-Dawley (SD) rats made hypertensive by the Goldblatt procedure. These rats included: 2K1C Goldblatt rats with

systolic blood pressures at ~150mmHg and those with pressures greater than 200mmHg; SDs that had reverted back to normotensive values (~125mmHg) with Captopril treatment; SDs that remained normotensive because they had undergone sham operations; and rats that remained normotensive because they were not subjected to any surgery. In this present chapter, we construct and solve mathematical kinetic models based on the *Law of Mass Action* to describe a possible mechanism to explain these results; this mechanism looks at the transcription factor as point of regulation. First we examine the steady state form of the model and compare with Chapter 4's data. We argue that, since the time scale for blood pressure adjustment after the Goldblatt procedure is on the order of weeks, much longer than the time scale of protein regulation (tens of hours (Walsh and Wright 1995)), Chapter 4's observed aquaporin-1 concentrations are most likely pseudo-steady (Levenspiel 1999). We thus use these data to extract the regulatory rate parameter, which is the only parameter not available from the literature. We then use these parameters to solve time dependent model equations using Matlab® 7.3.0.

Our group has carried out chemically blocked AQP1 both on BAECs monolayers and whole rat vessels *ex vivo* using $HgCl_2$ and tetraethylammonium (TEA) chloride, followed by Lp measurements of the monolayers. To complement these studies, we have used siRNA technology to knock down AQP1 protein expressions and repeated these measurements. siRNAs are short strands of RNA that interfere with the mRNA pathway resulting in mRNA degradation (Schonthal 2004)and are believed to yield a 'cleaner" and much more specific experiment than chemically blocking. Since siRNA interferes with the protein transcription/translation mechanism, our model should be able to address,

describe and guide these experiments. It may also help suggest and predict new experiments and effects.

II. MODELS AND METHOD OF SOLUTION

Protein synthesis can conceptually be divided into two phases: transcription and translation. Transcription takes place in the nucleus of eukaryotes and occurs when the information in a DNA sequence (gene) is copied into an RNA sequence, termed a messenger RNA transcript (mRNA). Translation occurs when these transcripts are then transported from the nucleus to the cytoplasm where they are converted into the amino acid sequence of a polypeptide; this takes place on the ribosome. Both of these two phases occur in three steps: initiation, elongation and termination (Sadava, Heller et al. 2006).

Here we construct a simplified transcription kinetic model in an attempt to understand the regulation of AQP1 in response to chronic pressure. We adopt some of the kinetic rate parameters and assumptions in our model from Yang et al.'s (2007) model. Yang et al. were able to derive an analytical rate expression for gene transcription mediated by transcription factors. They estimated their kinetic rate constants based on Cranz et al.'s *in vitro* experiments on the Gcnp4 system, a *Saccharomyces cerevisiae* master gene regulator. Equations 1 and 2 show the mechanisms we adopt for transcription and Table 1 lists all the rate constants.

$$TF + D \xrightarrow{k_2} mR + D + TF \qquad \textbf{1}$$

$$TF \xrightarrow{k1} 0 \qquad \mathbf{2}$$
$$\xleftarrow{\quad} \mathrm{k_{6(\Delta P)}}$$

Here TF is the transcription factor, D is the DNA template and mR is the messenger RNA transcript. In principle, DNA is tightly coiled and needs to unlock structurally, a process known as chromatin remodeling, so that the TFs can bind to it. Yang et al.'s (2007) simplified these processes by assuming that chromatin remodeling is fast compared with TF binding and therefore they do not explicitly model the former. While searching for specific DNA sequence, TFs may slide along the DNA template by one-dimensional diffusion or they may hop between sequences in three-dimensions. This motion results an initial non-specific binding, which their model also ignores.

Equation 1 in our model states that TF and D bind and produce mR without any loss of TF or of D. We have assumed that the initial concentration of D ($[D_O]$) remains unchanged during the reaction. This assumption allows us to combine [D] with the second order rate constant $\mathbf{k_2}$ into a pseudo first order rate constant $\mathbf{k_2' := k_2[D_O]}$. Since $\mathbf{k_2}$ was obtained from *in vitro* experiments at 6^0C, and rate constants are generally strong Arrhenius functions of temperature, we employ a widely used rule of thumb that chemical reaction rates ~ doubles for every 10^0C rise in temperature, to give a k_2 value at 37^0C typical of the *in vivo* situation. We have also assumed that the point of pressure regulation is TF. That is, we assume that the rate of production of TF is some empirical function $\mathbf{k_6}(\Delta P)$ of the transmural (or systolic, which is what our experiments measure) pressure ΔP that we shall determine from our experimental results, as discussed below.

We have also assumed that, since TF is a protein, it is degraded with a first order rate constant similar to that of the protein AQP1 synthesized in the translation phase; therefore **k1=k5**.

For translation, we adopt the simplified mechanism in equations 3-5

$$mR \xrightarrow{k_3} P \quad \textbf{3}$$

$$mR \xrightarrow{k_4} 0 \quad \textbf{4}$$

$$P \xrightarrow{k_5} 0 \quad \textbf{5}$$

Here an mRNA produces a protein molecule (and is itself destroyed in the process) with rate constant **k3**, both molecules are degraded with rate constants **k4** and **k5** respectively.

To summarize, we model protein synthesis kinetics by the following elementary rate reactions:

$$\frac{d}{dt}[TF] = k_6 - k_1[TF] \quad \textbf{6}$$

$$\frac{d}{dt}[mR] = k_2'[TF] - k_3[mR] - k_4[mR] \quad \textbf{7}$$

$$\frac{d}{dt}[P] = k_3[mR] - k_5[P] \quad \textbf{8}$$

Rate constants $\mathbf{k_1}$, $\mathbf{k_3}$, $\mathbf{k_4}$ and $\mathbf{k_5}$ are first order rate constants and $\mathbf{k_2}$ is pseudo first order. Again, the rate $\mathbf{k_6}$ of TF production is a function of pressure ΔP. We shall determine $\mathbf{k_6}$ at each experimental ΔP by noting that the time scale of rat blood pressure change after Goldblatt surgery is weeks (see fig.1 in chapter 4), whereas the time scale of protein upregulation is typically tens of hours (Walsh and Wright 1995). As a result, at each experimental ΔP one can assume that protein regulation is at the steady state commensurate with the rat's instantaneous blood pressure. As such, comparison of the model steady state with the data will yield $\mathbf{k_6}$ at each experimental ΔP.

siRNA Knockdown Experiments

Our group and many others carry out knockdown experiments. One introduces a certain concentration of an siRNA specially-designed against a protein of interest into cultured cells and expects a significant reduction. siRNA molecules interfere with the mRNA pathway; they do this by cleaving the mRNA molecules at specific sites, which are then rapidly degraded by RNases.

Table 1: Rate constants used in this work

Constant	Value	Units	Reference
k_1	4.81×10^{-5}	s^{-1}	(Leitch, Agre et al. 2001)
k_2'	0.726	s^{-1}	(Cranz, Berger et al. 2004)
k_3	$5.5 \pm 1.16 \times 10^{-3}$	s^{-1}	(Jungbauer, Bakke et al. 2006)
k_4	2.7×10^{-5}	s^{-1}	(Sharova, Sharov et al. 2009)
k_5	4.81×10^{-5}	s^{-1}	(Leitch, Agre et al. 2001)
k_8	2.0×10^{-6}	s^{-1}	(Dharmacon.com)

This action prevents the mRNAs from coding for protein therefore the mechanism shown in equation 3 is affected in some manner (Kurreck 2009). As the siRNA is depleted, one expects protein levels to return to near normal. Protein knockdown typically vary between 70% and 90% over two days and recovery values vary between 56% to total recovery of the original expression amount over a period of one week or so. (Konnikova, Kotecki et al. 2003; Zhou, Lou et al. 2004; Miyawaki-Shimizu, Predescu et al. 2006; Mulkeen, Silva et al. 2006; Fishel, He et al. 2008). Since the above mathematical model describes transcription and translation, it is natural to extend it to include the effects of siRNA and to use it to investigate the dynamics of protein knockdown and of protein recovery.

First we note that, in our experiments, we transfect our aortic endothelial cells simply with Lipofectamine 2000 that is a cationic liposome based reagent. Thus, in any given experiment, one prescribes the amount or concentration of siRNA placed in with the cells, and the product of this concentration with the transfection efficiency determines the concentration inside the cells. Clearly different cell lines and different transfection methods will yield different tranfection efficiencies. Another experimental parameter is the seeding density of cells. These parameters all affect the optimal initial amount of siRNA used in the experiment in order to obtain maximal knockdown (Dalby, Cates et al. 2004). Although it is known that siRNA cleaves mRNA, the actual reaction mechanism by which this occurs and the final fate of the siRNA molecules is still debatable. Below, we extend our model to include the action and degradation of siRNA by three alternative mechanisms. The goal is to see how different siRNA degradation mechanisms affect the dynamics of protein recovery as a function of initial siRNA amount (or, equivalently, transfection efficiency). Scheme 1 assumes that siRNA reacts equimolarly and irreversible with the mRNA, killing off the mRNA in a second order process, but itself remaining conserved at the end of the reaction (equation 9). This scheme allows for an inherent, first-order siRNA degradation (equation 10). Equation 11 is the rate equation for siRNA in this scheme.

Scheme1

$$siRNA + mR \xrightarrow{k_7} siRNA \qquad \mathbf{9}$$

$$siRNA \xrightarrow{k_8} 0 \quad \textbf{10}$$

$$\frac{d}{dt}[siRNA] = -k_8[siRNA] \quad \textbf{11}$$

In scheme 2, the siRNA is degraded both when it reacts with mRNA and in an inherent, first order reaction. The second order process also degrades the mRNA, as in the first scheme. Equations 12 and 13 show these irreversible reactions and equation 14 shows the equation for the time rate of change of siRNA.

Scheme 2

$$siRNA + mR \xrightarrow{k_7} 0 \quad \textbf{12}$$

$$siRNA \xrightarrow{k_8} 0 \quad \textbf{13}$$

$$\frac{d}{dt}[siRNA] = -k_7[siRNA][mR] - k_8[siRNA] \quad \textbf{14}$$

Scheme 3 is the limiting case of case of scheme 2 where the degradation rate constant $\mathbf{k_8}$ goes to zero. The rate equation for siRNA associated with this scheme is equation 16

Scheme 3

$$siRNA + mR \xrightarrow{k_7} 0 \qquad \textbf{15}$$

$$\frac{d}{dt}[siRNA] = -k_7[siRNA][mR] \qquad \textbf{16}$$

Naturally, each of these schemes couples to the model's rate equations 6-8, modified to include an additional term in the equation for the time-rate-of-change of mRNA; thus equation 17 replaces equation 7.

$$\frac{d}{dt}[mR] = k_2'[TF] - k_3[mR] - k_4[mR] - k_7[siRNA][mR] \qquad \textbf{17}$$

As before, all rate constants are known except for $\mathbf{k_7}$, the rate constant for the action of a specific siRNA and its target mRNA. An ineffective siRNA would have a very low value for $\mathbf{k_7}$ and every siRNA-mRNA pair will have its own $\mathbf{k_7}$. Typical siRNA amounts used are in the 10-100pM per 141,000 cell range (as per Invitrogen protocol) and transfection efficiencies are claimed to lie between 40-99% (www.invitrogen.com 2009). Since the transcription efficiency only enters as a factor multiplying the initial siRNA charge, and since all reactions involving siRNA are linear in its concentration, at fixed $\mathbf{k_7}$, changing this product by changing either factor has the same effect. As such, when we speak of

changing the initial siRNA amount, we could equally well be writing of changing the transcription efficiency.

III. RESULTS

By setting all of the time derivatives to zero (equation 18) we find the model's steady state concentration as

$$\frac{d}{dt}=0 \qquad \textbf{18}$$

$$\left[TF\ \right]=\frac{k_6}{k_1} \qquad \textbf{19}$$

$$\left[mR\right]=\frac{k_2^{'}k_6}{\left(k_3+k_4\right)k_1} \qquad \textbf{20}$$

$$\left[P\right]_{[\Delta P]}=\frac{k_3k_2^{'}k_6}{\left(k_3+k_4\right)k_1k_5} \qquad \textbf{21}$$

By comparison with our data (Chapter 4), Figure 1 finds that $\mathbf{k_6}$ increases ~ 2.25 fold from $1.42\text{x}10^{-8}$ nMs^{-1} (125mmHg) to $3.14\text{x}10^{-8}$ nMs^{-1} as the pressure rises from 125 to

150 and another ~1.18 fold to 3.69 ±0.5 x10^{-8} nMs^{-1} as the pressure reaches >200mmHg. Figure 2 fits this parameter to the exponential function in equation 22

$$k_6 = a * \exp(-b * x) + c \quad \textbf{22}$$

with three unknown parameters, whose best fit values are a = 3.82e-08, b = -7.68e-06 and

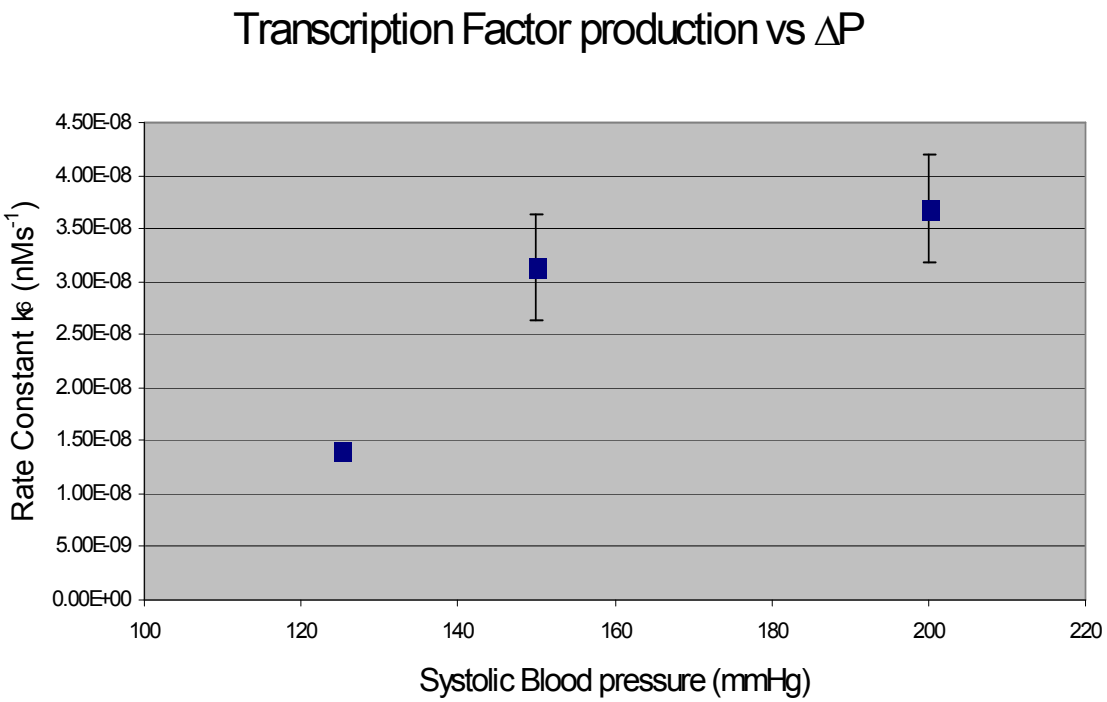

Figure 1 Transcription factor upregulation constant as function of systolic pressure

c = 0.04623. Figures 4, 5 and 6 now investigate the time-dependent behavior of the model in response to a step change (at t=0.5 days) in chronic systolic pressure from an initial value of 125mmHg (and all the species concentrations i.e. TF, mR and P at the corresponding steady state from equations 19-21) to either 150mmHg or >200mmHg.

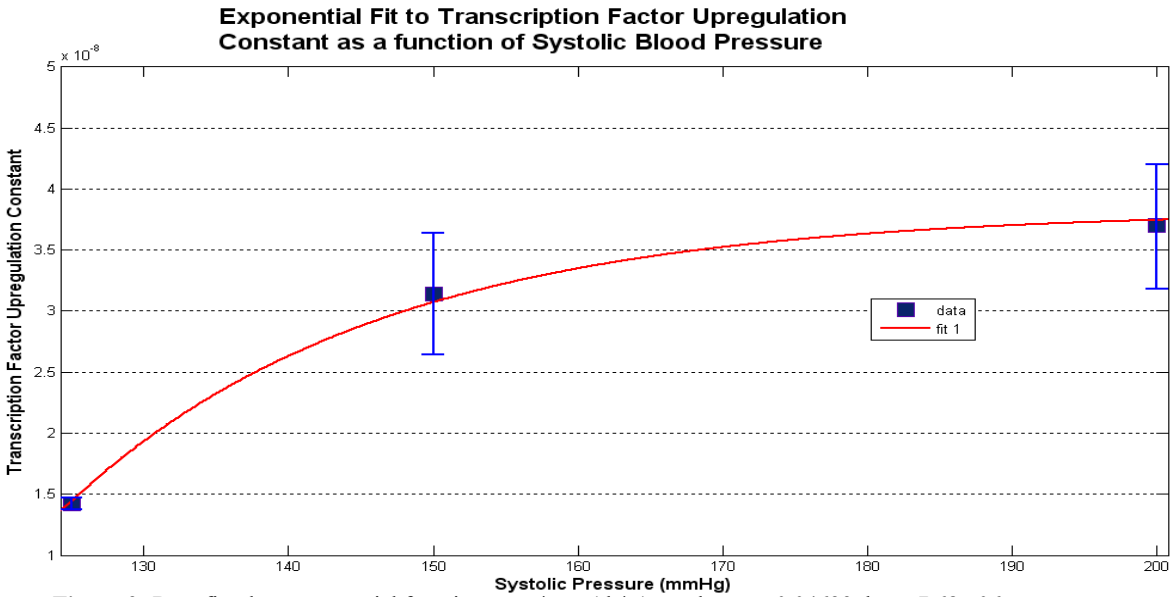

Figure 2: Data fitted to exponential function y = a*exp (-b*x)+c where a =0.04623, b = -7.68e-06 and c = 0.04623, R^2=1 obtained from Igor® Pro 6

The figures follow the concentrations with time until they achieve their next steady state.

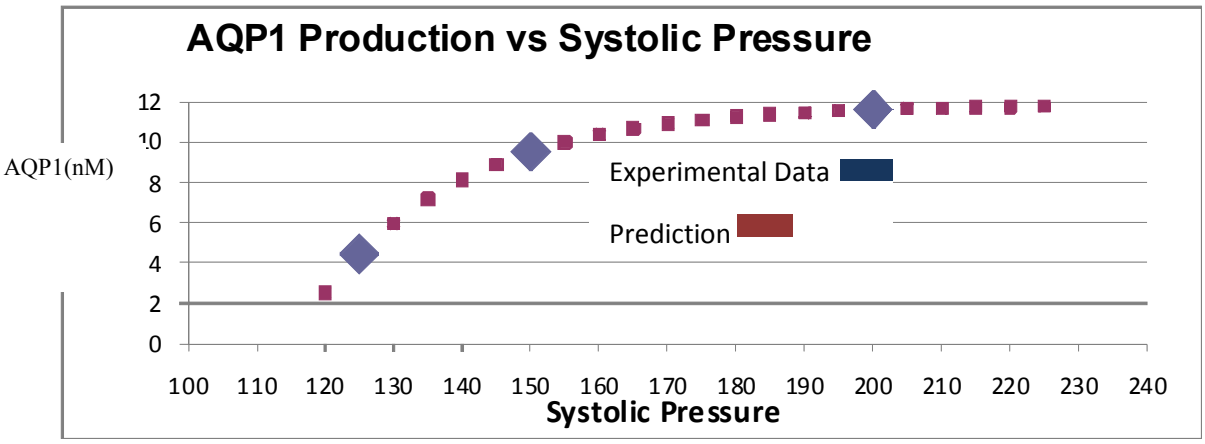

Figure 3: Prediction of AQP1 steady state concentration vs ΔP using figure 2's exponential fit

The figures show that the concentrations of TR and of mRNA achieve their new steady state in ~0.5 days, whereas the downstream protein levels need ~1.5 days to adjust to its new steady values.

Systolic Pressure (mmHg)	***Steady State Concentration of Species*** (nM) Equation / Matlab®		
	Protein	mRNA	TF
125	***4.48 / 4.48***	***3.89e-2 / 3.89e-2***	***2.9e-4 / 2.9e-4***
150	***9.9 / 9.8***	***0.082/ 0.085***	***6.53e-4 /6.54e-4***
>200	***11.62 / 11.53***	***0.09/ 0.1***	***7.67e-4 / 7.68e-4***

Table 2: Steady State values of TF, mRNA and protein concentration obtained by steady state model and Matlab®

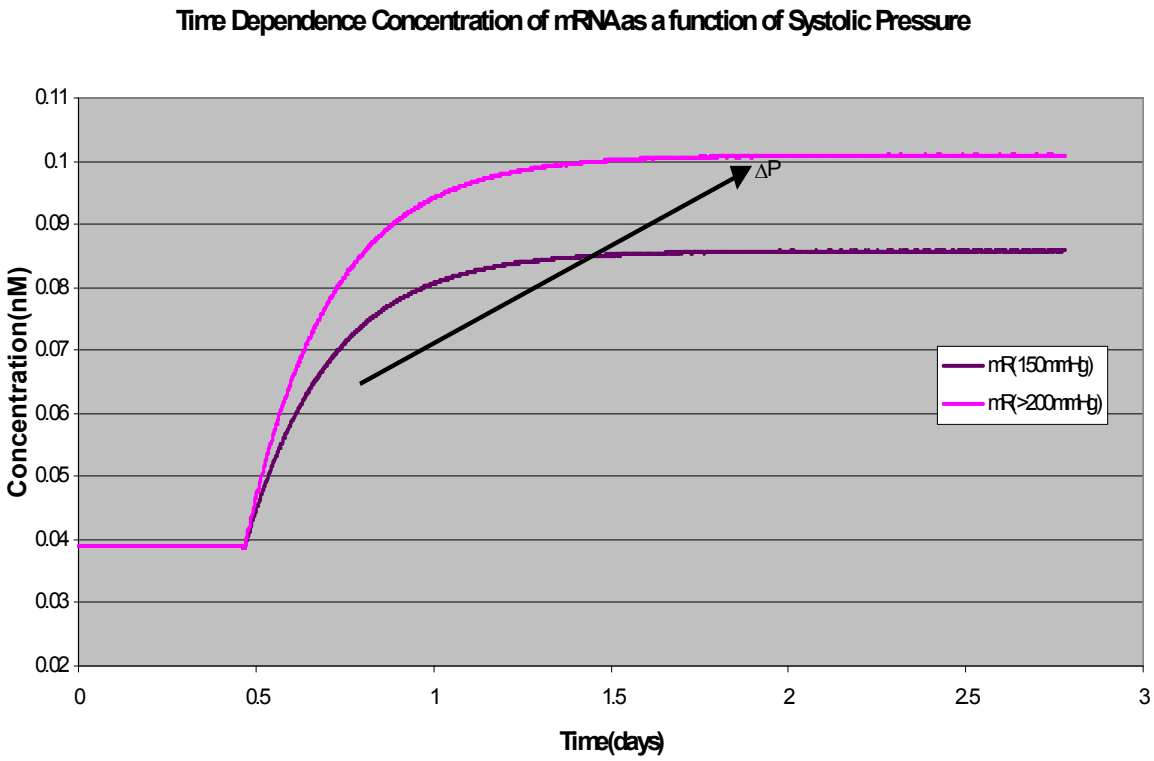

Figure 4: Upregulation of mRNA concentration with increase in rat systolic pressure. System reaches steady state within ~0.5 days when systolic pressure is increased to either 150mmHg or >200mmHg

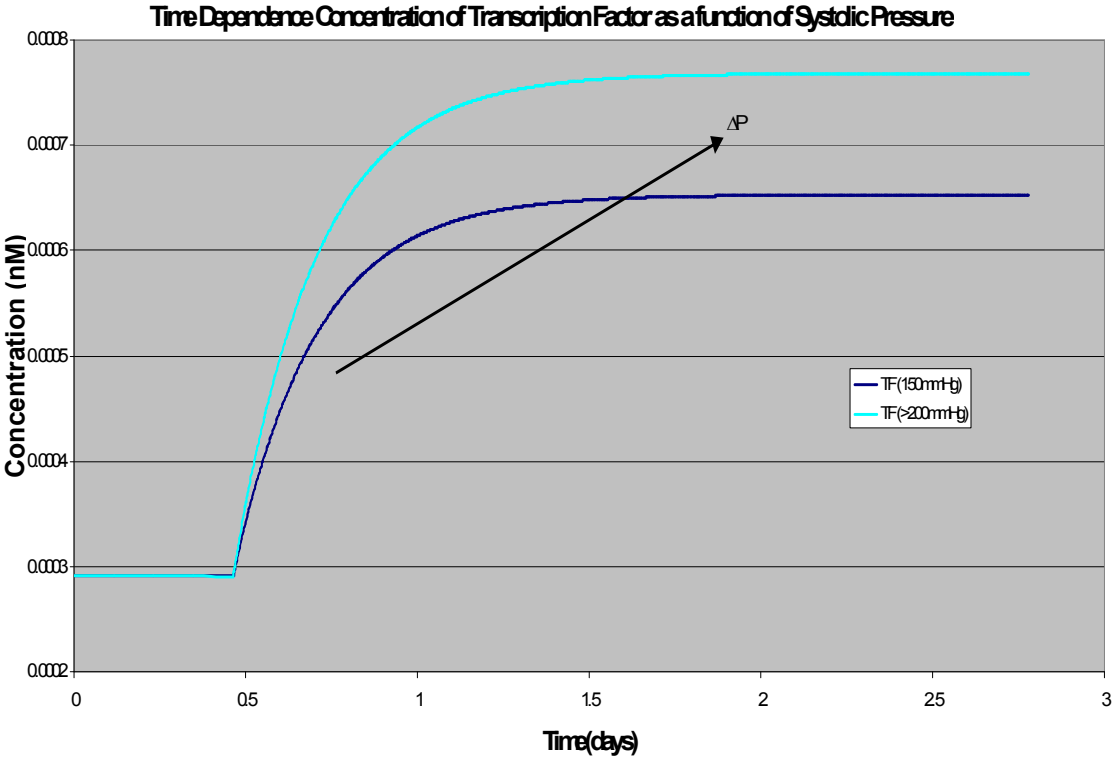

Figure 5: Upregulation of transcription factor concentration with increase in rat systolic pressure. System reaches steady state within ~0.5days when systolic is pressure is increased to either 150mmHg or >200mmHg

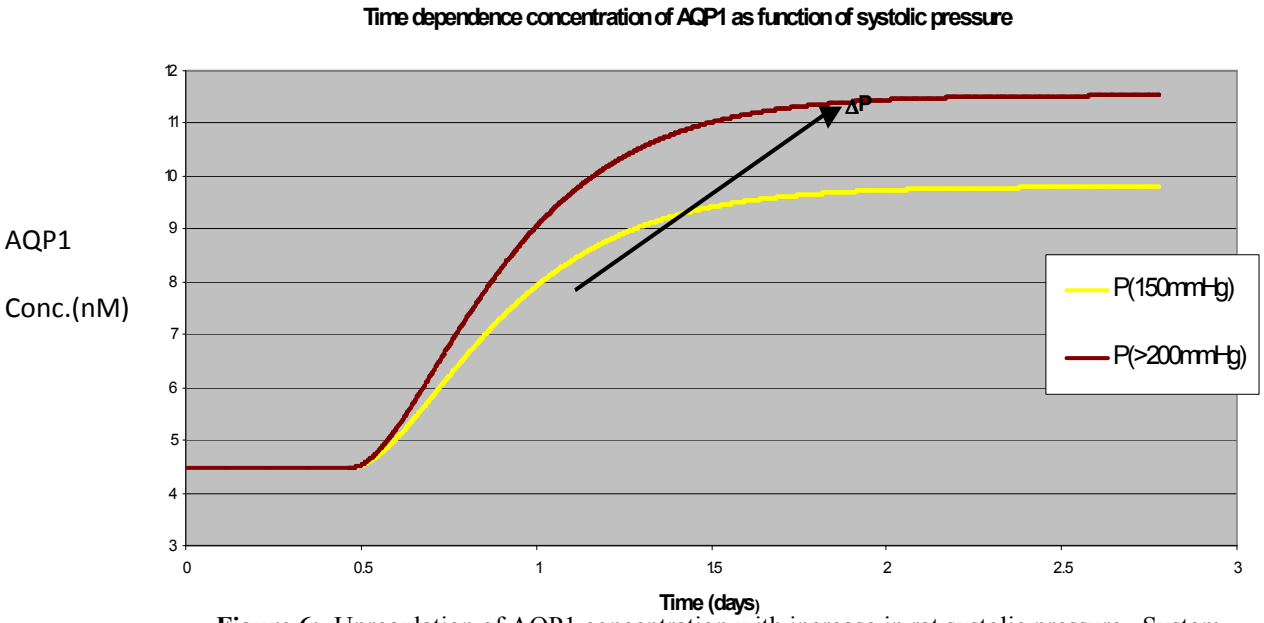

Figure 6: Upregulation of AQP1 concentration with increase in rat systolic pressure. System reaches steady state within one day when systolic pressure increased to either 150mmHg or >200mmHg

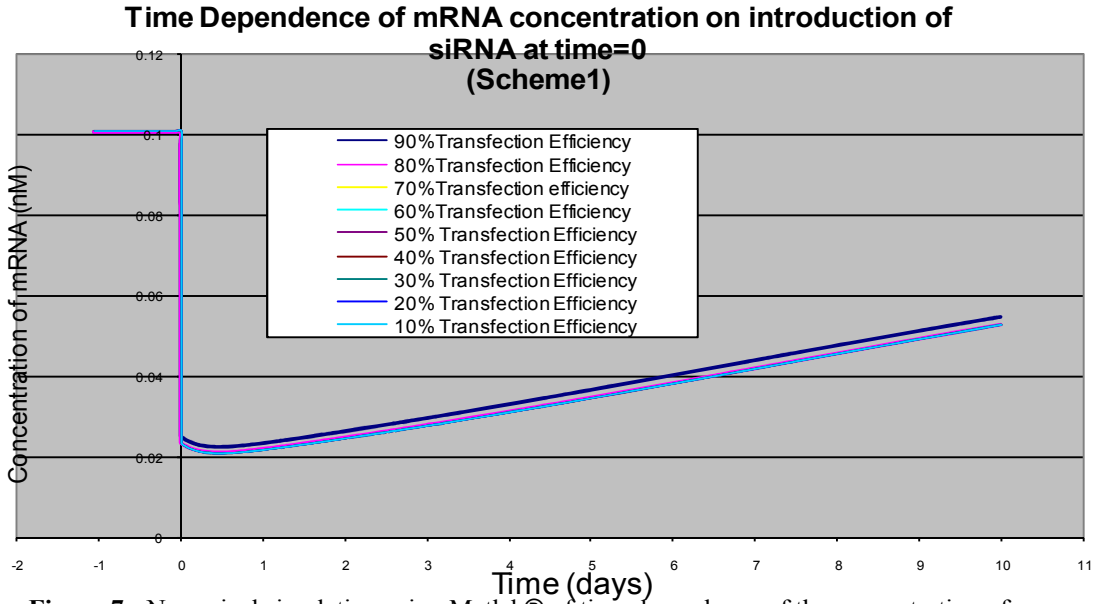

Figure 7: Numerical simulation using Matlab® of time dependence of the concentration of mRNA on introduction of siRNA at time=0 shows that it is downregulated at a constant rate to its lowest level over <1 day. The minimum of each curve is independent of the transfection efficiency. Curves recover with a constant rate but are independent of transfection efficiency below 80%.

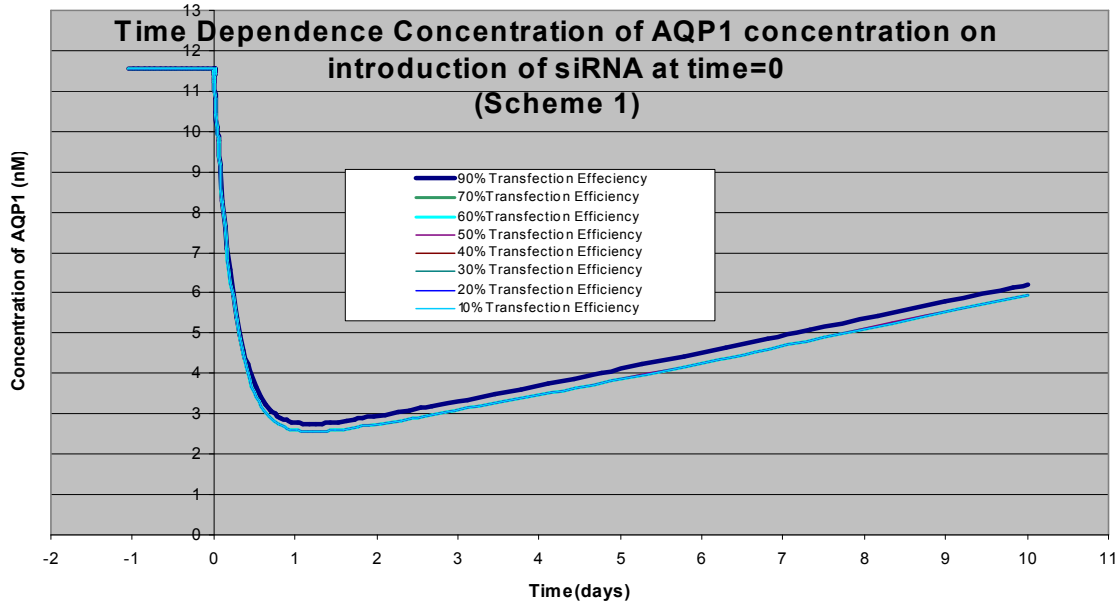

Figure 8: Numerical simulation using Matlab® of time dependence of the concentration of AQP1 on introduction of siRNA at time=0 shows that it is downregulated at a constant rate to its lowest level over 1.5 days. The minimum of each is independent of the transfection efficiency. Curves recover with a constant rate but are independent of transfection efficiency

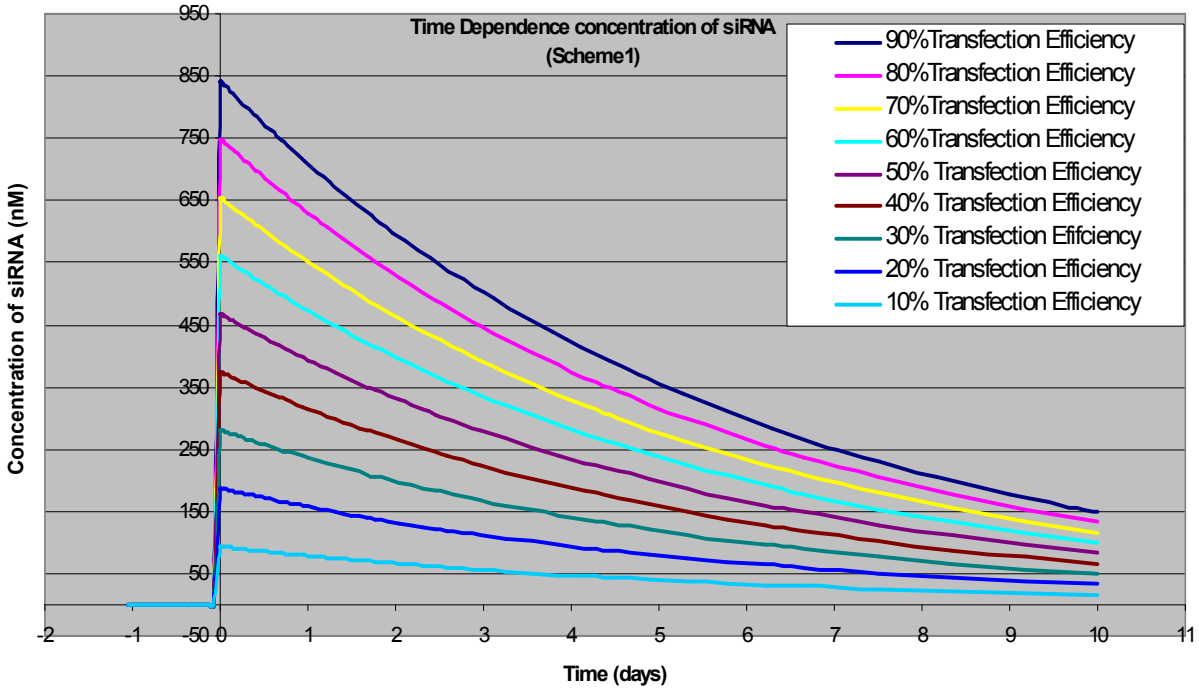

Figure 9: Introduction of siRNA at time=0 and its degradation of siRNA at different transfection efficiencies

Transfection Efficiency %	Rate Constant (k7)		
	Scheme 1	Scheme 2	Scheme3
90	0.0829	0.1024	0.0493
80	0.0933	0.1188	0.0565
70	0.1066	0.1415	0.0662
60	0.1244	0.1753	0.0798
50	0.1492	0.2306	0.1006
40	0.1866	0.3386	0.1364
30	0.2487	0.6675	0.2135
20	0.3731	--------	0.5347
10	0.7462	---------	--------

Table 3: Optimized Rate Constant (k7), Initial siRNA charge is 9.36×10^3 pM

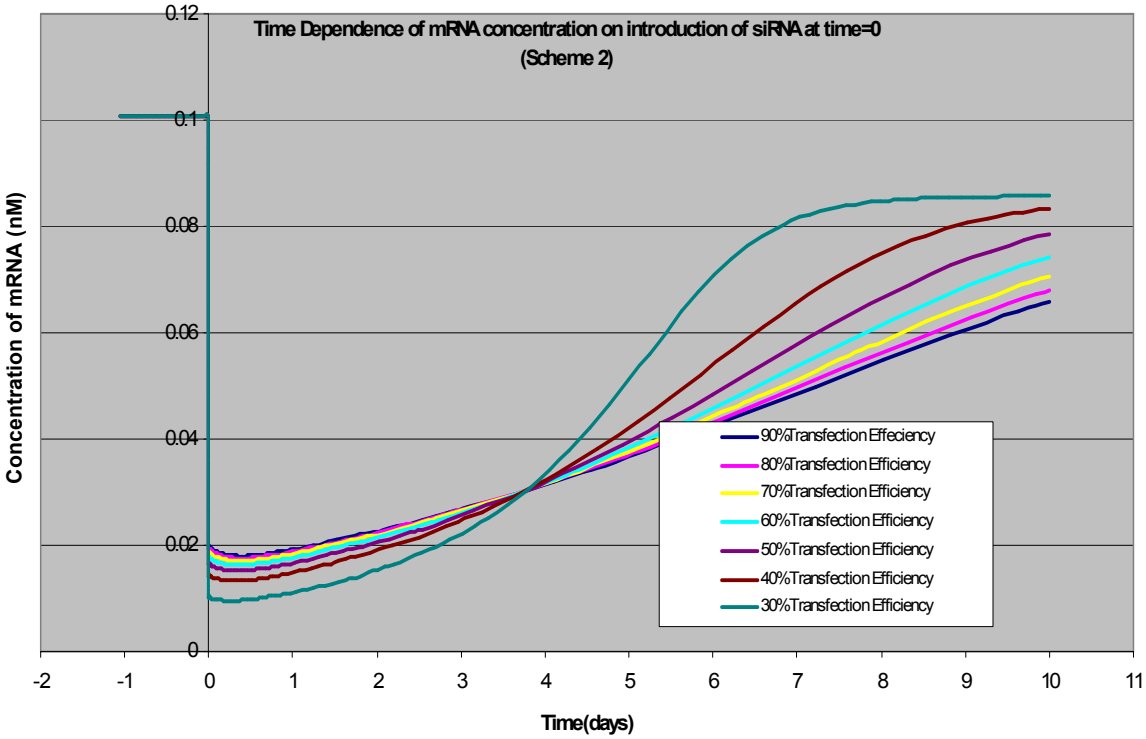

Figure 10 Numerical simulation using Matlab® of time dependence of the concentration of mRNA on introduction of siRNA at time=0 shows that it is downregulated at a constant rate to its lowest level < 1 day. The minimum of each curve depends on the transfection efficiency. They all recover with an almost constant rate for transfection rates 90% to 50%. From 40% transfection efficiency, the recovery curve appears sigmoidal in shape.

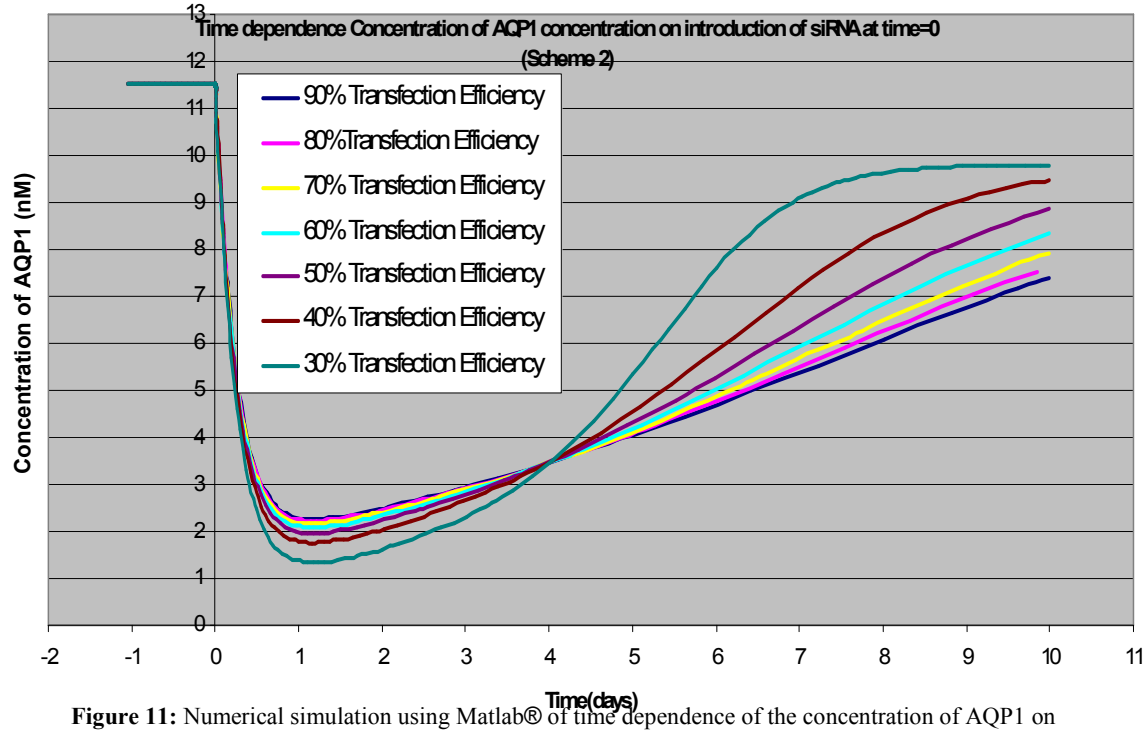

Figure 11: Numerical simulation using Matlab® of time dependence of the concentration of AQP1 on introduction of siRNA at time=0 shows that it is downregulated at a constant rate to its lowest level over 1.5 days. The minimum of each curve depends on the transfection efficiency. They all recover with an almost constant rate for transfection rates 90% to 50%. From 40% transfection efficiency, the recovery curve appears sigmoidal in shape.

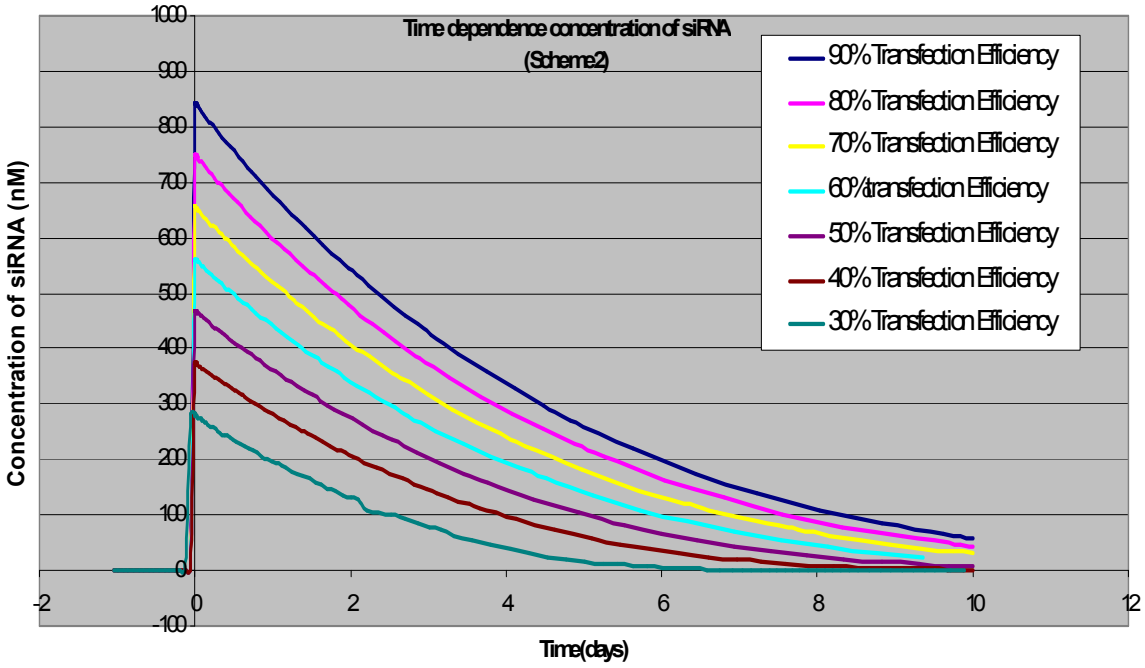

Figure 12: Introduction of siRNA at time=0 and its degradation of siRNA at different transfection efficiencies

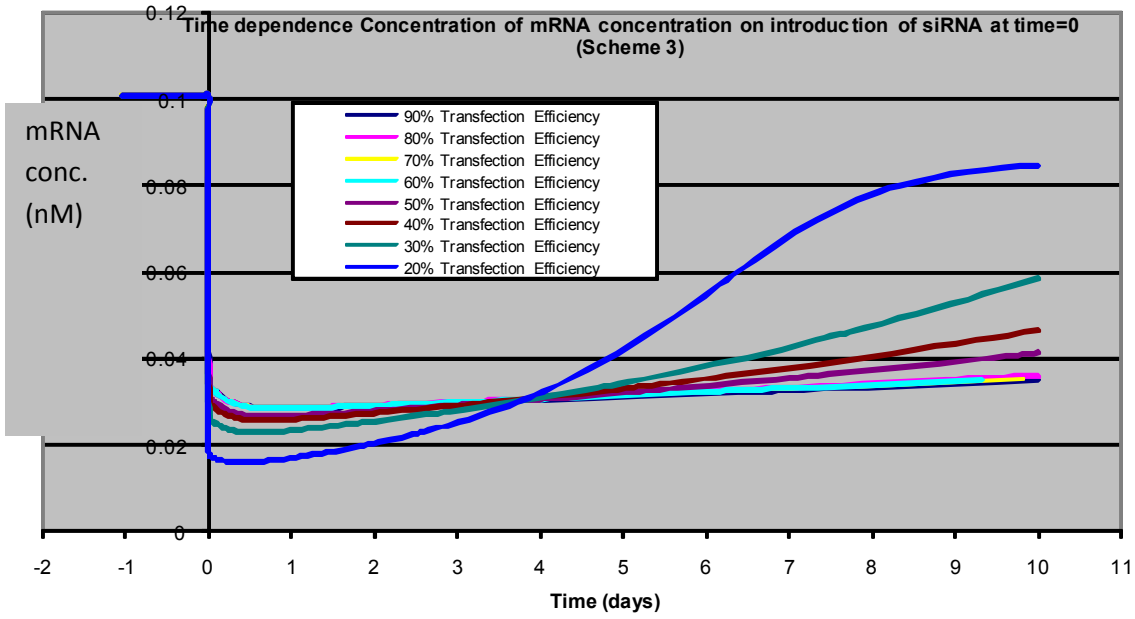

Figure 13: Numerical simulation using Matlab® of time dependence of the concentration of mRNA on introduction of siRNA at time=0 shows that it is downregulated at a constant rate to its lowest level < 1 day. The minimum of each curve depends on the transfection efficiency. They all recover with an almost constant rate for transfection rates 90% to 40%. From 30% transfection efficiency, the recovery curve tends toward sigmoidal in shape.

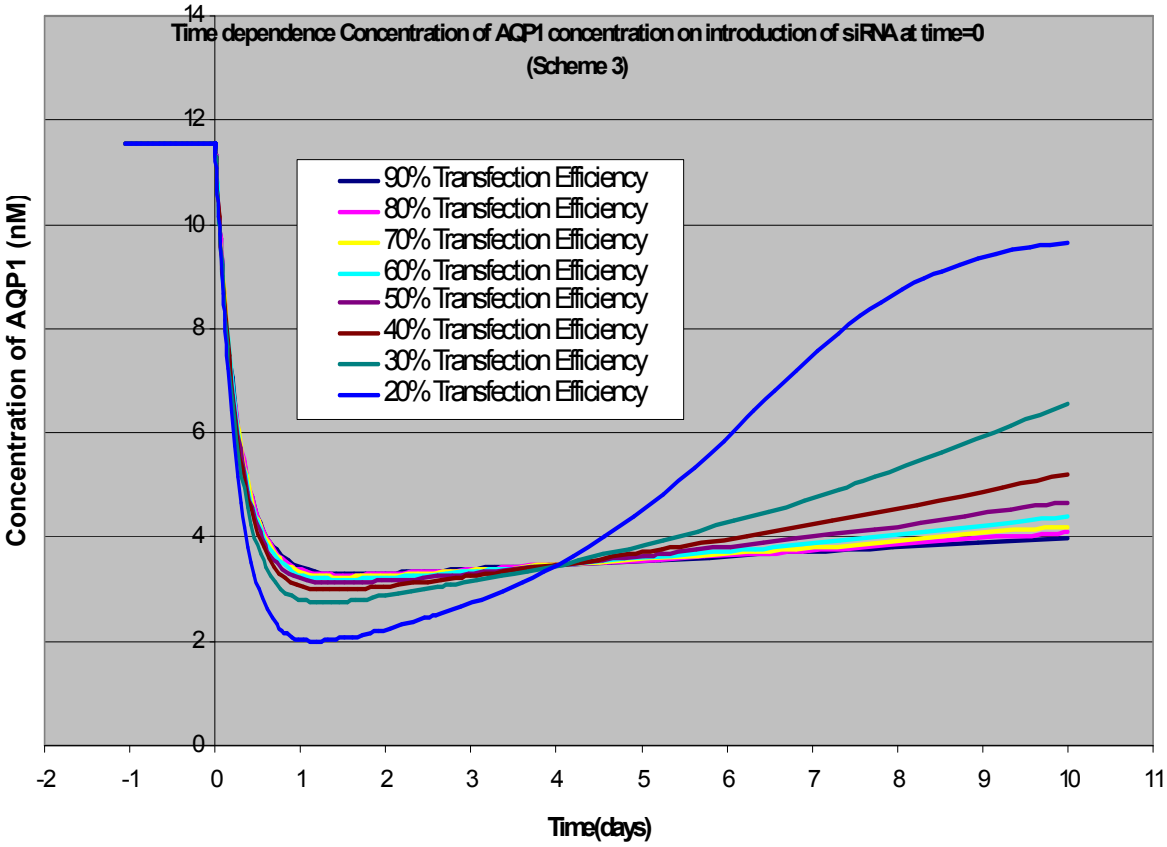

Figure 14: Numerical simulation using Matlab® of time dependence of the concentration of AQP1 on introduction of siRNA at time=0 shows that it is downregulated at a constant rate to its lowest level over 1.5 days. The minimum of each curve depends on the transfection efficiency. They all recover with an almost constant rate for transfection rates 90% to 40%. From 30% transfection efficiency, the recovery curve tends toward sigmoidal in shape.

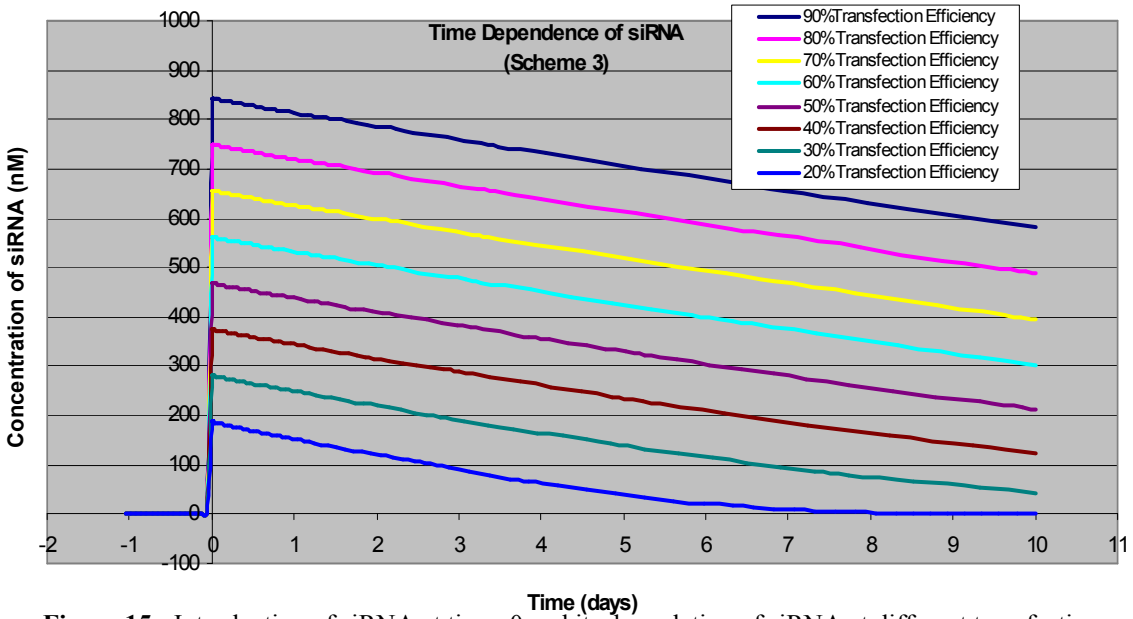

Figure 15: Introduction of siRNA at time=0 and its degradation of siRNA at different transfection efficiencies

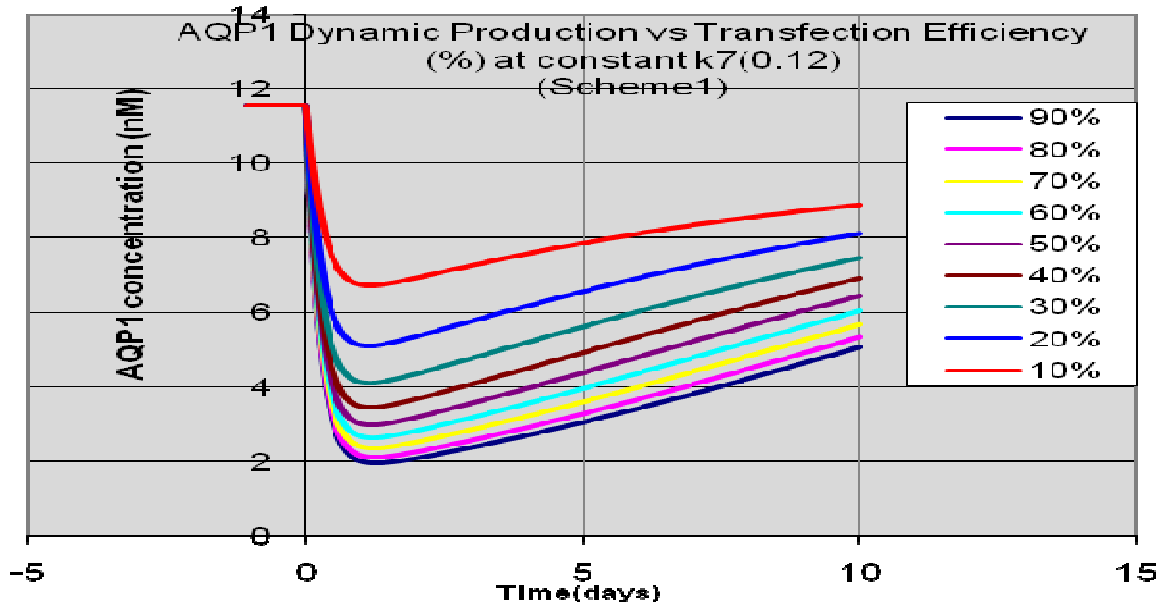

Figure 16: AQP1 production (Scheme1) at constant k7 (0.12)

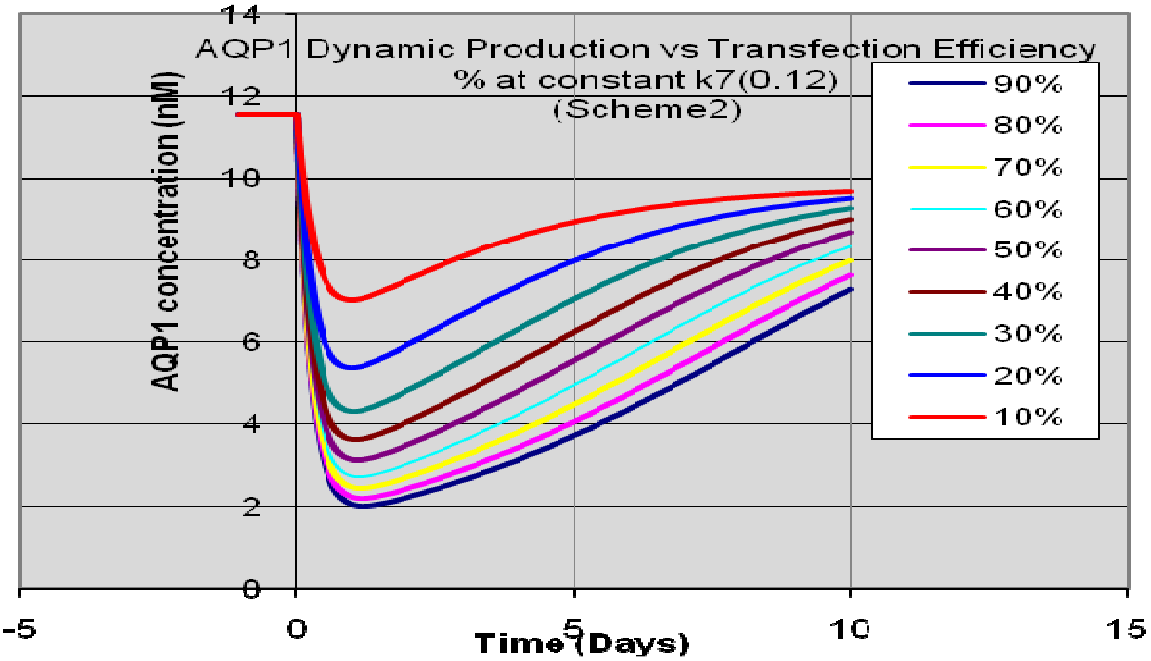

Figure 17: AQP1 production (Scheme2) at constant k7 (0.12)

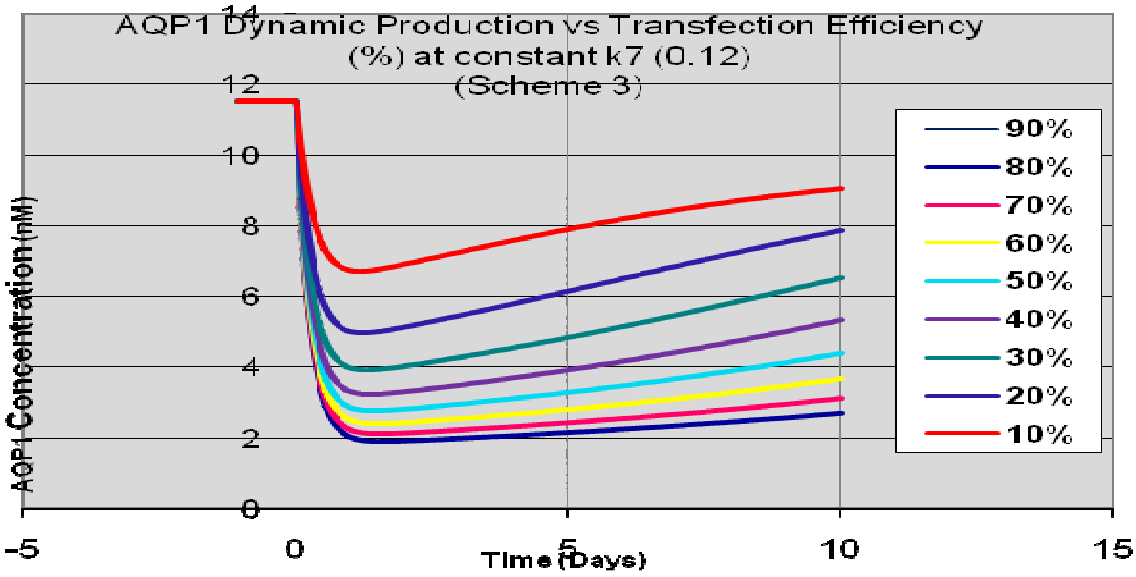

Figure 18: AQP1 production (scheme3) at constant k7 (0.12)

In the three model variants describing the siRNA knockdown experiments, in order to determine $\mathbf{k_7}$ for a given initial siRNA-transcription efficiency product, we require that $\mathbf{k_7}$ be such that the system achieves 70% knockdown in ~2days. As such, in the first set of results we plot (Figures 8-9, 11-12 and 14-15) the time evolution of both protein and siRNA for different initial siRNA charges, each with a different value of $\mathbf{k_7}$ optimized to satisfy this condition. Table 3 gives the corresponding values of $\mathbf{k_7}$. We do this so that the protein minima for all siRNA charges will be essentially the same, and we can compare the effect of initial siRNA charge on protein recovery. We do this initially for all three models. We then choose one value of $\mathbf{k_7}$ for each model and plot (Figures 16-18) the effect of the initial siRNA charge on these two evolutions at fixed $\mathbf{k_7}$. Naturally we shall find these latter plots show that the higher the initial siRNA charge, the stronger the

maximal knockdown. We shall examine how this maximal knockdown and its recovery compare for the three models in question

IV. DISCUSSION

We noted that chapter 4's aquaporin concentrations as a function of systolic transmural pressures were most likely quasisteady values. With this assumption, we solved for the rate, $\mathbf{k_6}$, of production of transcription factor by comparing these data with our steady state model (eqs 19-21), and then inserted this value into the dynamic model. Figure 1 plots $\mathbf{k_6}(\Delta P)$ with error bars. Although Figure 2 fits its three data points to an exponential function, the error bars and the paucity of data points, i.e., pressures, suggest we remain cautious about extrapolating this curve. Figure 3 cautiously predicts steady protein concentrations at ΔPs intermediate between the data and extrapolates slightly outside this range. It appears to suggest a leveling off of steady AQP1 expression with pressures much above 200mmHg and a further drop below 125mmHg.

Turning now to the dynamic model, we examine how the system, initially at steady state, responds to a step change in pressure. As expected we find (Figure 6) that the aquaporin concentration reaches steady state – and does so in about 1 1/2 days. This justifies our assumption that chapter 4's data were quasisteady. Figures 4-5 show that the TF and mR concentrations reach steady state in half a day, even faster than the protein. This makes sense, since the model assumes that regulation acts directly at the TF level, and that protein regulation is a downstream consequence of this TF control. These time scales are the same whether the step is to 150mmHg or to >200mmHg from the base systolic pressure of 125mmHg.

For our siRNA studies, in addition to the rate parameters ($\mathbf{k_1}$-$\mathbf{k_5}$) which were taken from the literature, we also used the average transcription upregulation factor rate constant ($\mathbf{k_6}$) value obtained at systolic blood pressure, 150mmHg, shown in figure1 and an siRNA degradation rate constant ($\mathbf{k_8}$) value supplied by the siRNA manufacturer, Dharmacon. For each transfection efficiency, along with the conditions that were set as described above, we optimized for a $\mathbf{k_7}$ value. Optimizing for $\mathbf{k_7}$ was done using the absolute concentration numbers for the AQP1 protein in our studies (Table 2) and our previously calculated absolute amount of AQP1 in a single rat aortic endothelial cell or RAEC, (Chapter 4), (~1,000,000). In an siRNA experiment one typically varies the initial charge of siRNA from 10-100pM per 141,000 cells. Moreover, a vector, in our case Lipofectamine® 2000, must carry or transfect the siRNA across the cell membrane into the cell. Transfection efficiencies however typically range from 20 % up to 96% based on the type of cell (Ohki, Tilkins et al. 2001; Dalby, Cates et al. 2004; Hagerkvist, Mokhtari et al. 2005), as a result, we include both initial siRNA concentration in the cell medium and the transfection efficiency (they appear only as a product) in our model and observe how this product affects the dynamics of each of the three model systems.

Clearly, equation 6 shows that the dynamics of the TF are only affected by $\mathbf{k_1}$ and $\mathbf{k_6}$; therefore unlike the mRNA and protein, the addition of siRNA does not affect the concentration of TF in any of the three schemes.

Upon introduction of the siRNA at time t=0, Figures 7-8, show that mR and AQP1 are depleted to their lowest values, mRNA in far less than one day and AQP1 in ~1 day. The recovery curves appear to increase at a constant rate. This figure, which uses $\mathbf{k_7}$ values fit

independently for each initial siRNA charge so as to give a constant maximal knockdown, shows that the protein recoveries in model 1 displays a complete insensitivity to initial charge or, equivalently, to transcription efficiency; in fact, the siRNA recoveries simply scale with the initial charge. This is because, when the only way to destroy the siRNA is by a first-order degradation (eq.10), the siRNA concentration decays exponentially with time and the program that fits $\mathbf{k_7}$ simply does so based on the equation for mRNA. Since, in that equation, $\mathbf{k_7}$ multiplies [siRNA] and the transcription efficiency, ε, for each initial siRNA charge or transcription efficiency ε, it finds the same optimal value of the product $\mathbf{k_7}$[siRNA]ε. Table 3 illustrates this. Note that, since model 1 allows explicit analytic solution for [siRNA] as an exponential decay, independent of the concentrations of any of the other species, the rate of reaction 7 is now linear (in [mRNA]) with a coefficient that is an explicit function of time. As such, the entire model 1 lends itself to analytic solution. Whereas we have calculated this solution, we present numerical solutions of all three models because models 2 and 3 do not lend themselves to analytic solution since their reaction 7's rate is nonlinear.

As in model 1, models 2 and 3 show a sharp, very rapid drop in mRNA and an ~1 day drop in protein concentration, followed by a wide (~2-3 day) minimum before recovery gets under way. The situation regarding $\mathbf{k_7}$ from model 1 is completely different in model 2, where there is, in addition to the first order siRNA degradation, the nonlinear, second order process that is mRNA-dependent. In model 3, there is only the latter method for eliminating siRNA. In each of these models, the optimization process to find $\mathbf{k_7}$ finds an unrelated optimum for each initial siRNA charge. Models 2 and 3 shows that varying the initial siRNA charge indeed strongly affects protein recovery, with a lower initial charge

leading to a faster and more complete recovery than a higher initial siRNA charge. This effect is more pronounced in model 3 than in model 2 because, in model 3, the only method for eliminating siRNA is via the nonlinear kinetic reaction. For the higher transfection efficiencies, all recovery curves appear ~linear up to ten days, whereas for the lower efficiencies (or initial siRNA charges), the recoveries show a pronounced sigmoidal shape; we presume that at longer times, even the lower transcription efficiency curves will also turn sigmoidal.

It is worth noting that our $\mathbf{k_7}$ fitting scheme adjusted $\mathbf{k_7}$ for a given product of initial siRNA charge and transcription efficiency, until the protein knockdown was 70% at 2 days. In model 1, where siRNA is depleted independently of its action, increasing $\mathbf{k_7}$ can increase the knockdown almost to any desired degree. In contrast, in models 2 and 3, an increase in $\mathbf{k_7}$ not only depletes mRNA, but also the siRNA itself. As such, there will be products of initial siRNA charge and transcription efficiency that are simply too low for a value of $\mathbf{k_7}$ to exist that satisfies the said criterion. This is indeed the situation that we found numerically.

We turn now to figures 16-18, where we have chosen a single $\mathbf{k_7}$ for all curves for each model and also for all three models. As expected, in all three models, the higher the product of the initial charge of siRNA and the transfection efficiency, the lower the maximal knockdown and the lower the extent of recovery at 10 days. Interestingly, the knockdown phase, including the time to and extent of maximal knockdown is nearly identical for all three models. The reason for this is that the three models differ in their modes of siRNA degradation. Since siRNA degradation is negligible over the time scales

(~12 hrs) of maximal knockdown, we shouldn't expect any significant difference between models.

For each model, the deeper the protein minimum, the less its recovery at 10 days. The extent of recovery in ten days varies dramatically between models. In model 3, the 90% transfection efficiency curve recovers to only ~2.5nM from a minimum of ~2nM. In contrast, in model 2 it the same curve recovers to ~7.5nM and in model one it recovers to ~5nM from the same minimum. The rate of recovery is hampered by the presence of siRNA. In model 2, siRNA is degraded the fastest – by two mechanisms, and that is why recovery is the fastest. In contrast, in model 3, siRNA is only degraded by its deactivation of mRNA, and so none of it "goes to waste." As such, recovery is slower. In model 1, siRNA degradation is independent of its action and $\mathbf{k_7}$ (not $\mathbf{k_8}$) governs the rate of recovery. If $\mathbf{k_7}$ were very large (small), this model's recovery would be fastest (slowest). However, since all three models have the same $\mathbf{k_7}$, its recovery is intermediate between the other two.

Finally, let's examine the shapes of the recovery curves. For the ten day period, nearly all of them look like straight lines, although the lower transcription efficiency curves in model 2 show a leveling off. Clearly, we expect that, at sufficiently only times, all for the recovery curves will have this shape; ten days are just not long enough for these other curve.

Naturally, these models do not include experimental artifacts – or other effects of the siRNAs that, in practice at high concentrations, lead to lower, rather than higher knockdowns. Thus, in practice, there is generally an initial siRNA charge that is optimal in the sense that it leads to a higher maximal knockdown than either higher or lower

initial siRNA charges. We note that, at fixed $\mathbf{k_7}$, for each model, all of the curves have similar shapes, unlike the earlier comparisons of curves with different $\mathbf{k_7}$s, each optimized separately for its particularl initial loading-transcription efficiency product. Arginine vasopressin is a vasoconstricting hormone that causes the contraction of smooth muscle cells, resulting in the increase of arterial blood pressure (Holmes, Landry et al. 2004). Evidence has shown that arginine vasopressin can upregulate AQP1 in several cell types (Patil, Han et al. 1997; Belkacemi, Beall et al. 2008). At present, our lab is attempting to use this hormone to upregulate AQP1 in BAEC monolayers and to see how such an upregulation might affect monolayer Lp. It would be interesting to test whole rats, both normotensive and Goldblatt-induced hypertensive, to find their arginine vasopressin levels. It would also be interesting to manipulate their arginine vasopressin levels and see if and how these levels affect arterial EC AQP1 expression and arterial Lp, both with normal and increased blood pressure.

V. SUMMARY

We construct a simplified transcription kinetic model in an attempt to understand the regulation of chapter 4‘s aquaporin concentrations as a function of systolic transmural pressures. This mechanism looks at the transcription factor as point of regulation. First we solve the steady state form of the model and use its parameters in a dynamic model to show that the aquaporin reaches steady state concentration in 1 1/2 days while the TF and the mR takes ½ day when all are subjected to a step change in pressure. For our siRNA studies, we investigate the dynamics of protein knockdown and of protein recovery using

three different schemes. Interestingly, the knockdown phase, including the time to and extent of maximal knockdown is nearly identical for all three models, however the extent of recovery varies dramatically between models.

Works Cited

Agre, P., M. D. Lee, et al. (1997). "Aquaporins and ion conductance." Science **275**(5305): 1490; author reply 1492.

Agre, P., A. M. Saboori, et al. (1987). "Purification and partial characterization of the Mr 30,000 integral membrane protein associated with the erythrocyte Rh(D) antigen." J Biol Chem **262**(36): 17497-17503.

Alexander, R. W. (1995). "Theodore Cooper Memorial Lecture. Hypertension and the pathogenesis of atherosclerosis. Oxidative stress and the mediation of arterial inflammatory response: a new perspective." Hypertension **25**(2): 155-161.

Armitage, J. A., L. Lakasing, et al. (2005). "Developmental programming of aortic and renal structure in offspring of rats fed fat-rich diets in pregnancy." J Physiol **565**(Pt 1): 171-184.

Baltimore, D. (1995). "Discovery of the reverse transcriptase." FASEB J. **9**(15): 1660-1663.

Barton, G. M. and R. Medzhitov (2002). "Retroviral delivery of small interfering RNA into primary cells." Proc Natl Acad Sci U S A **99**(23): 14943-14945.

Batchelor, G. K. (1999). An introduction to fluid dynamics. Cambridge, U.K. ; New York, NY, Cambridge University Press.

Beitz, E., B. Wu, et al. (2006). "Point mutations in the aromatic/arginine region in aquaporin 1 allow passage of urea, glycerol, ammonia, and protons." Proc Natl Acad Sci U S A **103**(2): 269-274.

Bell, F. P., I. L. Adamson, et al. (1974). "Aortic endothelial permeability to albumin: focal and regional patterns of uptake and transmural distribution of 131I-albumin in the young pig." Exp Mol Pathol **20**(1): 57-68.

Bell, F. P., I. L. Adamson, et al. (1974). "Focal and Regional pattern of uptake and the transmural distribution of I-fibrinogen in the pig aorta in vivo." Exp Mol Pathol **20**: 281-292.

Bellingham, S. A., L. A. Coleman, et al. (2009). "Regulation of prion gene expression by transcription factors SP1 and metal transcription factor-1." J Biol Chem **284**(2): 1291-1301.

Bratzler, R. L., G. M. Chisolm, et al. (1977). "The distribution of labeled low-density lipoproteins across the rabbit thoracic aorta in vivo." Atherosclerosis **28**(3): 289-307.

Bretherton, K. N., A. J. Day, et al. (1977). "Hypertension-accelerated atherogenesis in cholesterol-fed rabbits." Atherosclerosis **27**(1): 79-87.

Brown, D., T. Katsura, et al. (1995). "Cellular distribution of the aquaporins: a family of water channel proteins." Histochem Cell Biol **104**(1): 1-9.

Bundgaard, M. (1984). "The three-dimensional organization of tight junctions in a capillary endothelium revealed by serial-section electron microscopy." J Ultrastruct Res **88**(1): 1-17.

Burnette, W. N. (1981). ""Western blotting": electrophoretic transfer of proteins from sodium dodecyl sulfate--polyacrylamide gels to unmodified nitrocellulose and radiographic detection with antibody and radioiodinated protein A." Anal Biochem **112**(2): 195-203.

Chen, T., H. L. He, et al. (1999). "Modeling gene expression with differential equations." Pac Symp Biocomput: 29-40.

Chen, Y. L., K. M. Jan, et al. (1997). "Relationship between endothelial cell turnover and permeability to horseradish peroxidase." Atherosclerosis **133**(1): 7-14.

Cherry, R. J. and C. I. Ragan (1986). Techniques for the analysis of membrane proteins. London ; New York, Chapman and Hall.

Chobanian, A. V., A. H. Lichtenstein, et al. (1989). "Influence of hypertension on aortic atherosclerosis in the Watanabe rabbit." Hypertension **14**(2): 203-209.

Chuang, P. T., H. J. Cheng, et al. (1990). "Macromolecular transport across arterial and venous endothelium in rats. Studies with Evans blue-albumin and horseradish peroxidase." Arteriosclerosis **10**(2): 188-197.

Connolly, D. L., C. M. Shanahan, et al. (1998). "The aquaporins. A family of water channel proteins." Int J Biochem Cell Biol **30**(2): 169-172.

Cowen, T., A. J. Haven, et al. (1985). "Pontamine sky blue: a counterstain for background autofluorescence in fluorescence and immunofluorescence histochemistry." Histochemistry **82**(3): 205-208.

Cranz, S., C. Berger, et al. (2004). "Monomeric and dimeric bZIP transcription factor GCN4 bind at the same rate to their target DNA site." Biochemistry **43**(3): 718-727.

Crick, F. (1970). "Central dogma of molecular biology." Nature **227**(5258): 561-563.

Crick, F. H. (1958). "On protein synthesis." Symp Soc Exp Biol **12**: 138-163.

Dalby, B., S. Cates, et al. (2004). "Advanced transfection with Lipofectamine 2000 reagent: primary neurons, siRNA, and high-throughput applications." Methods **33**(2): 95-103.

Davis, D. and M. J. Klainer (1940). "Studies in hypertensive heart disease1.The incidence of coronary atherosclerosis in cases of essential hypertension." Am Heart J **19**(2): 185-192.

de Jong, H. (2002). "Modeling and simulation of genetic regulatory systems: a literature review." J Comput Biol **9**(1): 67-103.

Denker, B. M., B. L. Smith, et al. (1988). "Identification, purification, and partial characterization of a novel Mr 28,000 integral membrane protein from erythrocytes and renal tubules." J Biol Chem **263**(30): 15634-15642.

Duncan, L. E., Jr., J. Cornfield, et al. (1962). "The effect of blood pressure on the passage of labeled plasma albumin into canine aortic wall." J Clin Invest **41**: 1537-1545.

Elbashir, S. M., J. Harborth, et al. (2001). "Duplexes of 21-nucleotide RNAs mediate RNA interference in cultured mammalian cells." Nature **411**(6836): 494-498.

Fan, X. Y., H. Ma, et al. (2009). "A novel differential expression system for gene modulation in Mycobacteria." Plasmid **61**(1): 39-46.

Fishel, M. L., Y. He, et al. (2008). "Knockdown of the DNA repair and redox signaling protein Ape1/Ref-1 blocks ovarian cancer cell and tumor growth." DNA Repair (Amst) **7**(2): 177-186.

Frank, J. S. and A. M. Fogelman (1989). "Ultrastructure of the intima in WHHL and cholesterol-fed rabbit aortas prepared by ultra-rapid freezing and freeze-etching." J Lipid Res **30**(7): 967-978.

Fry, D. L. (1983). "Effect of pressure and stirring on in vitro aortic transmural 125I-albumin transport." Am J Physiol **245**(6): H977-991.

Fry, D. L. (1985). "Mathematical models of arterial transmural transport." Am J Physiol **248**(2 Pt 2): H240-263.

Fry, D. L. (1987). "Mass transport, atherogenesis, and risk." Arteriosclerosis **7**(1): 88-100.

Garg, U. C. and A. Hassid (1989). "Nitric oxide-generating vasodilators and 8-bromo-cyclic guanosine monophosphate inhibit mitogenesis and proliferation of cultured rat vascular smooth muscle cells." J Clin Invest **83**(5): 1774-1777.

Georgianna, D. R., A. M. Hawkridge, et al. (2008). "Temperature-dependent regulation of proteins in Aspergillus flavus: whole organism stable isotope labeling by amino acids." J Proteome Res **7**(7): 2973-2979.

Guyton, A. C. and J. E. Hall (1996). Textbook of medical physiology. Philadelphia, W.B. Saunders.

Guyton, A. C. and J. E. Hall (2000). Textbook of medical physiology. Philadelphia, Saunders.

Hall, R. A., L. S. Ostedgaard, et al. (1998). "A C-terminal motif found in the beta2-adrenergic receptor, P2Y1 receptor and cystic fibrosis transmembrane conductance regulator determines binding to the Na+/H+ exchanger regulatory factor family of PDZ proteins." Proc Natl Acad Sci U S A **95**(15): 8496-8501.

Hall, R. A., D. Vullo, et al. (2008). "External pH influences the transcriptional profile of the carbonic anhydrase, CAH-4b in Caenorhabditis elegans." Mol Biochem Parasitol **161**(2): 140-149.

Hansson, G. K., Y. J. Geng, et al. (1994). "Arterial smooth muscle cells express nitric oxide synthase in response to endothelial injury." J Exp Med **180**(2): 733-738.

Hargrove, J. L. and F. H. Schmidt (1989). "The role of mRNA and protein stability in gene expression." Faseb J **3**(12): 2360-2370.

Hatakeyama, S., Y. Yoshida, et al. (2001). "Cloning of a new aquaporin (AQP10) abundantly expressed in duodenum and jejunum." Biochem Biophys Res Commun **287**(4): 814-819.

Haudenschild, C. C., J. Grunwald, et al. (1985). "Effects of hypertension on migration and proliferation of smooth muscle in culture." Hypertension **7**(3 Pt 2): I101-104.

Herrera, M., N. J. Hong, et al. (2006). "Aquaporin-1 transports NO across cell membranes." Hypertension **48**(1): 157-164.

Heymann, J. B. and A. Engel (1999). "Aquaporins: Phylogeny, Structure, and Physiology of Water Channels." News Physiol Sci **14**: 187-193.

Holm, L. M., T. P. Jahn, et al. (2005). "NH3 and NH4+ permeability in aquaporin-expressing Xenopus oocytes." Pflugers Arch **450**(6): 415-428.

Huang, A. L., K. M. Jan, et al. (1992). "Role of intercellular junctions in the passage of horseradish peroxidase across aortic endothelium." Lab Invest **67**(2): 201-209.

Huang, Y., K. M. Jan, et al. (1998). "Structural changes in rat aortic intima due to transmural pressure." J Biomech Eng **120**(4): 476-483.

Huang, Y., D. Rumschitzki, et al. (1994). "A fiber matrix model for the growth of macromolecular leakage spots in the arterial intima." J Biomech Eng **116**(4): 430-445.

Iliev, E. A., W. Xu, et al. (2002). "Transcriptional and posttranscriptional regulation of Arabidopsis TCH4 expression by diverse stimuli. Roles of cis regions and brassinosteroids." Plant Physiol **130**(2): 770-783.

Imai, H., H. Nakamoto, et al. (2001). "Renin-angiotensin system plays an important role in the regulation of water transport in the peritoneum." Adv Perit Dial **17**: 20-24.

Ishibashi, K., M. Kuwahara, et al. (1997). "Cloning and functional expression of a new water channel abundantly expressed in the testis permeable to water, glycerol, and urea." J Biol Chem **272**(33): 20782-20786.

Ishibashi, K., M. Kuwahara, et al. (1998). "Cloning and functional expression of a new aquaporin (AQP9) abundantly expressed in the peripheral leukocytes permeable to water and urea, but not to glycerol." Biochem Biophys Res Commun **244**(1): 268-274.

Issaq, H. J., T. P. Conrads, et al. (2002). "Methods for fractionation, separation and profiling of proteins and peptides." Electrophoresis **23**(17): 3048-3061.

Itoh, T., T. Rai, et al. (2005). "Identification of a novel aquaporin, AQP12, expressed in pancreatic acinar cells." Biochem Biophys Res Commun **330**(3): 832-838.

Jacob, F. and J. Monod (1961). "Genetic regulatory mechanisms in the synthesis of proteins." J Mol Biol **3**: 318-356.

Jung, J. S., G. M. Preston, et al. (1994). "Molecular structure of the water channel through aquaporin CHIP. The hourglass model." J Biol Chem **269**(20): 14648-14654.

Jungbauer, L. M., C. K. Bakke, et al. (2006). "Experimental and computational analysis of translation products in apomyoglobin expression." J Mol Biol **357**(4): 1121-1143.

Kannel, W. B., J. D. Neaton, et al. (1986). "Overall and coronary heart disease mortality rates in relation to major risk factors in 325,348 men screened for the MRFIT. Multiple Risk Factor Intervention Trial." Am Heart J **112**(4): 825-836.

Kao, C. H., J. K. Chen, et al. (1994). "Ultrastructure and permeability of endothelial cells in branched regions of rat arteries." Atherosclerosis **105**(1): 97-114.

Karakotchian, M. and I. S. Fraser (2007). "An ultrastructural study of microvascular inter-endothelial tight junctions in normal endometrium." Micron **38**(6): 632-636.

Kass, M., A. Witkin, et al. (1998). "Snakes: Active contour models." International Journal of Computer Vision **1**(4): 321-331.

Konnikova, L., M. Kotecki, et al. (2003). "Knockdown of STAT3 expression by RNAi induces apoptosis in astrocytoma cells." BMC Cancer **3**: 23.

Kopecky, R. T., F. D. Thomas, et al. (1987). "Furosemide augments the effects of captopril on nuclear studies in renovascular stenosis." Hypertension **10**(2): 181-188.

Koyama, N., K. Ishibashi, et al. (1998). "Cloning and functional expression of human aquaporin8 cDNA and analysis of its gene." Genomics **54**(1): 169-172.

Kozono, D., M. Yasui, et al. (2002). "Aquaporin water channels: atomic structure molecular dynamics meet clinical medicine." J Clin Invest **109**(11): 1395-1399.

Krueger, C., C. Danke, et al. (2006). "A gene regulation system with four distinct expression levels." J Gene Med **8**(8): 1037-1047.

Kurien, B. T. and R. H. Scofield (2003). "Protein blotting: a review." J Immunol Methods **274**(1-2): 1-15.

Kurreck, J. (2009). "RNA interference: from basic research to therapeutic applications." Angew Chem Int Ed Engl **48**(8): 1378-1398.

Kurtz, T. W. and R. C. Morris, Jr. (1987). "Biological variability in Wistar-Kyoto rats. Implications for research with the spontaneously hypertensive rat." Hypertension **10**(1): 127-131.

Kyte, J. and R. F. Doolittle (1982). "A simple method for displaying the hydropathic character of a protein." J Mol Biol **157**(1): 105-132.

Lark, M. W., T. K. Yeo, et al. (1988). "Arterial chondroitin sulfate proteoglycan: localization with a monoclonal antibody." J Histochem Cytochem **36**(10): 1211-1221.

Leach, L., M. J. Lammiman, et al. (2000). "Molecular organization of tight and adherens junctions in the human placental vascular tree." Placenta **21**(5-6): 547-557.

Leitch, V., P. Agre, et al. (2001). "Altered ubiquitination and stability of aquaporin-1 in hypertonic stress." Proc Natl Acad Sci U S A **98**(5): 2894-2898.

Levenspiel, O. (1999). Chemical Reaction Engineering, John Wiley & Sons.

Lever, M. J., M. T. Jay, et al. (1996). "Plasma protein entry and retention in the vascular wall: possible factors in atherogenesis." Can J Physiol Pharmacol **74**(7): 818-823.

Libby (2001). The Vascular Biology of atherosclerosis. Braunwald's Heart Disase: A textbook of Cardiovascular Medicine. P. L. E. Braunwald. Philadelphia, WB Saunders**:** 995-1009.

Lin, S. J., K. M. Jan, et al. (1990). "Role of dying endothelial cells in transendothelial macromolecular transport." Arteriosclerosis **10**(5): 703-709.

Lin, S. J., K. M. Jan, et al. (1988). "Enhanced macromolecular permeability of aortic endothelial cells in association with mitosis." Atherosclerosis **73**(2-3): 223-232.

Lin, S. J., K. M. Jan, et al. (1989). "Transendothelial transport of low density lipoprotein in association with cell mitosis in rat aorta." Arteriosclerosis **9**(2): 230-236.

Lindsay, J. (1979). The Aorta. New York, Grune & Stratton.

Lopez Farre, A., J. R. Mosquera, et al. (1996). "Endothelial cells inhibit NO generation by vascular smooth muscle cells. Role of transforming growth factor-beta." Arterioscler Thromb Vasc Biol **16**(10): 1263-1268.

Majno, G., G. E. Palade, et al. (1961). "Studies on inflammation. II. The site of action of histamine and serotonin along the vascular tree: a topographic study." J Biophys Biochem Cytol **11**: 607-626.

Marieb, E. N. (1999). Human Anatomy and Physiology. New york, Benjamin Cummings.

McGill, H. C., Jr., K. D. Carey, et al. (1985). "Effects of two forms of hypertension on atherosclerosis in the hyperlipidemic baboon." Arteriosclerosis **5**(5): 481-493.

McGuire, P. G., D. G. Brocks, et al. (1989). "Increased deposition of basement membrane macromolecules in specific vessels of the spontaneously hypertensive rat." Am J Pathol **135**(2): 291-299.

Michel, C. C. (1997). "Starling: the formulation of his hypothesis of microvascular fluid exchange and its significance after 100 years." Exp Physiol **82**(1): 1-30.

Michel, C. C. and M. E. Phillips (1987). "Steady-state fluid filtration at different capillary pressures in perfused frog mesenteric capillaries." J Physiol **388**: 421-435.

Miyawaki-Shimizu, K., D. Predescu, et al. (2006). "siRNA-induced caveolin-1 knockdown in mice increases lung vascular permeability via the junctional pathway." Am J Physiol Lung Cell Mol Physiol **290**(2): L405-413.

Morishita, Y., T. Matsuzaki, et al. (2005). "Disruption of aquaporin-11 produces polycystic kidneys following vacuolization of the proximal tubule." Mol Cell Biol **25**(17): 7770-7779.

Mulkeen, A. L., T. Silva, et al. (2006). "Short interfering RNA-mediated gene silencing of vascular endothelial growth factor: effects on cellular proliferation in colon cancer cells." Arch Surg **141**(4): 367-374; discussion 374.

Mulvany, M. J. (1993). "Remodeling of resistance vessel structure in essential hypertension." Curr Opin Nephrol Hypertens **2**(1): 77-81.

Mulvany, M. J. (1993). "Vascular remodelling in hypertension." Eur Heart J **14 Suppl C**: 2-4.

New, D. I., A. M. Chesser, et al. (2004). "Structural remodeling of resistance arteries in uremic hypertension." Kidney Int **65**(5): 1818-1825.

Nielsen, S., B. L. Smith, et al. (1993). "Distribution of the aquaporin CHIP in secretory and resorptive epithelia and capillary endothelia." Proc Natl Acad Sci U S A **90**(15): 7275-7279.

Nievelstein, P. F., A. M. Fogelman, et al. (1991). "Lipid accumulation in rabbit aortic intima 2 hours after bolus infusion of low density lipoprotein. A deep-etch and immunolocalization study of ultrarapidly frozen tissue." Arterioscler Thromb **11**(6): 1795-1805.

Owens, G. K., P. S. Rabinovitch, et al. (1981). "Smooth muscle cell hypertrophy versus hyperplasia in hypertension." Proceedings of the National Academy of Sciences of the United States of America **78**(12): 7759-7763.

Owens, G. K. and S. M. Schwartz (1983). "Vascular smooth muscle cell hypertrophy and hyperploidy in the Goldblatt hypertensive rat." Circ Res **53**(4): 491-501.

Packham, M. A., H. C. Rowsell, et al. (1967). "Localized protein accumulation in the wall of the aorta." Exp Mol Pathol **7**(2): 214-232.

Palade, G. E. (1953). "Fine structures of blood capillaries(abstract)." J. Applied Physiol **24**: 14-24.

Palmer, R. M., D. S. Ashton, et al. (1988). "Vascular endothelial cells synthesize nitric oxide from L-arginine." Nature **333**(6174): 664-666.

Patton, F., Hille, Scher, Steiner (1989). Textbook of physiology. Philadelphia, Saunders.

Pereira, L. M., D. G. Bezerra, et al. (2004). "Aortic wall remodeling in rats with nitric oxide deficiency treated by enalapril or verapamil." Pathol Res Pract **200**(3): 211-217.

Presnell, J. and M. Schreibman (1979). Animal Tissue techniques. Baltimore, The John Hopkins University Press.

Preston, G. M. and P. Agre (1991). "Isolation of the cDNA for erythrocyte integral membrane protein of 28 kilodaltons: member of an ancient channel family." Proc Natl Acad Sci U S A **88**(24): 11110-11114.

Preston, G. M., T. P. Carroll, et al. (1992). "Appearance of water channels in Xenopus oocytes expressing red cell CHIP28 protein." Science **256**(5055): 385-387.

Preston, G. M., J. S. Jung, et al. (1993). "The mercury-sensitive residue at cysteine 189 in the CHIP28 water channel." J Biol Chem **268**(1): 17-20.

Rippe, B., B. I. Rosengren, et al. (2002). "Transendothelial transport: the vesicle controversy." J Vasc Res **39**(5): 375-390.

Rudi, B. and M. Alexander (1990). "Induction of nitric oxide synthase by cytokines in vascular smooth muscle cells." FEBS Lett **275**(1,2): 87-90.

Saadoun, S., M. C. Papadopoulos, et al. (2005). "Impairment of angiogenesis and cell migration by targeted aquaporin-1 gene disruption." Nature **434**(7034): 786-792.

Saboori, A. M., B. L. Smith, et al. (1988). "Polymorphism in the Mr 32,000 Rh protein purified from Rh(D)-positive and -negative erythrocytes." Proc Natl Acad Sci U S A **85**(11): 4042-4045.

Scanu, A. M. (1973). The structure of human serum low and high density lipoprotein. Atherogenesis: Initiating Factors. Ciba Foundation Symposium 12 (new series). Amsterdam New York**:** viii, 288 p. illus. 225 cm.

Schonthal, A. (2004). Checkpoint Controls and Cancer: Activation and Regulation protocols, Springer.

Schwartz, S. M. (1980). "Role of endothelial integrity in atherosclerosis." Artery **8**(4): 305-314.

Schwartz, S. M. and E. P. Benditt (1977). "Aortic endothelial cell replication. I. Effects of age and hypertension in the rat." Circ Res **41**(2): 248-255.

Schwartz, S. M., C. M. Gajdusek, et al. (1980). "Maintenance of integrity in aortic endothelium." Fed Proc **39**(9): 2618-2625.

Schwartz, S. M., C. M. Gajdusek, et al. (1981). "Vascular wall growth control: the role of the endothelium." Arteriosclerosis **1**(2): 107-126.

Shanahan, C. M., D. L. Connolly, et al. (1999). "Aquaporin-1 is expressed by vascular smooth muscle cells and mediates rapid water transport across vascular cell membranes." J Vasc Res **36**(5): 353-362.

Sharova, L. V., A. A. Sharov, et al. (2009). "Database for mRNA half-life of 19 977 genes obtained by DNA microarray analysis of pluripotent and differentiating mouse embryonic stem cells." DNA Res **16**(1): 45-58.

Shou, Y., K. M. Jan, et al. (2006). "Transport in rat vessel walls. I. Hydraulic conductivities of the aorta, pulmonary artery, and inferior vena cava with intact and denuded endothelia." Am J Physiol Heart Circ Physiol **291**(6): H2758-2771.

Sprague, E. A., M. A. Frankel, et al. (1980). Observation on vascular surface membranes charge distribution. Hemodynamics and Arterial wall. R. M. Nerem and J. R. Guyton. Houston,TX, University of Houston Press**:** 11-18.

Sui, H., B. G. Han, et al. (2001). "Structural basis of water-specific transport through the AQP1 water channel." Nature **414**(6866): 872-878.

Tarbell, J. M. (2003). "Mass transport in arteries and the localization of atherosclerosis." Annu Rev Biomed Eng **5**: 79-118.

Tedgui, A. and M. J. Lever (1984). "Filtration through damaged and undamaged rabbit thoracic aorta." Am J Physiol **247**(5 Pt 2): H784-791.

Tedgui, A. and M. J. Lever (1985). "The interaction of convection and diffusion in the transport of 131I-albumin within the media of the rabbit thoracic aorta." Circ Res **57**(6): 856-863.

Tedgui, A. and M. J. Lever (1987). "Effect of pressure and intimal damage on 131I-albumin and [14C]sucrose spaces in aorta." Am J Physiol **253**(6 Pt 2): H1530-1539.

Temin, H. M. (1976). "The DNA provirus hypothesis." Science **192**(4244): 1075-1080.

Truskey, G. A., W. L. Roberts, et al. (1992). "Measurement of endothelial permeability to 125I-low density lipoproteins in rabbit arteries by use of en face preparations." Circ Res **71**(4): 883-897.

Trusky, F. Y. D. K. G. A. (2004). Transport Phenomena in Biological Systems. New Jersey, Pearson Prentice Hall.

Turner, C. A., S. B. Flagel, et al. (2008). "Cocaine interacts with the novelty-seeking trait to modulate FGFR1 gene expression in the rat." Neurosci Lett **446**(2-3): 105-107.

Underwood, E. (1970). Quantitative Stereology.

Vargas, C. B., F. F. Vargas, et al. (1979). "Hydraulic conductivity of the endothelial and outer layers of the rabbit aorta." Am J Physiol **236**(1): H53-60.

Veflingstad, S. R. and E. Plahte (2007). "Analysis of gene regulatory network models with graded and binary transcriptional responses." Biosystems **90**(2): 323-339.

Wagner, R. C. and S. C. Chen (1991). "Transcapillary transport of solute by the endothelial vesicular system: evidence from thin serial section analysis." Microvasc Res **42**(2): 139-150.

Walsh, P. J. and P. Wright (1995). Nitrogen metabolism and excretion. Boca Raton, Fla., CRC Press.

Weinbaum, S., G. Tzeghai, et al. (1985). "Effect of cell turnover and leaky junctions on arterial macromolecular transport." Am J Physiol **248**(6 Pt 2): H945-960.

Wiebel, E. (1980). Stereological Methods:Practical methods for biological morphology.

Wight, T. N. and V. C. Hascall (1983). "Proteoglycans in primate arteries. III. Characterization of the proteoglycans synthesized by arterial smooth muscle cells in culture." J Cell Biol **96**(1): 167-176.

Wolinsky, H. (1972). "Long-term effects of hypertension on the rat aortic wall and their relation to concurrent aging changes. Morphological and chemical studies." Circ Res **30**(3): 301-309.

Wong, A. P., N. Nili, et al. (2008). "Expansive remodeling in venous bypass grafts: novel implications for vein graft disease." Atherosclerosis **196**(2): 580-589.

Wu, C. H., J. C. Chi, et al. (1990). "Transendothelial macromolecular transport in the aorta of spontaneously hypertensive rats." Hypertension **16**(2): 154-161.

Wuertz, K., J. P. Urban, et al. (2007). "Influence of extracellular osmolarity and mechanical stimulation on gene expression of intervertebral disc cells." J Orthop Res **25**(11): 1513-1522.

www.invitrogen.com (2009) "Lipofectamine 2000 transfection reagent." 1.

www.uhnresearch.ca/facilities/wcif/PDF/Autofluorescence.pdf. (2000). "Autofluorescence Causes and Cures." Retrieved 07/13/2005, 2005, from www.uhnresearch.ca/facilities/wcif/PDF/Autofluorescence.pdf.

Yasa, M., Z. Kerry, et al. (1999). "Effects of treatment with FK409, a nitric oxide donor, on collar-induced intimal thickening and vascular reactivity." Eur J Pharmacol **374**(1): 33-39.

Yasui, M., T. H. Kwon, et al. (1999). "Aquaporin-6: An intracellular vesicle water channel protein in renal epithelia." Proc Natl Acad Sci U S A **96**(10): 5808-5813.

Yuan, F., S. Chien, et al. (1991). "A new view of convective-diffusive transport processes in the arterial intima." J Biomech Eng **113**(3): 314-329.

Yuan, Y. V., D. D. Kitts, et al. (1998). "Interactive effects of increased intake of saturated fat and cholesterol on atherosclerosis in the Japanese quail (Coturnix japonica)." Br J Nutr **80**(1): 89-100.

Zeidel, M. L., S. V. Ambudkar, et al. (1992). "Reconstitution of functional water channels in liposomes containing purified red cell CHIP28 protein." Biochemistry **31**(33): 7436-7440.

Zeidel, M. L., S. Nielsen, et al. (1994). "Ultrastructure, pharmacologic inhibition, and transport selectivity of aquaporin channel-forming integral protein in proteoliposomes." Biochemistry **33**(6): 1606-1615.

Zhou, H. W., S. Q. Lou, et al. (2004). "Recovery of function in osteoarthritic chondrocytes induced by p16INK4a-specific siRNA in vitro." Rheumatology (Oxford) **43**(5): 555-568.

Zhu, F., E. Tajkhorshid, et al. (2002). "Pressure-induced water transport in membrane channels studied by molecular dynamics." Biophys J **83**(1): 154-160.